HYDROGEOLOGICAL CHARACTERIZATION OF A HIGH-DISCHARGE COASTAL FRESHWATER KARST SPRING SYSTEM

MARIA JHONNIE Z. VILLAREAL

JOHN W. JENSON

ROMINA P. KING

EDGARDO L. ABAN

WATER AND ENVIRONMENTAL RESEARCH INSTITUTE
OF THE WESTERN PACIFIC
UNIVERSITY OF GUAM

TECHNICAL REPORT NO. 176

MAY 2022

HYDROGEOLOGICAL CHARACTERIZATION OF A HIGH-DISCHARGE COASTAL FRESHWATER KARST SPRING SYSTEM

Maria Jhonnie Z. Villareal[1], John W. Jenson[1],

Romina P. King[2,3], & Jose Edgardo L. Aban[2]

[1] Water and Environmental Research Institute of the Western Pacific – University of Guam, Mangilao, Guam 96923

[2] College of Liberal Arts and Social Sciences – University of Guam Mangilao, Guam 96923

[3] Micronesian Area Research Center – University of Guam Mangilao, Guam 96923

Technical Report No. 176

May 2022

ABSTRACT

Studies of the distribution, modes, and geologic associations of coastal freshwater discharge provide clues to the internal characteristics or “natural plumbing” of island karst aquifers. This study employed field surveys and geospatial analyses of remotely sensed data from the Northern Guam Lens Aquifer to characterize *Ayuyu Cave*, the *Pugua Fault Zone*, and the relationship between them. Ayuyu Cave discharges the singularly highest-volume spring flow on Guam’s northwest coast. The Pugua Fault Zone is the dominant geologic feature of the interior area containing the hydrologic catchment of the Ayuyu Cave spring. Ayuyu Cave extends 65 m (210 ft) perpendicular to the northeast-trending coastline, with a volume of 3,486 m^3 (123,107 ft^3). The latest measurement of discharge is 8,700 m^3/day (2.3 MGD). The Pugua Fault Zone intersects the coast along the location of the cave, striking north-northwest and extending 4 km (2.4 mile) into the interior. The interior area is the site of a new military installation that will support at least 5,000 additional active-duty personnel and require development of at least 6,400 m^3/day (1.7 MGD) of additional groundwater production.

Field survey and mapping of the cave revealed a complex assemblage of features disparately characteristic of vadose, phreatic, and flank margin origins. These are overprinted such that the sequence, timing, and durations of genetic conditions and associated events cannot be discerned. The inscrutable speleological complexity of Ayuyu Cave testifies of an intricate history that includes the many cycles of Pleistocene eustatic sea level fluctuation, along with episodes of tectonic uplift and subsidence of unknown timing and magnitude, contemporaneous with the emergence of the Northern Guam Plateau.

Analysis of LiDAR imagery produced new insights into the structural characteristics of the interior area. Pugua Fault was originally mapped as a classic normal fault, downthrown on the southwest side, but DEM analyses of LiDAR imagery reveal features diagnostic of a left-lateral strike-slip fault with extensional components. Brecciated zones in the cave are consistent with structural deformation characteristic of strike-slip displacement. Cross-cutting relationships between the fault and the top-most units suggest the fault is likely to still be active. Strike-slip deformation is consistent with assumptions of previous studies that the Pugua Fault occupies a zone of enhanced hydraulic conductivity.

Keywords: *carbonate island karst, flank margin cave, submarine groundwater discharge, fault hydrogeology*

TABLE OF CONTENTS

LIST OF FIGURES

LIST OF TABLES

LIST OF APPENDICES

ACKNOWLEDGEMENT

I am honored to be part of a research that provides scientific groundwork for a better understanding of the Northern Guam Lens Aquifer, to ensure that the community of Guam have safe water to drink for generations to come. The opportunity to conduct this research, was carried under the generous funding of NASA Hawaii EPSCOR.

My heartfelt gratitude goes to my advisor – Dr. John Jenson, for his patience, overwhelming support and whose guidance goes beyond academics and into practical life advice.

I am extremely fortunate to have in my committee – Dr. Romina King and Dr. Jose Edgardo Aban for the insightful conversations and brainstorming calls that have helped shape the outcome of this thesis. My off-campus counsel – Todd Presley, deserves the same gratitude for his practical guidance on how to tread graduate school.

I drew wisdom from those who explored and studied the karst and caves of Guam before me – John Jocson, Danko Taborôši, Blaz Miklavič and Ida Shalilian. Their insights are relevant then and now.

Fieldwork was always fun with my reliable cave buddies: Charles Paulino Jr., for his enthusiasm to go back to Ayuyu cave anytime and Kaylyn Bautista whose pregnancy did not deter her from donning a helmet and crawling in tight spaces in support of me and this cave research project. Much appreciation to all others who on short notice were able to assist in my fieldworks - Aja, Jerson, Frank, and Anthony. President Krise, curious to know what we do inside the cave, joined us in one of our trips, merits a very special thank you for supporting the research that we do.

Special thanks to Eliana Walker for piloting the drone that has become my eyes of what's above the cave and Carl Henderson for piloting and lending us his submersible rover, for us to see what's underwater in Ayuyu cave pool.

In the sidelines, but equally important to the success of this project are the boat services, WERI admin and laboratory staff. Awesome boat captains who brought us back and forth safely to Ayuyu Cave – Todd Generaux, Barnaby, and UOG Marine Lab's - Jason Miller and John Peralta; Ms. Gema and Anthony for making sure we are on track on this project; WERI lab for processing my water samples.

From back home, I have my GEC caving friends to give thanks, for lending me Disto-X and for sharing their talent and expertise whenever needed.

This thesis is dedicated to my family who supported my dream to pursue graduate school. They may not understand why someone would want to go inside caves for fun and even more so to study them, still they were with me all the way in this journey. And lastly, my heart goes to Gerard, *l'amour de ma vie*.

CHAPTER 1. INTRODUCTION

1.1 Project Motivation and Application: Management of The Northern Guam Lens Aquifer:

The Northern Guam Lens Aquifer (NGLA) is a carbonate island karst aquifer (Mylroie *et al*., 2001) from which 40-44 MGD of freshwater is withdrawn from 100 to 120 production wells, to supply 90% of the drinking water for the island's 159,358 residents (USCB, 2020) which also—as will be explained in detail below—has some uniquely challenging geological qualities. One manifestation is that this portion of the aquifer discharges a disproportionately large volume of the total aquifer discharge, and that the mode of the discharge is spring flow from fractures and caves, rather than the classic distributed seepage associated with Darcian[1] flow.

Studies of coastal discharge provide hydrogeologists with important clues and insights into the internal plumbing of aquifers. This study focused on a field survey of the singularly highest-volume concentrated spring flow on the northwest coast of Guam and its relationship to prominent geologic and geomorphic features of the interior area containing its catchment.

Field study of coastal discharge from the NGLA has been a basic component of WERI groundwater research for the past two-and-a-half decades (Jenson *et al*., 1997; Jocson *et al*., 1999; Taborosi, 2004; Jenson *et al*., 2006; Taborosi *et al*., 2012; Shalilian, 2017). This project builds on this established line of research using new tools and focusing on specially selected features to provide new insights into the hydrogeologic properties of this complex part of the aquifer at a crucial time when new development directly affecting it is underway.

1.2 Coastal discharge and its clues to NGLA aquifer properties

The NGLA is a sole source aquifer with an unconfined fresh groundwater lens in a highly permeable limestone bedrock underlain by an impermeable volcanic basement unit (Mink and Vacher, 1997). The permeable aquifer bedrock is hosted within the limestone plateau of northern Guam, classified as a carbonate island type of aquifer (Jenson *et al.,* 2006). In young carbonate islands like northern Guam, unique karst features are known to develop from the complex relationship of diagenetically immature host rock with various factors such as tropical climate, autogenic recharge, sea level position and tectonics.

1 Darcian flow is fluid flow through porous medium based on the results of flow experiments through beds of sand by Henry Darcy and described by the Darcy's Law equation.

Coastal freshwater seeps and springs and submarine groundwater discharge (SGD) are characteristic features of the NGLA (Figure 1.1). These features were first documented for the northwest coast of Guam by Jenson *et al.* (1997) and Jocson *et al.*, (1999) who systematically explored and mapped for freshwater coastal discharge from 1995 to 1999. Two types of discharge were noted: diffuse seepage and concentrated discharge. Diffuse seepage is exemplified on Tumon Bay beach, where groundwater discharges in ubiquitous, persistent, but migrating seepages in and above the tidal zone, along the sandy beach. The Tumon Bay beach also exhibits scattered concentrated discharge forming brackish springs above the tide level and small boils of *vruljas* where the discharge is underwater. Further north, where the coast is dominated by rock benches and cliffs, concentrated coastal discharge emerges from fractures and caves. Taborôi *et al.* (2012) identified three characteristic coastal geomorphological environments: (1) linear beaches, (2) enscalloped embayments (such as Tumon Bay), and (3) rocky, cliff-dominated zones in the coast of the northern Guam plateau, and described the contributions of diffuse seepage, and concentrated discharge by beach springs, fracture springs, and conduit springs relative to each of the three environments.

Various modeling studies (Contractor, 1982; Contractor and Srivastava 1989, 1992; Jocson *et al*., 2002; Gingerich, 2013) have estimated coastal discharges from the NGLA. Gingerich (2013) estimated coastal freshwater discharge from the entire NGLA using a concurrently-built water budget (Johnson, 2012) and estimated distributions of interior hydraulic conductivity from tidal-signal attenuation in 34 wells across the aquifer (Rotzoll *et al*., 2012). The discharge estimate from the NGLA is 163 MGD, of which 72 MGD, i.e., 44%, discharges along the 10-km coast from Haputo Bay to Tumon Bay, which comprises only 37% of the entire NGLA coast. Discharge along this stretch of coast thus averages 7.2 MGD/km and is 20% more concentrated than if coastal discharge were uniformly distributed around the entire aquifer.

1.3 The uniqueness of Carbonate Island Karst aquifers

Karst aquifers present special challenges because they are characterized by complex “plumbing” composed of three-dimensional networks of fractures and conduits. Water infiltrates a porous, deeply weathered surficial epikarst, through the vadose bedrock to the water table, where it is transported horizontally in the phreatic zone to discharge at base-level springs (Ford and Williams, 2007). Among karst aquifers, carbonate island karst aquifers are even more complex because the limestone bedrock retains much of its original porosity, and the fresh groundwater resides in dynamic equilibrium in a typically lens-shaped layer atop the underlying saltwater. The base level of carbonate island karst aquifers rises and falls with both ordinary tidal cycles and seasonal-to-geological changes in sea level (Jenson *et al*, 2006).

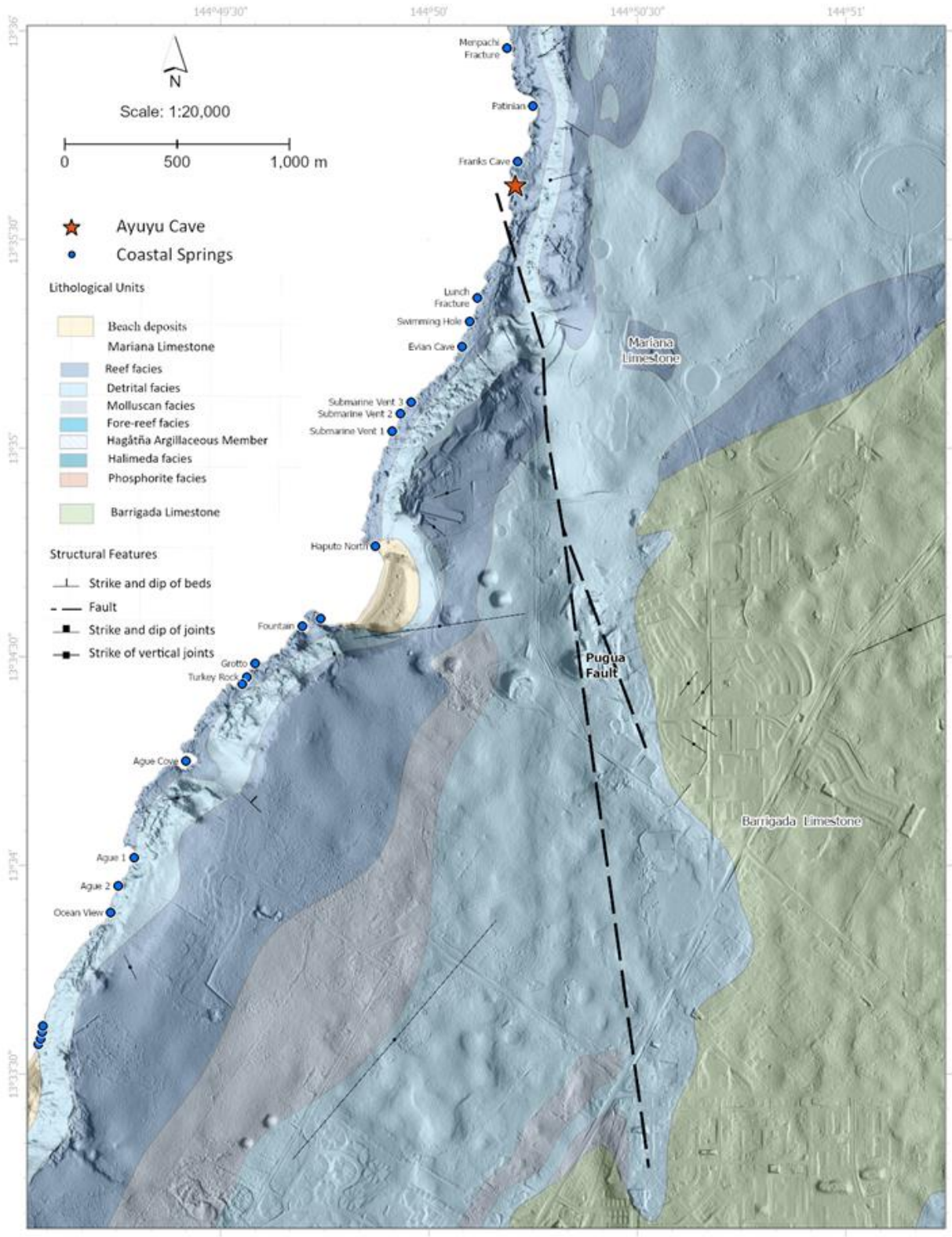

Figure 1.1 Study area in the context of geologic formations and coastal discharge features in Northwest Guam.

1.4 Prospective theoretical models and field assessment of hypotheses: Guam's NW coast

Coastal and submarine discharge from the NGLA is interpreted and explained in terms of the current theoretical models of island karst and coastal cave development: the Carbonate Island Karst Model (CIKM) and the Flank Margin Cave Model (FMCM). The CIKM summarizes the features that develop in young carbonate rocks based on their unique post-depositional history, retention of high original porosity, the effects of sea-level change and associated speleogenesis, and the relationship between volcanic basement rock, the overlying carbonate bedrock, and the origins and distribution of recharging surface waters. Mylroie and Jenson (2000) and Mylroie *et al.* (2001) applied the CIKM to interpreting the karst features and characterizing the hydrogeology of Guam. Jenson *et al.* (2006) subsequently documented its application to all of the Mariana Islands.

The flank margin cave model was to explain the unique morphology and features of caves that develop on the flanks of carbonate islands along the distal margin of the fresh-water lens (Mylroie and Carew, 1990; Jenson and Mylroie, 2006). The role of freshwater and its interaction with karst at the surface, subsurface, and submarine zones in both models is essential. *This study is aimed at advancing our understanding of coastal freshwater discharge along the northwest coast of Guam, with the ultimate goal of improving our conceptual models of groundwater transport in carbonate island karst aquifers.* Previous research (Jenson *et al.,*1997; Jocson *et al.,* 1999; Taborosi *et al.,* 2012; Gingerich, 2013) indicates that discharge is not only especially concentrated in the study area, but suggests, moreover, that discharge is dominated by point concentration from flowing fractures and caves.

On the northwest coast, the most striking concentrated discharge is from *Ayuyu Cave*, which produces the single greatest measured volume discharge from the northwest coast, perhaps from the entire aquifer (Jocson *et al.,*1999; Taborosi, 2004). Jocson (1998) found the cave and named it after Ayuyu or coconut crabs that lived there. Taborosi (2006) created the first map of Ayuyu Cave (Appendix 1a). Ayuyu Cave was described as a simple flank margin cave with an entrance at sea level and continuous groundwater discharge. The discharge from Ayuyu Cave is best observed during low tide when seawater significantly recedes, whereas during high tide, seawater and freshwater mixing creates a blurry, shearing effect. Shalilian (2017) further explored the cave and updated Taborosi's map, with the addition of narrow passages that extend to a brecciated room (Appendix 1b). Shalilian (2017) also measured the concentrated discharge in Ayuyu Cave to be 2.3 MGD. The large volume of concentrated groundwater discharge from Ayuyu Cave may be associated with to its proximity to the end of *Pugua Fault* (Figure 1.1), interpreted by Tracey *et al.* (1964) as a normal fault downthrown to the southwest, with a broad damage and brecciation zone. Shalilian hypothesized that the discharge from

Ayuyu Cave may be flowing along the Pugua Fault and calculated an estimate of the hydraulic conductivity of the fault from tidal-signal data collected from an inland cenote located along the fault. Although the cave has been mapped before and its coastal discharge measured (Shalilian, 2017), the previous maps were general, preliminary, and there has been no systematic or comprehensive, much less definitive assessment of the structural, stratigraphic, and hydrologic controls of the groundwater discharge in Ayuyu Cave.

This work builds on the previous work cited above and broadens it to include examination of speleogenetic processes and evidence for them that might provide additional insights into coastal zone hydrogeology for carbonate island karst aquifers. We seek to improve our understanding of the local geologic conditions of the study area and what general conclusions can be drawn from this case study regarding the geologic pathways and processes by which carbonate island karst aquifers store, transmit and discharge groundwater.

The subject, objectives, scope, and conceptual framework of the study are outlined in the next section.

1.5 Subject and Objectives: Hydrogeology of Ayuyu Cave and Implications for Discharge

In this study, we explored and mapped Ayuyu Cave in detail to discover, document and better understand defining feature of large-volume concentrated discharge in the NGLA, and in particular to characterize the contributions and constraints wrought by geologic structure, speleogenesis, and groundwater hydrology. *The central objective of this study was to examine and document the defining geological characteristics of* Ayuyu Cave *and their relationships to the coastal groundwater discharge associated with it.*

Field study objectives thus included:

(1) Characterizing surface and subsurface karst morphologies

(2) Determining structural controls on the development of Ayuyu Cave

(3) Assessing the contribution of Pugua Fault to the concentrated discharge in Ayuyu Cave

(4) Ascertaining cave characteristics attributable to climatic and sea-level history

1.5.1 Scope of Study: Research Questions

The research questions asked included:

(1) What are the structural, speleogenetic, and hydrogeological controls of the occurrence and distribution of coastal discharge from Ayuyu Cave?

(2) What is the relationship of the cave and the associated discharge to Pugua Fault and other structural features proximal to the cave?

(3) What generalizations can be drawn from them for applications elsewhere?

1.6 Conceptual Framework

The conceptual framework for evaluating and interpreting observable features of coastal caves exhibiting large-volume concentrated flow includes the Carbonate Island Karst Model (*cf.*, Jenson *et al*., 2006), the Flank Margin Cave Model (*cf.*, Mylroie and Carew, 1995), and conceptual models of Submarine Groundwater Discharge (SGD) phenomena (*cf.* Fleury *et al,* 2004; Burnett *et al.,*2006). The relevant aspects of these models that form the conceptual framework for this study are summarized below.

1.6.1 The Carbonate Island Karst Model

Carbonate island karst (Mylroie and Jenson, 2000; Mylroie and Mylroie, 2007) is a unique form of tropical karst characterized by the following traits and processes; 1) the karst is *eogenetic* (Vacher and Mylroie, 2002) i.e., it has developed in geologically young (Neogene to Pleistocene) carbonate rocks that have never been buried beyond the range of meteoric diagenesis and have thus retained substantial primary inter-particle porosity; 2) cavities form in the limestone bedrock from enhanced dissolution at the water table and at the base and margin of the freshwater lens; 3) glacio-eustasy has episodically repositioned the freshwater lens up and down leaving laterally-distributed sets of cavities—from the interior to the coast, where they are expressed as *flank margin caves*—at various levels above and below the modern sea level, over a vertical range of more than 100 m; 4) tectonic subsidence and uplift can also reposition the freshwater lens, with the same effects; 5) four categories of carbonate islands (Figure 1.2) are defined by the stratigraphic relationships of the island's non-soluble basement core to sea level and the island surface, and by the presence or absence of structural features (e.g., fractures and faults), stratigraphic discontinuities (e.g., bedding planes, disconformities), and concomitant secondary fracture and conduit porosities: a) simple, b) carbonate cover, c) composite, and d) complex. Simple carbonate islands have no basement core standing above sea level. Carbonate cover islands have basement core standing above sea level

but not cropping out at the surface. Composite carbonate islands have basement core cropping out at the surface but are not modified by structural features. Complex carbonate islands have the characteristics of composite islands plus further complexity wrought by presence of structural features and associated secondary porosities. Aquifers on composite and complex islands receive allogenic as well as autogenic recharge. Secondary (conduit) porosity develops along basement-bedrock contacts in carbonate cover, composite, and complex islands. Networks of dissolution-enhanced factures and associated conduits may be present in complex islands.

The low-standing, tectonically quiescent islands of the western Atlantic tend to be simple or carbonate cover islands. In the tectonically active Mariana Islands, Saipan is the archetype for the complex model. In Guam, the Northern Guam Plateau has provinces that fit each of the four models (see Vann *et al.,* 2014). Given that the northwest portion of the plateau has no outcrops of basement rock but contains a major fault, the study area of this project may be best described as a structurally modified carbonate cover province within the Northern Guam Lens Aquifer.

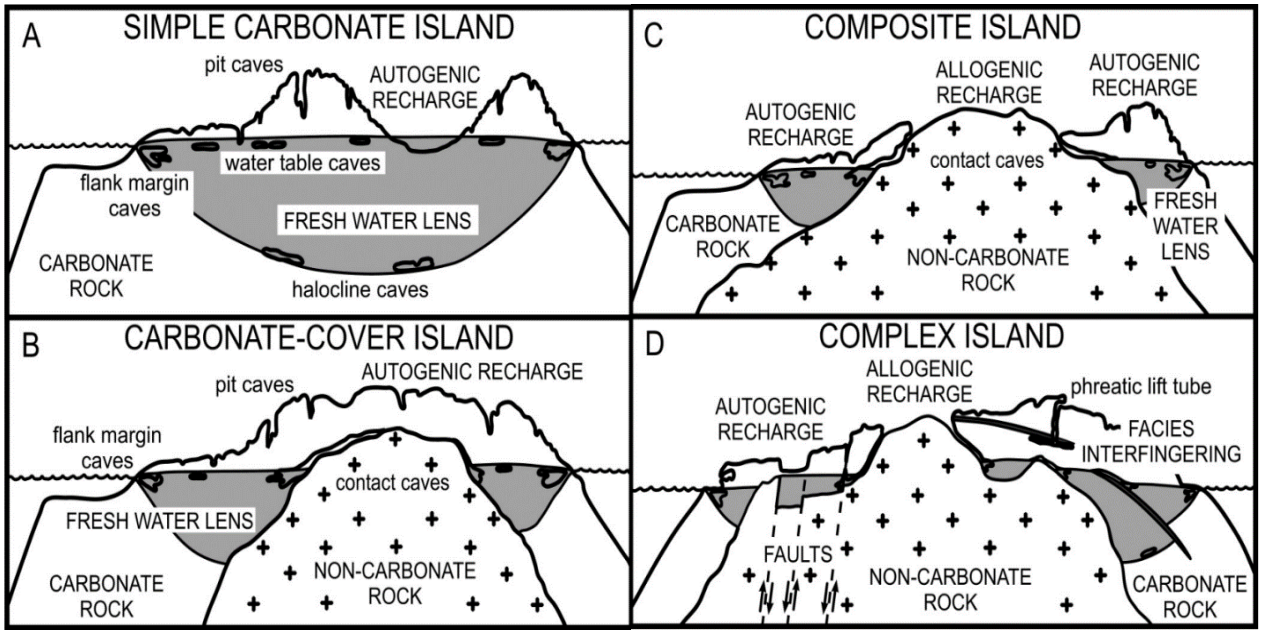

Figure 1.2. Island types of the *Carbonate Island Karst Model (Adapted from Jenson et al.,2006)* Schematic conceptual models of the four types carbonate islands (Jenson *et al.,*2006, and Mylroie and Mylroie, 2014): (1) **Simple carbonate islands,** when only carbonate rocks are present and catchment is entirely autogenic; (2) **Carbonate-covered islands,** when carbonate rocks blankets non-carbonate rocks and catchment is entirely autogenic; (3) **Composite islands**, when both carbonate and non-carbonate rocks are exposed at the surface and catchment can be autogenic and allogenic; (4) **Complex islands,** where carbonate and non-carbonate rocks exhibit a complex geological relationship (e.g. depositional or faulting).

The Carbonate Island Karst Model (CIKM) (Mylroie and Jenson, 2000) originated from pioneering work by Mylroie and Carew (1990) to explain the karst features on young carbonate islands in the Caribbean and Western Atlantic. Subsequent studies of the Marianas Islands from 1998 to 2005 (Mylroie and Jenson, 2000; Jenson *et al.,* 2006; Mylroie and Mylroie, 2007; Stafford *et al.,* 2009; Taborošı *et al.,*2003, 2009, 2012;), however, showed that island karst in general can be even more complex than previously observed and reported for Caribbean-Atlantic islands. The CIKM was thus developed by Mylroie and Jenson (2000) as a general model that accommodates the more complex islands of the Pacific (Mylroie and Mylroie, 2007, 2009, 2012).

1.6.2 Flank Margin Caves

Like the Carbonate Island Karst Model, the Flank Margin Cave Model originated from field studies of coastal caves in the Bahamas and Bermuda (Mylroie and Carew, 1990, 1995, 1999; Roth, 2006; Mylroie and Mylroie, 2011) which demonstrated caves on the flanks of carbonate islands (coincident with the margin of the lens, and hence the zone of freshwater discharge) have a characteristic morphology dominated by globular chambers that are horizontally broad but are vertically restricted (Mylroie and Carew, 1995). According to the model, flank margin caves originate by dissolution in the subsurface, without a visible opening at the surface (Mylroie and Carew, 1990, Mylroie and Carew, 1995, Mylroie and Mylroie, 2007). Dissolution begins from mixing corrosion (Kaufmann, 2003) at microscopic scales, in between matrix spaces and minute pores of rock.[2] Flank margin caves have been characterized as mixing chambers unassociated with conduits and turbulent flow (Roth, 2006). Mature morphology tends towards large globular chambers that extend towards the back of the cave as cross-linked, ramifying passages (Figure 1.3). Flank margin caves are important markers of past and present sea levels, have freshwater lens discharge horizons (Mylroie and Mylroie, 2014).

In Northern Guam, flank margin caves are ubiquitous in cliff faces at modern sea level and are interpreted as indicators of previous sea-level still stands (Figure 1.4). The spacing of the cave horizons is consistent with global and regional sea level curves bracketing the latest interglacial (Marine Isotope Stage 5e) and modern sea level. Intermediate cave horizons between the Mid-Holocene Highstand at 2 m above mean modern sea level and the MIS 5e Highstand at 7 m above mean modern sea level indicate intermediate stillstands that are most likely explained by episodes of local tectonic uplift and subsidence (Miklavič, 2012).

2 The Flank Margin Cave Model (Mylroie and Carew, 1990) invokes mixing-corrosion to explain the genesis and evolution of their characteristic morphology. Gulley (2015) have recently proposed that carbon dioxide derived from the vadose zone may be more important for dissolution and karstification, with mixing dissolution making only minor contribution to the speleogenesis of flank margin caves.

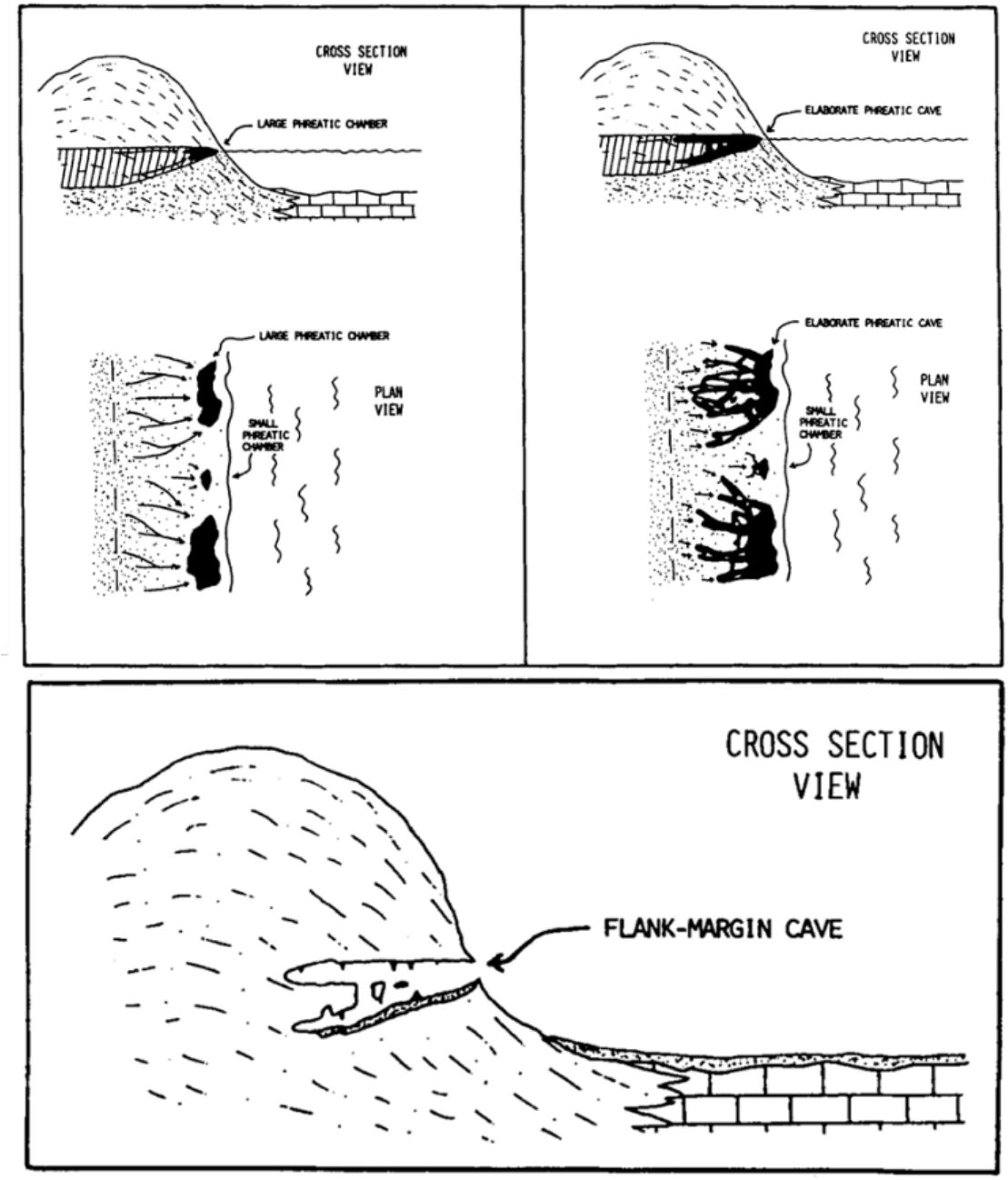

Figure 1.3. Flank margin cave formation (Adapted from Mylroie and Carew, 1990)

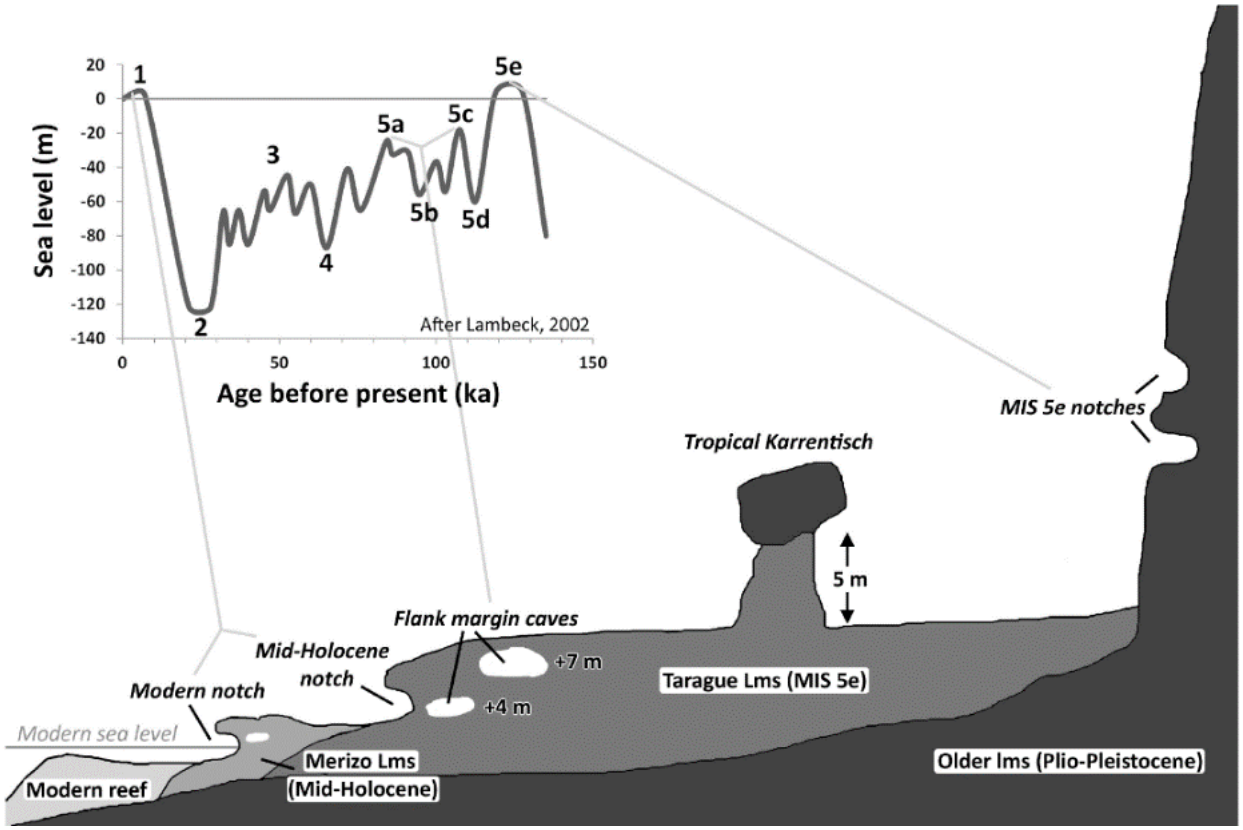

Figure 1.4. Cross-sectional sketch of flank margin cave horizons at several sea-level still stands in NW Guam (Adapted from Miklavič et al, 2012).

1.6.3 Submarine Groundwater Discharge

The contribution of freshwater from land to sea is called *Submarine Groundwater Discharge (SGD)* and refers to any flow of water out across the seafloor without regard to its composition, origin, and flow mechanism (Moore, 1996; Burnett, 2006). Among marine geologists and geochemists (*e.g.*, Burnett *et al.,*2003, 2006) there has been great interest during the past two decades in coastal groundwater discharge as a source of ocean solutes. For other than karst aquifers, such discharge is normally diffuse seepage distributed across beaches at and below the tidal level (Figure 1.5). In karst aquifers, however, coastal discharge can be concentrated in springs positioned in the tidal zone, or from *vruljas*, which are generally interpreted to have been coastal springs that formed at previously lower sea levels. In this study, the term *coastal groundwater discharge (CGD)* (Figure 1.5) will be applied to discharge in the tidal zone and reserve the term SGD for discharge from seeps or vents below the tidal zone.

As noted earlier, Taborosi *et al.* (2012) identified three characteristic geomorphological environments for the coast of northern Guam: (1) linear beaches, (2) enscalloped embayments, and (3) rocky, cliff-dominated zones. As also noted earlier, the study area

consists almost entirely of the third type and exhibits two striking characteristics: 1) although it occupies 37% of the aquifer coastline it is calculated to account for 44% of total discharge, and 2) the mode of discharge appears to be predominantly coastal spring from fractures or caves in the cliff face. Submarine vents have been observed in the reef platform fronting the cliff face (Jocson *et al.,*1999).

Submarine groundwater discharge is very difficult to find, much less to quantify. Although we are mindful of the prospects for submarine discharge, and were watchful for it during our fieldwork, the scope of this study is the characteristics and contributions of a selected significant source of concentrated spring flow from a coastal cave. Our search for related SGD was limited to provenance of Ayuyu Cave, and duly reported in Chapter 4, Results. We turn next to identify and describe the other relevant aspects of the study area geology.

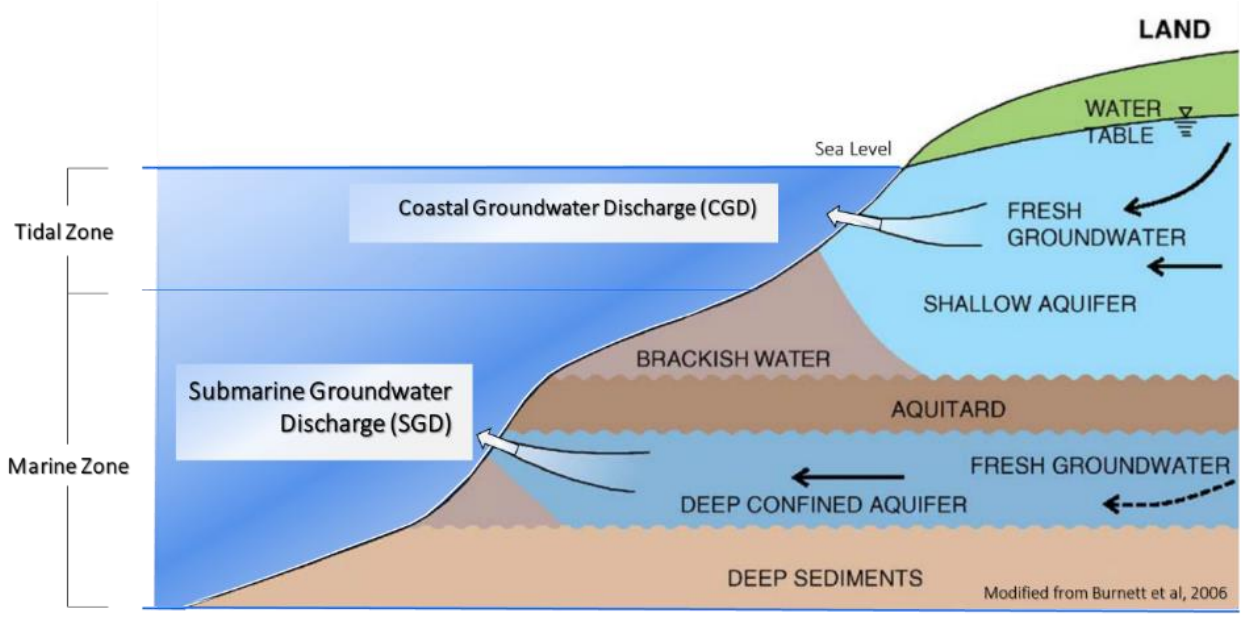

Figure 1.5. Land-sea interface of Submarine Groundwater Discharge (Modified from Burnett et al, 2006)

CHAPTER 2. GEOLOGIC CONTEXT AND LOCAL CHARACTERISTICS OF THE STUDY SITE

2.1 Regional Tectonic Setting

The Mariana Island Arc system is a crescent-shaped, tectonically active region in the western Pacific Ocean attributed to the oblique subduction of the Pacific Plate beneath the Philippine Sea Plate. It extends about 2,800 km from Guam in the south to Japan in the north characterized as a broad arc system under strong extension (Stern *et al.,* 2003). From west to east, the morpho-tectonic feature of the Mariana Island Arc system includes the Mariana Trench, Mariana Ridge (forearc), Mariana Trough (back-arc) and the West Mariana Ridge (remnant arc) (Figure 2.1).

The surface expression of the Pacific Plate subduction zone is the Mariana Trench, 2,554 km long and 11 km deep. Subduction along the Mariana Trench was initiated in Late Eocene (45 Ma), about the same time the Philippine Sea Plate was undergoing major reorganization and the Pacific Plate was changing from a northerly to westerly motion (Stern and Bloomer, 1992). Near Guam, the subduction rate along the Mariana Trench is estimated at 60-70 mm/year (Kato *et al.,* 2003).

Soon after the development of the subduction zone, the forearc also rapidly developed, likened to a type of seafloor spreading that suggests a strongly extensional environment (Stern and Bloomer, 1992). The forearc is composed of uplifted Eocene igneous basement blanketed by reef limestone especially in its southern end (Stern *et al.,* 2003). The Mariana Islands chain is the subaerially exposed part of the Mariana Fore-Arc (Hickey-Vargas and Reagan, 1987), Guam being the largest and southernmost, 48 km long and 6-19 km wide, with an area of 550 km^2. Petrologic and paleontological data of the oldest rock formations in Guam (Tracey *et al.,* 1964) and Saipan (Cloud *et al.,* 1956) concurs with the estimated initiation of subduction along the Mariana Trench.

The Mariana Trough is a well-developed, actively spreading, back arc basin located between the active volcanic arc (immediate west of the forearc) and the remnant arc. It marks the western divergent boundary of the Mariana Arc system with the Philippine Sea Plate. Spreading in the Mariana Trough began prior to 5 Ma, and motion surveys imply a spreading rate of 45 mm/year near Guam (Kato *et al.,* 2003).

The remnant arc, i.e., the West Mariana Ridge, is an arcuate edifice of single and coalesced submarine volcanic peaks that are generally younger toward the south. It is thought to have become dormant by about 7 Ma, but geomorphic characterizations provide evidence of active uplift (Gardner, 2010).

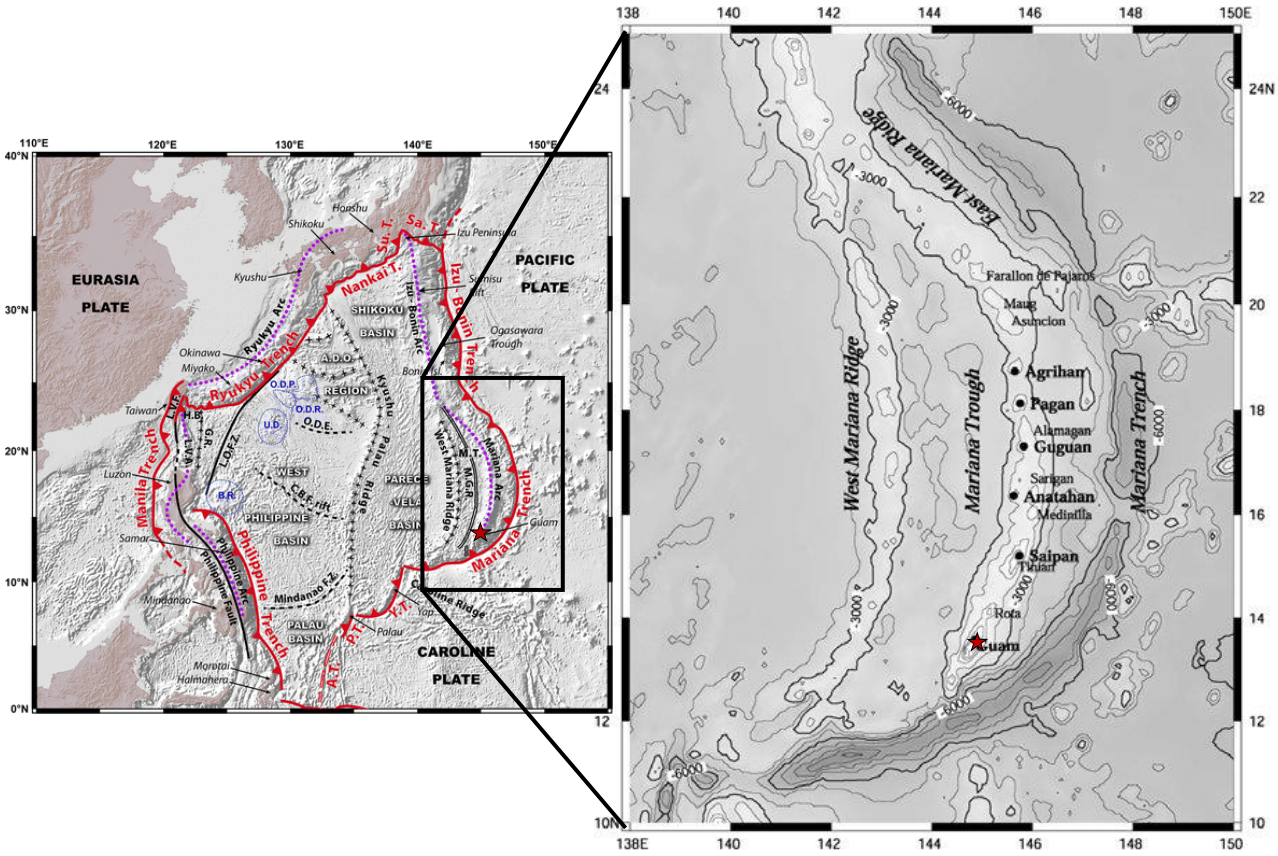

Figure 2.1. Regional tectonics and physiographic map of the NW Pacific Ocean showing the Mariana Subduction Zone and associated arc features. (Modified from Lallemand, 2016 and Kato et al., 2003)

2.2 Geological Setting

Detailed reports on the geology of Guam date back to the 1960's. Tracey *et al.* (1964) published the general geology, for which Schlanger (1964) did the petrological study of Guam's limestones. Reagan and Meijer (1984) later reclassified the volcanic rock units, and Siegrist and Randall (1992) revisited and reinterpreted the carbonate geology of Guam. In 2008, Siegrist and Reagan updated the geologic map of Guam of Tracey's report, incorporating these revisions.

Guam is divided by the *Pago-Adelup Fault*[3] into two distinct physiographic provinces of almost equal surface area: the island-karst limestone plateau of northern Guam (212 km^2) and the deeply weathered volcanic upland of southern Guam (330 km^2) (Figure 2.2). Northern Guam is composed mostly of carbonate rocks, the major series of which are the *Mariana* and *Barrigada Limestones*. Southern Guam is predominantly composed of three volcanic rock units, the *Facpi*, *Alutom* and *Umatac Formations*.

The oldest rock unit in the island is the Late Eocene *Facpi Formation*, which consists of mafic-to-ultramafic pillow lavas, hyaloclastites, tholeiitic basalts, and basaltic dikes that have undergone low-grade metamorphism and some lateritic weathering. The estimated thickness of the Facpi Formation ranges from 150 m to 240 m. Overlying the Facpi Formation are semi-contemporaneous series of volcanic breccias, conglomerates, turbidites and sandy limestones that comprise the Late Eocene-to-Early Oligocene *Alutom Formation*. The estimated thickness of this formation is 560 m to 610 m. Subsequent volcanic episodes deposited a series of volcaniclastic assemblages that altogether comprise the Oligocene-to- Miocene *Umatac Formation*, namely, the *Geus River Member*, the *Schroeder Flow Member*, *Bolanos Pyroclastic Member*, and the *Dandan Flow Member*. The total thickness of the Umatac Formation is estimated to be at least 670 m. The older volcanic formations in the south were uplifted and subaerially exposed during Miocene time, at about the same time that limestone deposition began in the north.

In the south, some minor sedimentary units—the *Maemong Limestone* (reef), *Bonya Limestone* (shallow inland embayment reef, pure to argillaceous), and *Talisay Member* (basal clayey conglomerate) of the *Alifan Limestone*—were deposited throughout the Miocene, unconformably overlying the older volcanic rocks. The more extensive Miocene limestone units—the *Barrigada Limestone* (massive to friable foraminiferal), *Janum Limestone* (argillaceous foraminiferal) and *Alifan Limestone* (massive, recrystallized reef) were deposited from Miocene through Pliocene time. The *Barrigada Limestone* is exposed at the surface in a ring-shape outcrop that dominates the north central interior of the northern plateau. *Alifan Limestone* occurs in the south as locally prominent remnant bedrock caps on the underlying dissected volcanic basement, and in the north as patches or fensters exposed where younger units have been eroded from above or were not deposited.

3 The *Pago-Adelup Fault* is a normal fault, striking N45°W sub-linearly across the middle of the island, dipping northeast, exhibiting folding, fractures, and irregular displacements or offsets. Although the relative vertical displacement is 300 feet downward on the dip-side (NE) both sides have undergone net uplift.

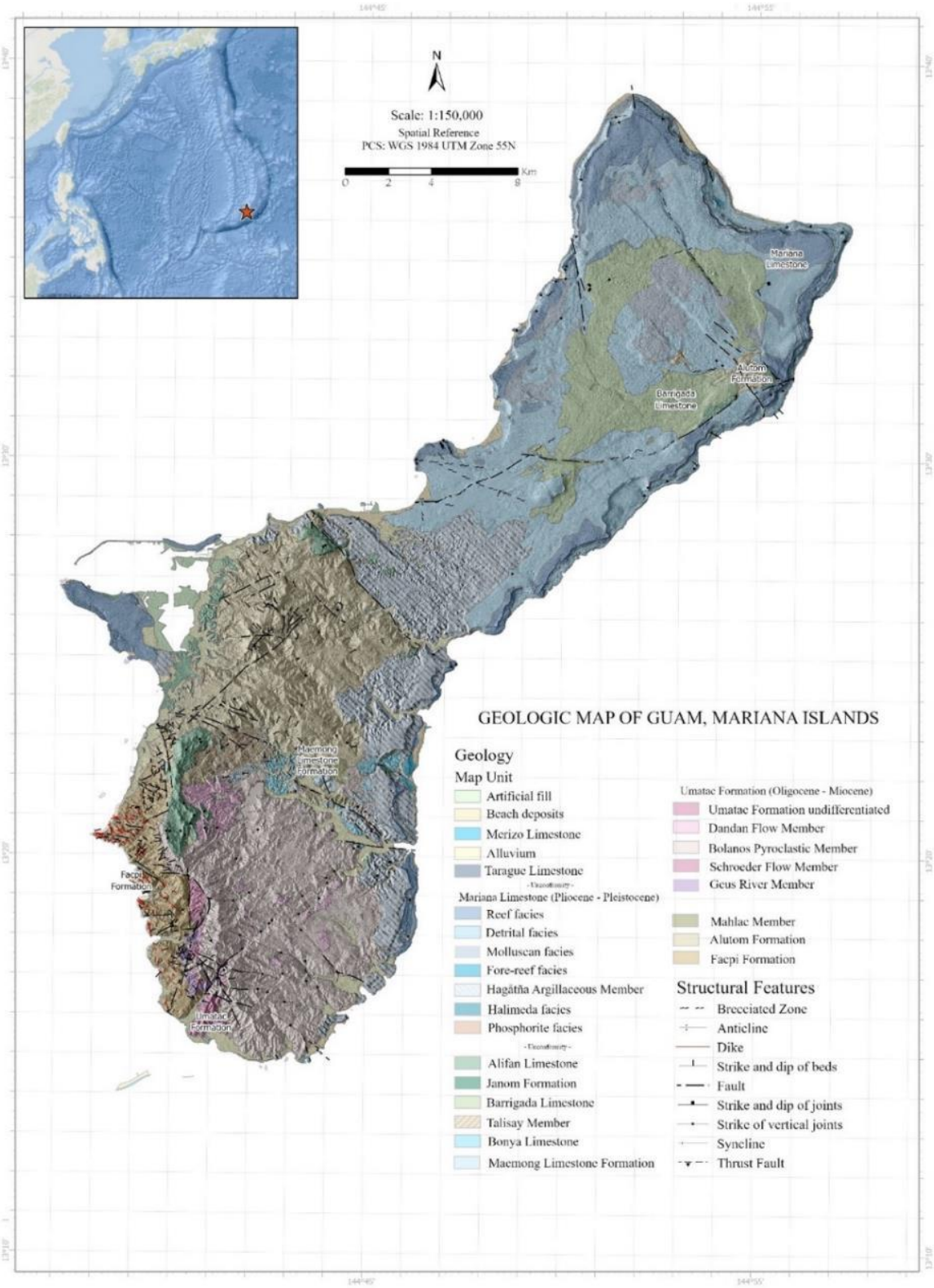

Figure 2.2. Geology of Guam (Adapted from Siegrist and Reagan, 2008)

The Pliocene to Recent is characterized by a quiescent period that allowed for uninterrupted and extensive limestone deposition, especially in the north, while the uplifted older volcanic rocks in the south underwent deep surficial weathering. The *Mariana Limestone*, which consists of seven facies, ranging from fore reef to interior lagoonal facies, was deposited during this quiescent period between Pliocene and Pleistocene. Aggregate thickness of the *Mariana Limestone f*acies is estimated to range from 165 m to 180 m. The massive reef facies of the Mariana limestone form the main part of the northern plateau's distinct marine terraces. The bedrock of the Northern Plateau is predominantly Mariana Limestone and Barrigada Limestone, overlying the *Alutom* Formation, which comprises the basement of the plateau. The two youngest limestone units in the island are accretional coral-algal reef limestones from fringing reefs that formed during the past two glacio-eustatic high stands: the last interglacial MIS 5e *Tarague Limestone*, (125,000 – 135,000 years old) and the mid-Holocene *Merizo Limestone* (2,500 – 4,800 years old) (Randall and Siegrist, 1996; Siegrist & Reagan, 2008; Miklavič, 2011). Each occurs in limited and distributed patches along the islands' coastlines.

2.2.1 Emergent Reefs, Sea Level and Uplift History

The presence of Pleistocene reef terraces or shore benches and emergent notches related to former sea levels has been documented in early studies (Tracey *et al.,* 1964; Bell and Siegrist, 1988; Randall and Siegrist, 1988) of the Mariana Islands. Reef terraces in Guam have been described at various elevations that have been correlated to limestones of comparable lithology in Saipan (Stearns, 1945; Tracey *et al.,*1964). Radiometric ages of the emergent reef and algal ridge on the north coast by Randall and Siegrist (1988) range from 810 ± 40 yr. BP to 4880 ± 80 yr. BP. However, the relationship of these geomorphic features to relative sea level is complex. Bell and Siegrist (1988) attributed the reef terraces in Guam to tectonic uplift, citing its location along an active arc. Based on geomorphic and geologic development of the Holocene reef, Kayanne *et al.,* (1993) concluded a gradual but steady rise in sea level to a maximum of 1.8 m between 6000 and 4200 yr. BP. After 4200 yr. BP., sea level is believed to have remained mostly stable with occasional episodes abrupt uplift and reef emergence thereafter.

The island's tectonic uplift began in Eocene time and has totaled several thousands of feet. The Pleistocene reef facies of the Mariana Limestone that tops the northern plateau would have risen several hundreds of feet in Pleistocene Time (Tracey *et al.,* 1964). In his study of flank margins in Guam, Miklavič (2011) estimated a cumulative uplift of the NGLA of ~22m (~0.18 mm/yr) or an average uplift rate of about 0.18 to 0.22 mm/yr considering as well, at least 8 m of denudation rate or an average rate of 0.064 mm/yr. over the past 125 ka years. Evidence to date (Tracey *et al.,* 1964; Miklavič, 2011)

suggests uplift of the was intermittent, with some setback periods of minor subsidence, obviously with net uplift from Late Eocene through Pleistocene time, through Pleistocene time, at least, juxtaposed against Pleistocene glacio-eustatic sea-level fluctuations.

2.2.2 Structural Features Relevant to the Study Area

Tracy *et al.* (1964) divided Guam into six structural blocks bounded by major faults (Appendix 2): *Machanao Block*, *Barrigada Block*, and *Santa Rosa Horst* in the north; *Tenjo Block* and *Orote Block* in central Guam; and *Bolanos Block* and *Cocos Block* in the south. The study area is within the *Machanao* Block. Randall (1988) preferred a simplified convention that considers the northern plateau as a structural province among three blocks separated by major fault zones. The interpretation of structural features in Guam has not been revisited or updated since. Tracey *et al*., (1964) remains the most comprehensive study of the structures of Guam.

Northern Guam has some prominent structural features, including regional-scale faults that may have pivotal influence on groundwater transport and discharge. As already noted earlier, previous workers have noted the possibility of a hydraulic connection between Pugua Fault and the discharge from Ayuyu Cave (e.g., Shalilian, 2017). Tracey *et al.* (1964) observed from cliffside exposures on the northeast coast of Guam that high-angle normal faults, cutting across Miocene Limestone units (Bonya and Janum limestones) do not extend upward into the Pliocene-Pleistocene Mariana Limestone, and hence must be older than about 5 Ma. The *Tamuning-Yigo Fault* is a high angle normal fault that separates the *Machana*o Block from the *Barrigada Block*. It transects the northern limestone plateau along a general northeast strike towards the perpendicular horst and graben, southwest bounding structure in Mt. Santa Rosa. The structures exposed in Mt. Santa Rosa are thrusts with evident crosscuts by high angle normal and strike-slip faults trending northwest (Tracey *et al.,* 1964). Hence, the age of Tamuning-Yigo fault can be estimated as Pliocene, no older than the Mariana Limestone.[4] In contrast, along the northwest coast the regional-scale, NNW-trending Pugua Fault cuts the top-lying Mariana Limestone (Figure 2.3). The Pugua Fault has thus been active since the 2-Ma-old Upper Pleistocene Reef Facies of the Mariana Limestone was deposited. This means that the Pugua Fault has been active in the geologically recent past (<2 Ma), which increases the odds that it may still be active.

4 Based on classic application of stratigraphic and cross-cutting relationships, the minimum relative age of a fault is the upper depositional age of the formation or facies that it cuts across.

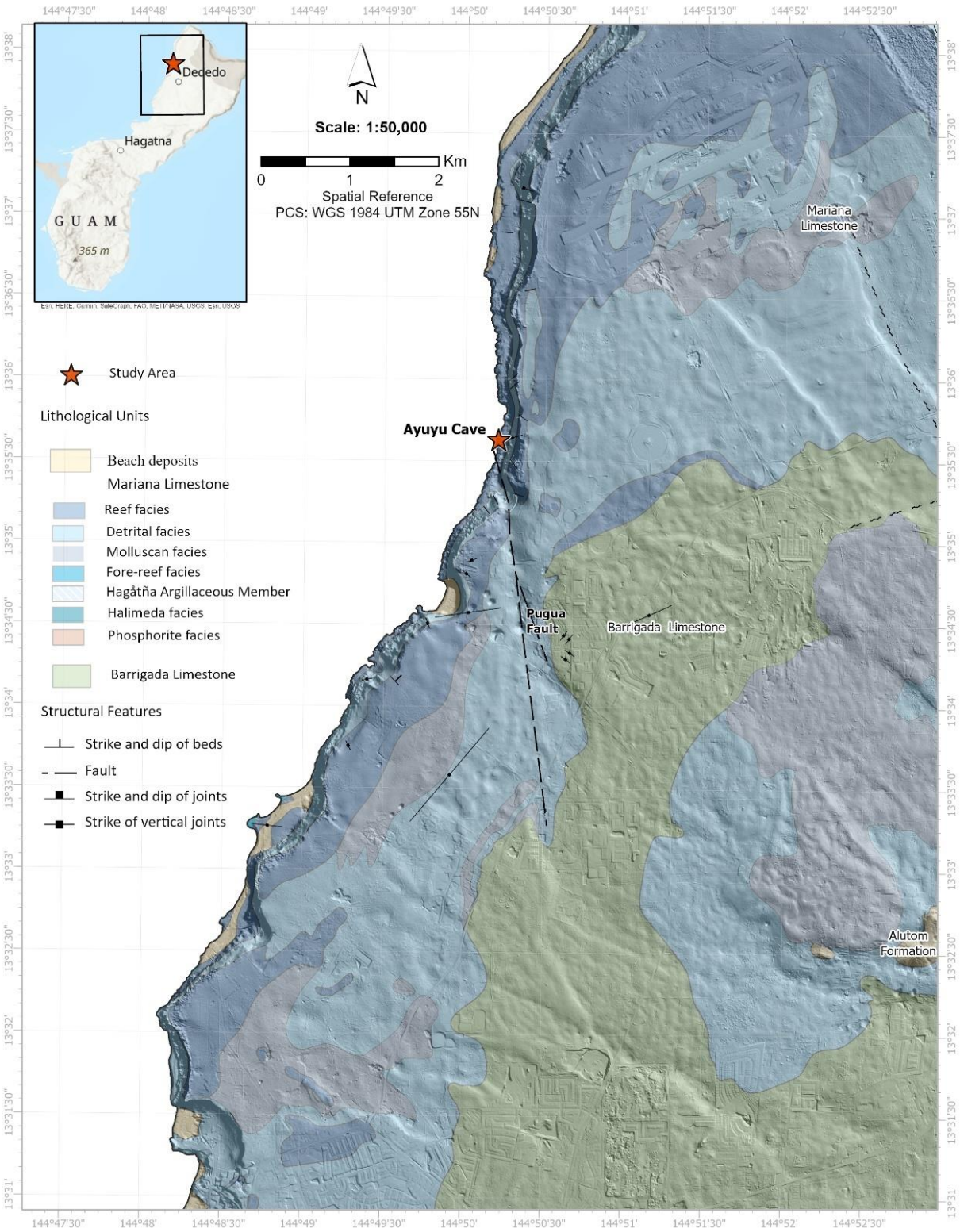

Figure 2.3. Structural features and lithological units in study area.

2.3 Hydrogeologic Setting and Previous Hydrological Studies Related to the Study Area

2.3.1 Hydrogeological Setting

Northern Guam is a gently undulating limestone plateau, devoid of surface streams because of the fast infiltration of water into the highly porous and permeable limestone formations that comprise the aquifer. The Miocene-Pliocene Barrigada Limestone forms the core and comprises most of the volume of the aquifer. The Pliocene-Pleistocene Mariana Limestone overlies and surrounds the Barrigada Limestone, covering most of the surface and thickening at the rim of the plateau. The two highly permeable limestone aquifer units form the bedrock of the plateau, unconformably overlying the much less permeable volcanic basement comprised by the *Alutom* Formation. Where the topography of the *Alutom* basement stands above sea level, it forms an aquiclude partitioning the aquifer into six hydrologically autonomous groundwater basins (Figure 2.4).

The study area is located in the Finegayan Basin in northwest Guam. Of the six NGLA aquifer basins, the Finegayan Basin receives the highest annual rainfall (105 inches; Lander and Guard, 2003) as well as the highest values of local hydraulic conductivity derived from pumping tests (900 to 1200 m/d; CDM, 1982, as cited in Shalilian, 2017). Water levels in observation wells were observed to rise in a matter of hours in response to heavy rainfall especially during wet conditions (Jocson *et al*., 1999). Under dry conditions, water levels do not respond as fast to heavy rainfall because water goes into storage in the vadose zone first before it percolates its way to the water table. This complex infiltration-storage feature of the NGLA is a characteristic attributed to geologically young, eogenetic limestones, which retain substantial intergranular primary porosity and thus high storage capacity. Modeling studies (Contractor, 1982; Contractor and Srivastava 1989, 1992; Jocson *et al.,* 1999, 2002*;* Rotzoll *et al.,* 2013; Gingerich, 2013) have successfully employed storativity values of about 20%. Rotzoll *et al.* (2012) used tidal-signal data from observation wells to calculate hydraulic conductivity for the interior of the aquifer ranging from 20,000 to 90,000 m/d. However, towards the island's periphery, the hydraulic conductivity decreased several orders of magnitude to only 20 to 800 m/d. The hydraulic conductivity drop was attributed to case hardening of limestone along the periphery. Significantly, the discharge zone of the Finegayan Basin (Figure 5 from Gingerich, 2013) proximal to Ayuyu Cave is located, constitutes a high-conductivity "breach" in the lower-conductivity wall of the adjacent rim of the plateau.

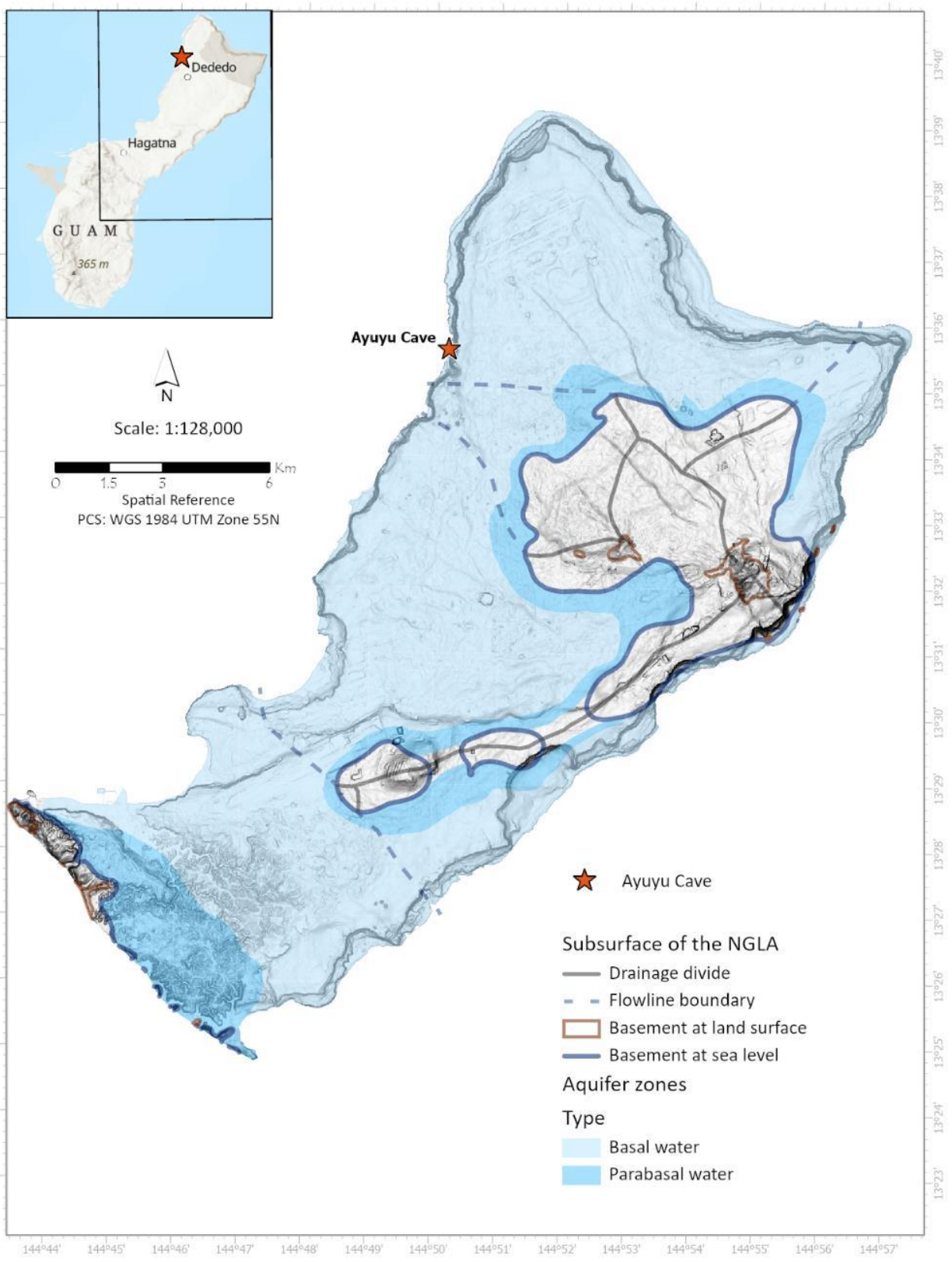

Figure 2.4. Hydrogeologic Map of the Northern Guam Lens Aquifer (Adapted from WERI)

2.3.2 Previous Hydrological Studies

Hydrogeological studies to explore and develop groundwater resources in Guam began with Stearns *et al.* (1937) of the USGS. Ward *et al.* (1964) prepared the USGS Professional paper on the *Hydrology of Guam* that accompanied Tracey's (1964) *General Geology of Guam*. Other reports in same series that are relevant to the hydrology of the study area include Schlanger's (1964) report on the *Petrology of the Limestones of Guam*, which describes the properties of the aquifer rocks; and Emery ***et al.'s*** (1964) report on the *Marine Geology of Guam*, which documented their discovery of four submarine terraces marking now-submerged former sea-level still-stands.

A decade later, private professional hydrogeologist John Mink was retained by the Public Utility Agency of Guam to prepare a water resources assessment including an estimate of aquifer sustainable yield (Mink, 1976), which was subsequently published as WERI Technical Report #1. Mink was retained again a few years later, by Guam Environmental Protection Agency, to lead the pivotal Northern Guam Lens Study (NGLS) (CDM, 1982) which still stands as the most comprehensive study of the basic properties of the aquifer. Ayers and Clayshulte (1984) contributed to the NGLS by analyzing a 500-foot limestone core drilled for the study and doing the first published calculations of regional hydraulic conductivity from tidal signal data. Mink (1991) prepared an update of the NGLS, which included some modeling results and a revised estimate of sustainable yield. These early works were later summarized by Mink and Vacher (1997) in a review paper on the Northern Guam Lens Aquifer. Numerous subsequent hydrogeological works cited earlier (e.g., Jenson *et al.,* 1997; Jocson *et al.,*1999; Contractor and Jenson, 2000; Gingerich, 2012; Rotzoll *et al.,*2012; Taborosi *et al.* 2012) have been conducted employing various methods to understand the properties of the NGLA.

CHAPTER 3. METHODS

To meet the research objectives, surface and subsurface geological features of Ayuyu Cave and adjacent parts of the study area were explored, mapped, and studied in the field using the CIKM, FMC, and CGD/SGD models as the theoretical framework for description and interpretation of observations to ascertain the conditions and processes that produce and constrain high-volume concentrated coastal freshwater discharge at this site. Related geospatial data, imagery, hydrological, and hydrogeological data were also analyzed and integrated. As summarized in Figure 3.1, the methodology included classical geologic and hydrogeologic field surveys, an inventory of regional structural features, and morphometric analyses of cave features to determine the origins and hydrologic properties of Ayuyu Cave.

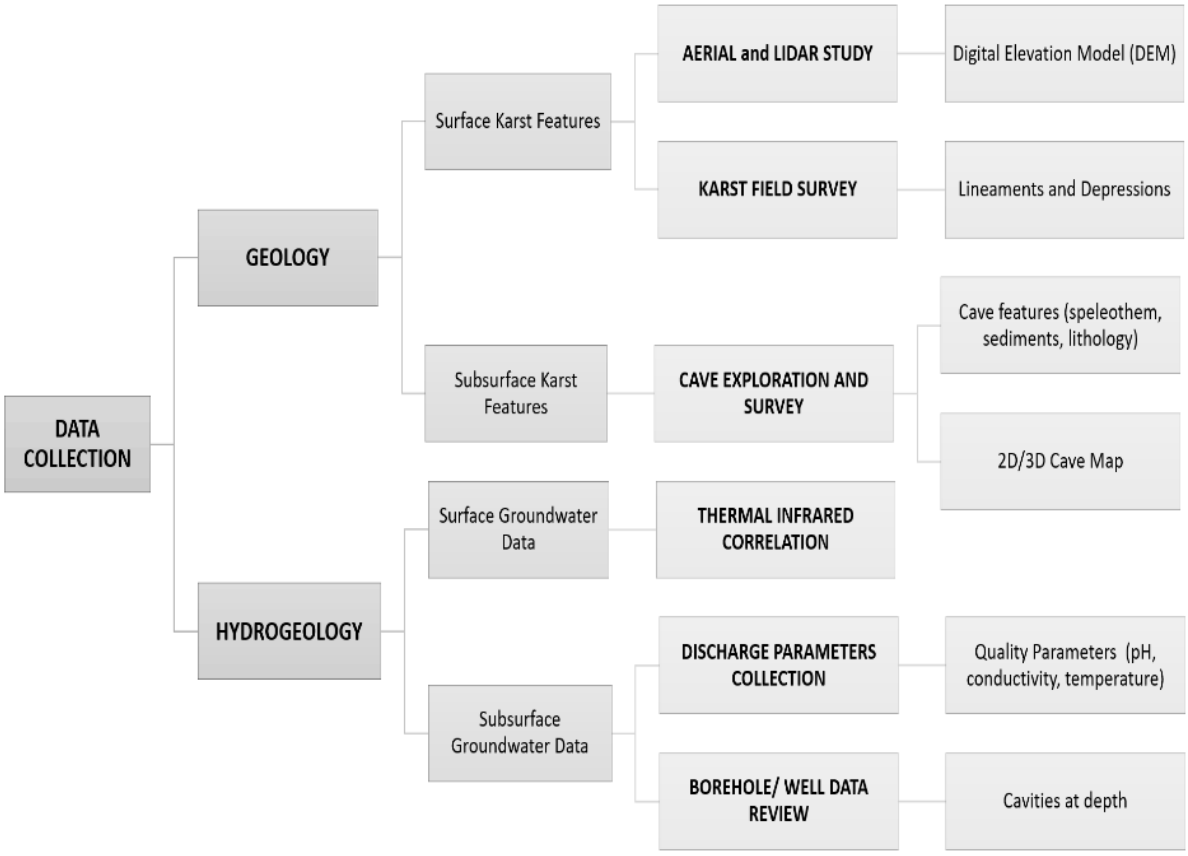

Figure 3.1. Methods Flowchart

3.1 Surface Karst Study

3.1.1 Aerial and LiDAR Study

LiDAR point cloud data (ver. 2012) of the study area were downloaded from the NOAA website and processed into digital elevation models (DEM) and digital surface models (DSM) using ARCGIS Pro Software. The DEM provides images of ground points or bare earth, while the DSM captures such "top-covering" features such as vegetation height and buildings. The DEM was processed further into various raster surfaces (Figure 2.6) namely as aspect, slope and hillshade to identify karst and linear structural features. Aspect raster surface is useful in identifying the compass direction of sloping terrain, while slope raster surface identifies the gradient of the terrain. Shaded reliefs by hill shading were also created using several azimuths and varying the orientation of the illumination source to highlight surface features at various angles. Generated contours from DEM were used for analyzing and correlating surfaces and identifying contour breaks in slope that may indicate structural features such as faults and offsets.

The raster surfaces were analyzed and studied to identify closed depressions attributed to karst dissolution as well as linear features and other geomorphic features such as truncated ridges, and sag ponds that may indicate faults. Identifying fault traces features in karst, whether in the field or from spatial imagery can be challenging because the high solubility of limestone means that surface terrain features that could have been fault indicators tend to be rapidly and thoroughly eradicated by dissolution. Identifying solution depressions (dolines) can also be challenging but benefits from DEM processing using the *Fill* and *Sink* spatial analyst tools. The Fill tool levels the anomalous sinks in the DEM data while the Sink tool identifies areas of internal drainage that could be associated with solutional depressions.

Using LiDAR imagery and other modern tools for remote sensing and geospatial analysis, however, this study revisited structural interpretations of Pugua Fault and delineated previously unmapped linear features in the study area.[5] Using surface raster maps created from LiDAR, the dominant structural feature of the study area, the Pugua Fault, was re-evaluated and retraced. Unfortunately, field verification of the re-interpreted lineaments was precluded access restrictions and pushed outside of the timeline of this research project by the COVID-19 pandemic. (Thus, we recommend revisiting the structural geology of Guam as a topic for future research.) This was a conservative delineation strictly based on conspicuous fault indicators such as offsets, scarps, and contour breaks that are readily observable in the raster surfaces. We interpret structural

5 In fact, it is widely noted among contemporary geologists who have used LiDAR imager that it reveals subtle differences in surface elevation that are obscured in the field by vegetation or are otherwise readily overlooked. Tracks of old dirt roads now covered with jungle and practically indiscernible in the field, even when standing on them, are readily visible on LiDAR images.

geologic features (Figure 4.2) in the study area in light of regional tectonics and identify how they are related to surface karst features.

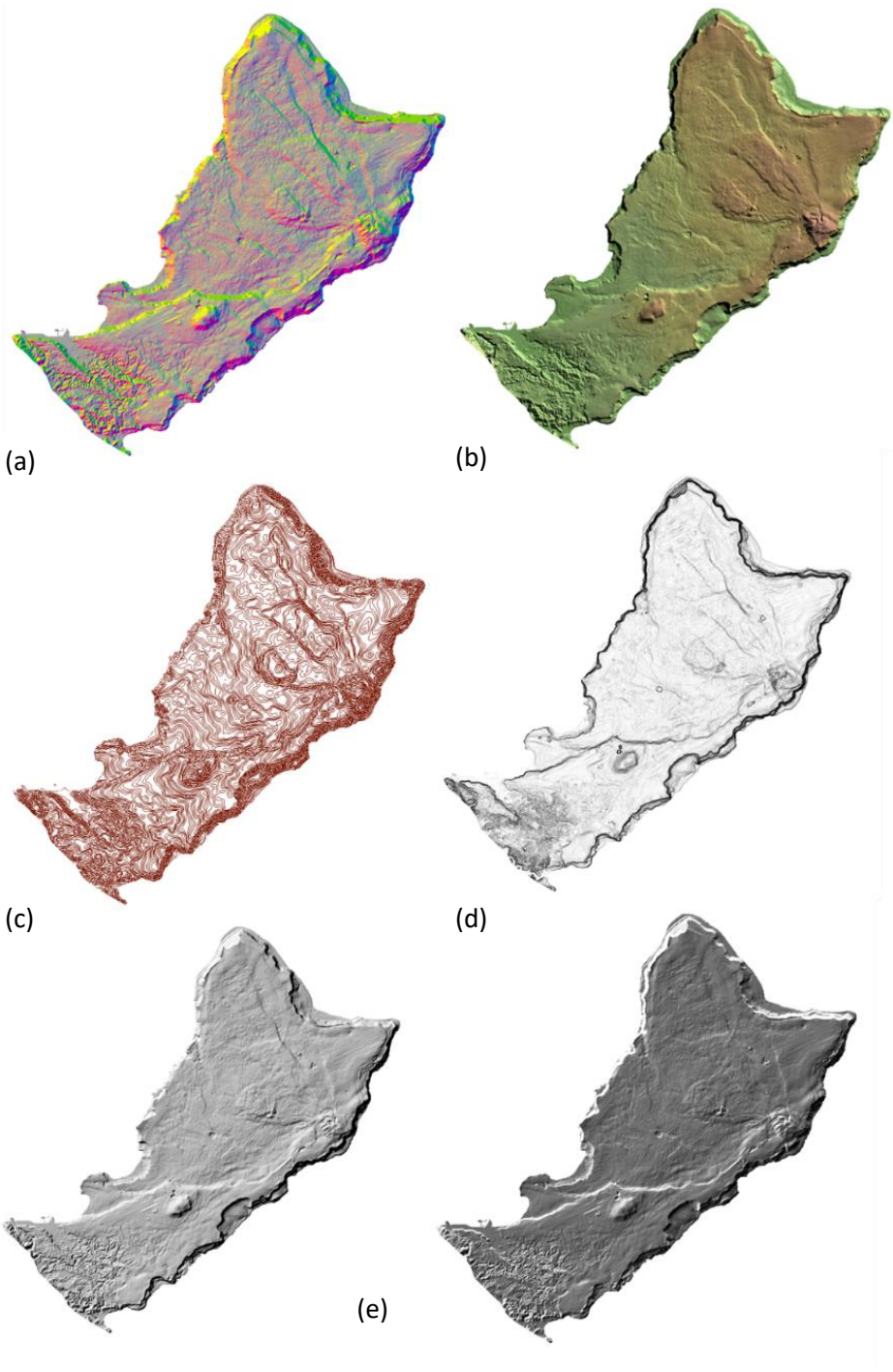

Figure 3.2. Raster surfaces processed from DEM include a) Aspect surface indicating slope direction; b) Colored 3D terrain representation; c) DEM generated contours; d) Slope surface showing change of elevation; e) Hill shade using various illumination source angles.

3.1.2 Karst Field Survey

Field verification of closed depressions and linear features delineated in the LiDAR study was precluded by access restrictions. The areas above Ayuyu Cave are part of a US military installation. Lockdowns and additional restriction caused by the global pandemic starting in March 2020 ruined our original field plan. Fortunately, Shalilian (2017) was able to gather field data and observations from the same general area particularly along the trace of Pugua Fault. Field photos, station waypoints and notes from Shalilian's (2017) work were reviewed and referenced in this work when relevant.

3.1.2.1 Thermal Infrared Imageries

Thermal infrared imageries were also available through complementary research by Walker (pers. comm., 2020). Using an Unmanned Aerial Vehicle (UAV) equipped with a thermal camera, Walker (2021) mapped the northwest coast of Guam to confirm locations of seeps and springs (initially mapped by Jenson *et al.,* 1999) to identify whether more exist. At Ayuyu Cave, where groundwater point discharge is highest, specific flight missions were conducted to observe the unique phenomenon. Imageries of the groundwater plume discharging from Ayuyu Cave were collected in summer 2019 during high tide and low tide conditions to characterize the behavior of the discharge (Walker, 2021). High resolution photos (courtesy of Walker) of the area above the cave were also collected using UAV in 2020. This was superimposed with the DEM in ARCGIS Pro to create the surface used in the 3D model of the cave.

3.2 Subsurface Karst Study

Ayuyu Cave fieldwork was undertaken in the summers of 2019 to 2021. The only means of travel to the study site is by boat. The requirements for suitable tide, surf, and weather conditions place tight restrictions on opportunities for safe and productive fieldwork. From March to June, surf and tide are calm enough to safely get to the entrance by either walking along the reef ledge or swimming straight in front of the cave. From July to December, wet weather, surf, and wind conditions are generally unfavorable for scheduling boat trips. Sometimes, even if getting to the study site is possible, rough surf can make the short swim from the boat to the entrance difficult to exhausting or even prohibitively dangerous, especially with equipment in tow.

3.2.1 Cave Exploration and Survey

To examine subsurface karst features and their relationship to surface karst features, one first needs an accurate cave map. Earlier map versions of Ayuyu Cave exist (Appendix 1), first drawn by Taborôsi and Plunkett (1999) and updated by Shalilian (2017); Both

mapped using the standard tape and compass survey method. Reconnaissance and later exploration of Ayuyu Cave for this study, reveals that the cave passage extends further than indicated in the earlier maps. Several unmapped rooms and a lower passage that leads to a water table pool have since been found from exploration undertaken in this work. Ayuyu Cave was resurveyed using digital cave survey tool, *Disto-X,* and tablet (Figure 3.3). Disto-X is a range finder specifically modified for cave surveys to measure distance, azimuth, and inclination. The Disto-X method uses the same survey principle as the classic tape and compass technique (See Dasher 1994). The digital method increases survey accuracy because more splay measurements can be taken with relative ease than are possible with the conventional method. Survey measurements were downloaded, stored, and processed in the *Topodroid* application in the tablet. Preliminary cave survey sketches were made onsite in Topodroid as well.

The next step was the conversion and migration of cave survey data to the desktop software, *Therion*, for final editing, drawing, and processing to create 2D and 3D cave maps. Several editing or processing platforms (e.g., Adobe Illustrator, ARCGIS Pro) were also utilized for georeferencing and creating DEM and rasters, which were later superimposed with the cave map. To create 3D cave maps, DEM resized to the extent of the cave were imported back to Topodroid. Relevant features inside the cave such as speleothems, cave pools, brecciated rocks, and fault diagnostic indicators were inventoried and characterized, and their locations accurately placed on the cave map created.

Figure 3.3. Digital cave survey tools (Disto-X and tablet) used to measure and map Ayuyu Cave.

3.2.2 Groundwater and Cave Conditions Baseline

To evaluate groundwater parameters, loggers were deployed in the bottom of the water table pool to measure conductivity, temperature, and depth (CTD) at 30-minute intervals (Figure 3.4a). The first set of CTD values was recorded from Sept. 28 to Dec. 12, 2019, when the pool was first discovered. Additional loggers became available later, which allowed measurement of atmospheric baseline conditions (e.g., temperature and pressure) in the cave, deployed at select chambers and passages (Figure 3.4c). More pool CTD measurements were collected from July 05, 2020, to Feb. 16, 2021, and Feb. 24, 2021 to Aug. 26, 2021. Water samples were synchronously collected at the water table pool and entrance (Figure3.4b) during specific trips to the cave. The water samples were analyzed for Ca, Mg, pH, total dissolved solids, and conductivity as additional baseline data. Whenever available, a multimeter tool was used to collect in-situ measurements as well. The collected water parameters are incidental data to our study.

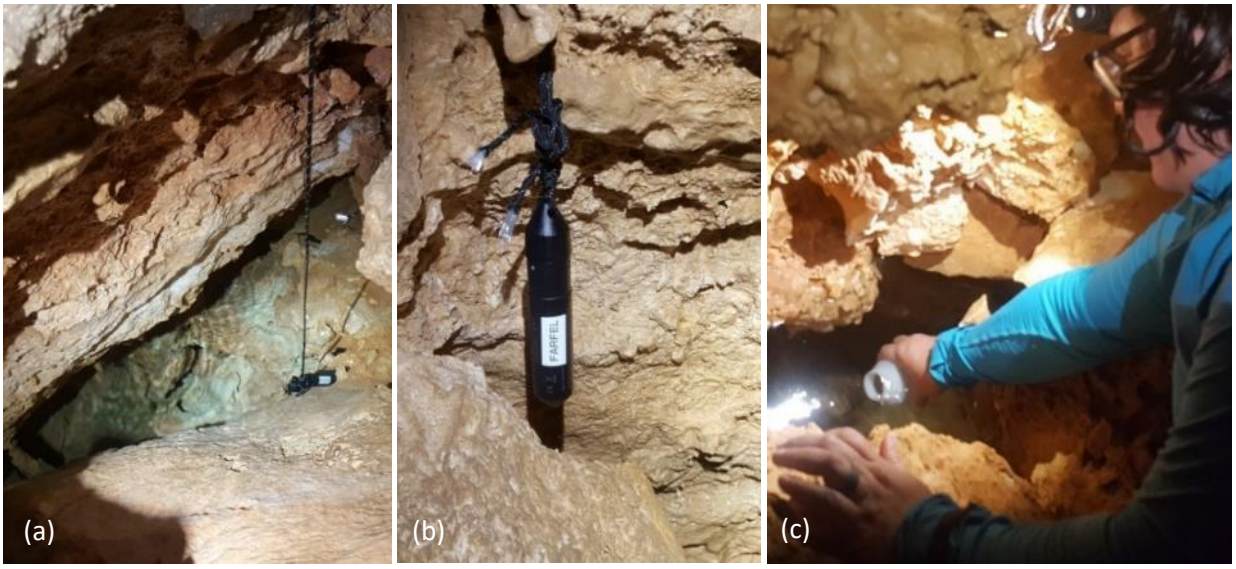

Figure 3.4. Hydrogeological characterization includes use of (a) CTD loggers to measure cave pool water parameters; (b) atmospheric temperature and pressure; and (c) water sampling.

3.2.3 Borehole Data Review

Based on borehole data logs, Taborośi (2006) observed that numerous wells encountered voids or cavities at depth suggesting the existence of subsurface horizons where conduits and cavities have preferentially developed. The subsurface evaluation of these wells is beyond the scope of this study, but it is prudent to cite this detail primarily due to the proximity of these subsurface features to Ayuyu Cave.

The programmed drilling of seven deep observation wells under the Groundwater Resources Program for the NGLA is timely for this research. The drilling program aims to expand the hydrologic monitoring, data collection, interpretation, trend analysis, groundwater modelling of the NGLA to promote sustainable management of the island's aquifer resource (USGS, 2016). Two of seven planned deep observation wells—NCSF-1 and NCSF-2—are located within and at the boundary of Finegayan Basin, respectively.

The drilling of the first well, NCSF-2, commenced in October 2021. NCSF-2 is located on the west flank of *Mataguac* Rise in an area that is both structurally and geomorphologically complex (Jenson, 2016). More importantly and why it is relevant to this research, NCSF-2 is straddled between the main Pugua Fault trace and its right splay (Figure 3.5). The well was programmed to be drilled to a depth of 585' to target past the freshwater-seawater transition zone. Borehole cuttings were collected by the drilling contractor at 5-foot intervals. Drilling reports and cuttings log were reviewed when available. Prior to the completion of the well, video logging done by the drilling contractor gave us a timely glimpse to the subsurface features within the structurally complex area of Pugua Fault. The information collected from the well provide real-time subsurface information but are incidental data as well.

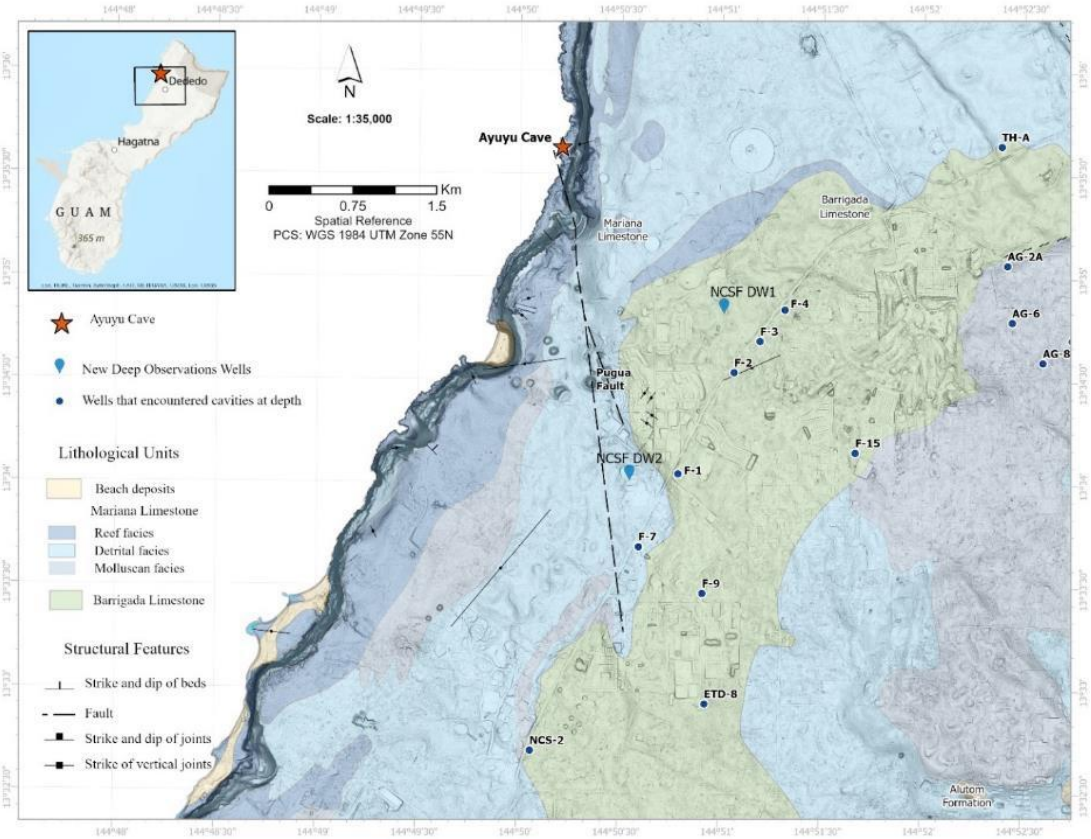

Figure 3.5. Location of wells that encountered voids/cavities and new observation wells–NCSF-1 and NCSF-2.

CHAPTER 4. RESULTS: MAPS OF *AYUYU* CAVE AND SURROUNDING GEOLOGY

Surrounding Surficial Geology: Geologic Context for Ayuyu Cave and Discharge

4.1 Surface Karst Landforms and Coastal Morphology

As stated in Chapter 2, the central objective of this research project was to determine and document the defining geological characteristics of Ayuyu Cave and their relationships to the coastal and submarine groundwater discharge associated with it. The first of the supporting objectives was to characterize the surface and subsurface karst morphologies. This chapter on the results of the project therefore begins with a description of the surrounding karst terrain, as determined, and mapped from remotely sensed data as well as field survey. After presenting maps of the surface features that are likely to determine the properties of the cave, the rest of the chapter presents the map of Ayuyu Cave built from our field survey and describes in detail features of the cave that are relevant to its origin and hydrogeologic characteristics.

Karst spring systems, such as the Ayuyu Cave system are formed by freshwater dissolution of a limestone surface catchment and the underground drainage network to which it is linked. Dissolution of the surface shapes it into a distinct karst landscape characterized by *karrenfeld* and *sinkhol*es. Over geologic time, these surface features become increasingly integrated into an increasingly efficient underground drainage network. The underground network consists of dissolution-widened fractures interconnected with linear cave conduits that are enlarged and extended by dissolution. Tributary conduits converge on a trunk that delivers the system discharge to a spring at the aquifer base level, which for an island aquifer is sea level. Karren is a deeply etched surface in soluble rock composed of simple to complex patterns of dissolutionally sculptured grooves or furrows, or pits, mounds, and pinnacles (Verress, 2020, Taborôsi *et al.,* 2003). In eogenetic limestones such as those that cover northern Guam, a uniquely rugged karren landscape (Figure 4.1a) develops from the diagenetically immature rock and the combined effects of their proximity to the ocean, autogenic recharge, and tropical climate (Taborôsi *et al.* 2004). Karren of carbonate island karst is characterized by solution pits up to a few meters deep, enclosed by sharp rims, with jagged pinnacles up to a few meters tall standing on the rims between adjacent the pits. The terrain is extremely rough and well drained. Even the most intense rainfall, such as from tropical cyclones, produces no runoff or ponding on the karrenfeld of island karst. In general, surface water does not accumulate and remain at the surface for long on the natural terrains, but and instead infiltrates rapidly into the weathered epikarst. Rainwater from low to moderate intensity percolates readily through the open matrix. Water from high-intensity storms is shunted into shafts and open fractures by which enters directly into subsurface drainage networks of the aquifer.

The term, “sinkhole” refers to any closed-contour depression on karst terrain formed by either of two processes: 1) *collapse sinkholes*, formed by mechanical collapse of rock into an underlying cavity, or 2) *solution dolines* formed by chemical dissolution and erosion of rock from the surface downward. On the northern Guam plateau, solution dolines are by far the most common.

The general morphology of the coastal area results from the combined effects of dissolution and erosion, enhanced locally where freshwater and saltwater mix. Sea arches, fracture caves and coastal tidal notches are the most common geomorphic features on the northwest coast. The sea arches are developed by erosion from constant wave and tide action (Figure 4.2b). Where there is structural weakness in the formation, fracture caves develop which also become preferential pathways for concentrated groundwater discharge towards the coast. Examples of fracture caves in the NW coast are No-Can (Figure 4.2c) and *Menpachi* fractures located north of Ayuyu Cave. Another important coastal feature is the tidal notch (Figure 4.2d), which indicate present and past mean sea levels. The modern notch is incised at 0.4 to 0.8m above the modern mean sea level (Miklavič, 2011) while the mid-Holocene notch is at 2-4m higher. Fracture cave without notch incision would be younger than Mid-Holocene (Taborosi *et al.,* 2013). Aside from notches, flank margin caves can also indicate past sea level positions.

4.1.1 Linear features interpreted using LiDAR

Although, as noted in the methods section our re-examination of the structural geology of the study area was not rigorous and exhaustive, it supports some important revisions, additions, and refinements of the structural geology of the study area, and yields some new insights into the hydrogeology, in addition to pointing the way toward promising new lines of research. The most important result from our reinterpretation of Pugua Fault, for example, is that the fault is not continuous but is instead comprised of several short segments along the same general N-S strike. On the geologic map of Guam (Siegrist and Randall, 2008, after Tracey *et al*., 1964), Pugua Fault is interpreted as a normal fault downthrown to the southwest. Our interpretation of Pugua Fault is that it is a strike-slip fault with an extensional component. Pugua Fault oversteps twice to the left, creating extensional bends in between. Although it is possible that differential weathering in the highly soluble karst surface creates the apparent segmentation, we suspect that the segmentation is from the overstepping of Pugua Fault.

The implications to surface hydrology of the new interpretations of Pugua Fault will be discussed in Chapter 5. Numerous lineaments cross-cutting Pugua Fault were delineated as well. After the lineaments were delineated, a linear density map was created using

ArcGIS Pro to visualize potential fracture density (Figure 4.3). The northern end of Pugua Fault towards the Ayuyu Cave is one of the three areas that have dense lineament and potentially high fracture density.

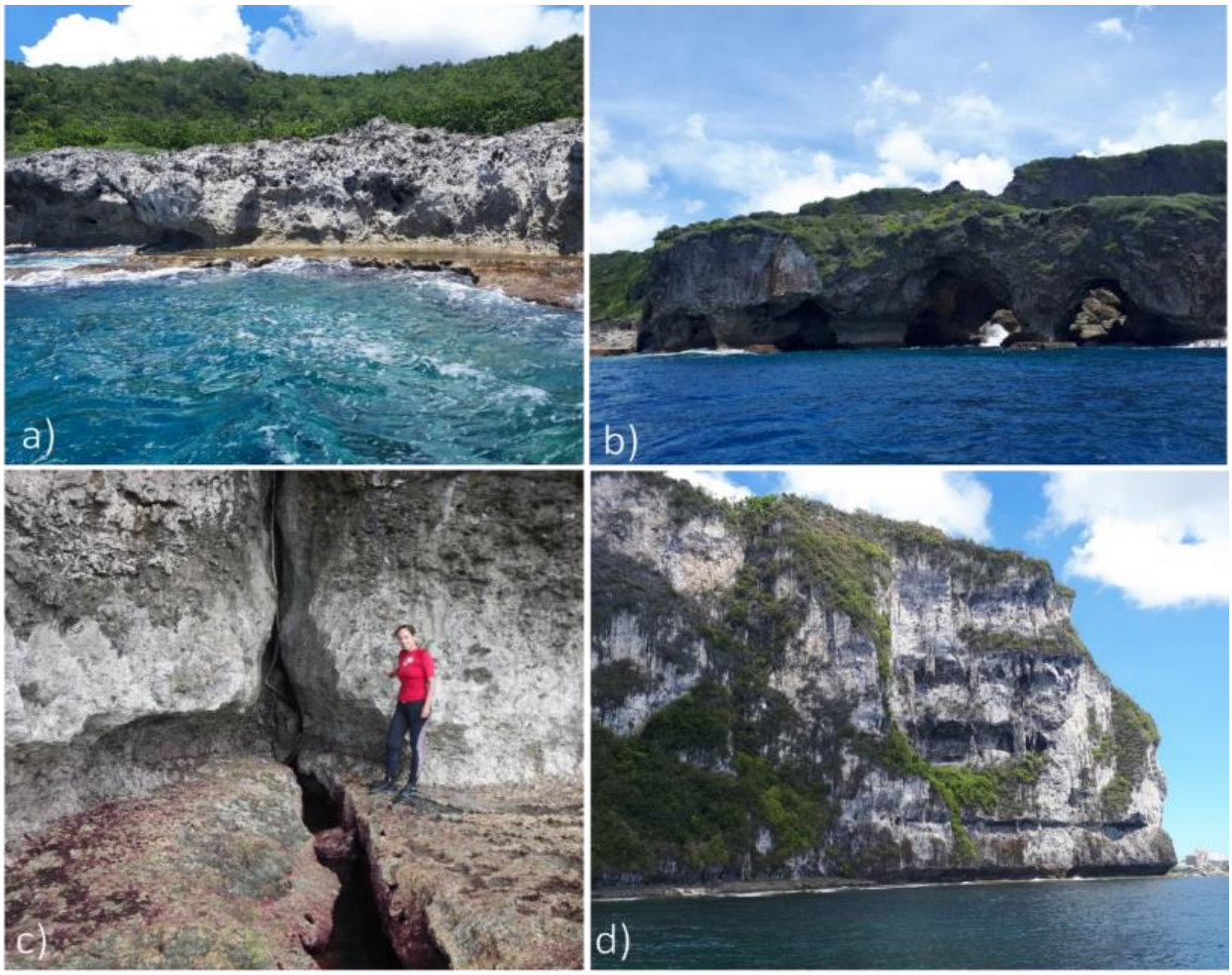

Figure 4.1. Coastal karst features and surface landforms in NW Guam a) Karren feature in young carbonate island karst such as Guam; b) Sea arches developed by erosion from wave and tide action; c) No Can Fracture Cave, d) Lateral cliff-face notches reflect past sea level still stands.

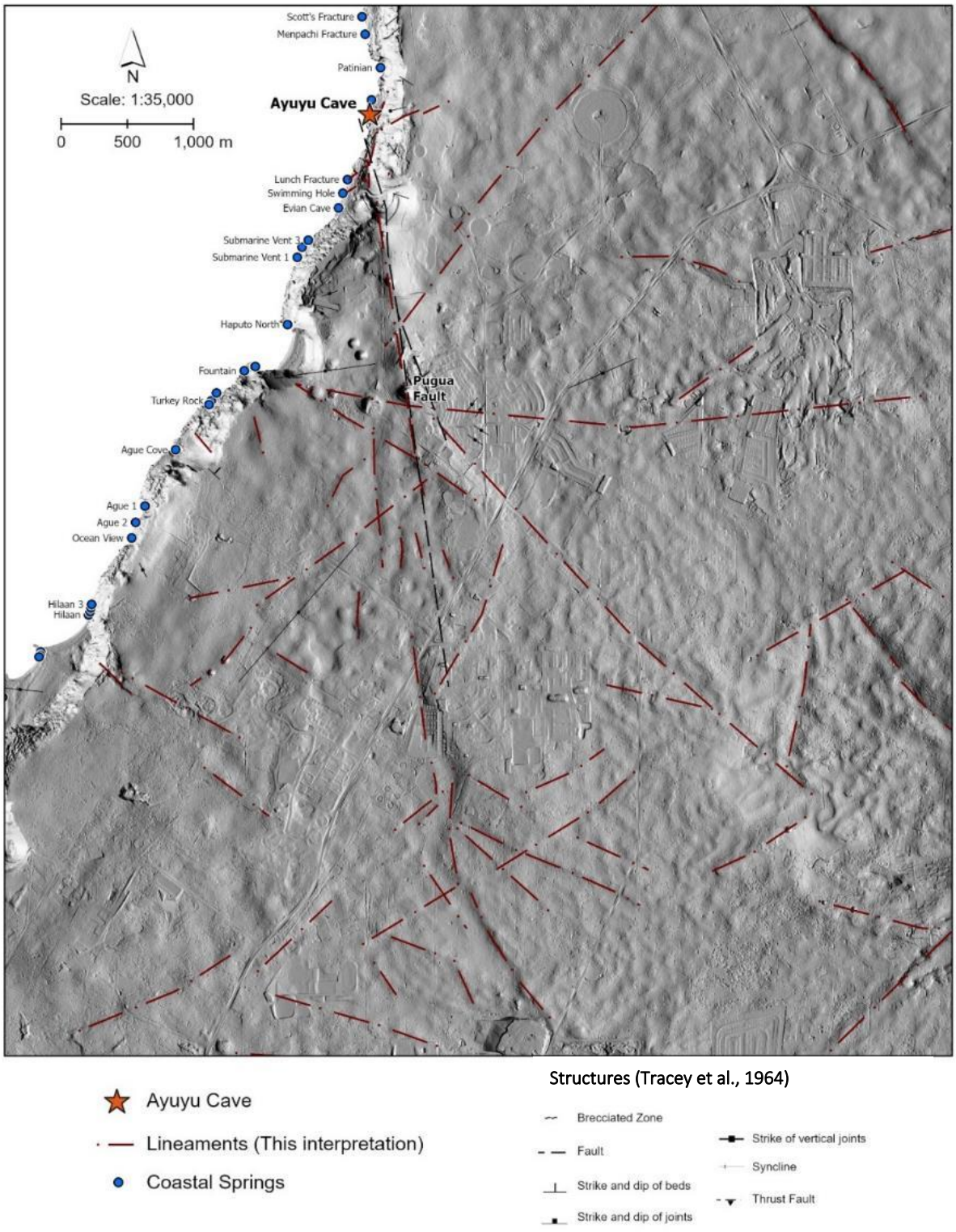

Figure 4.2. Lineaments interpreted from various raster surfaces

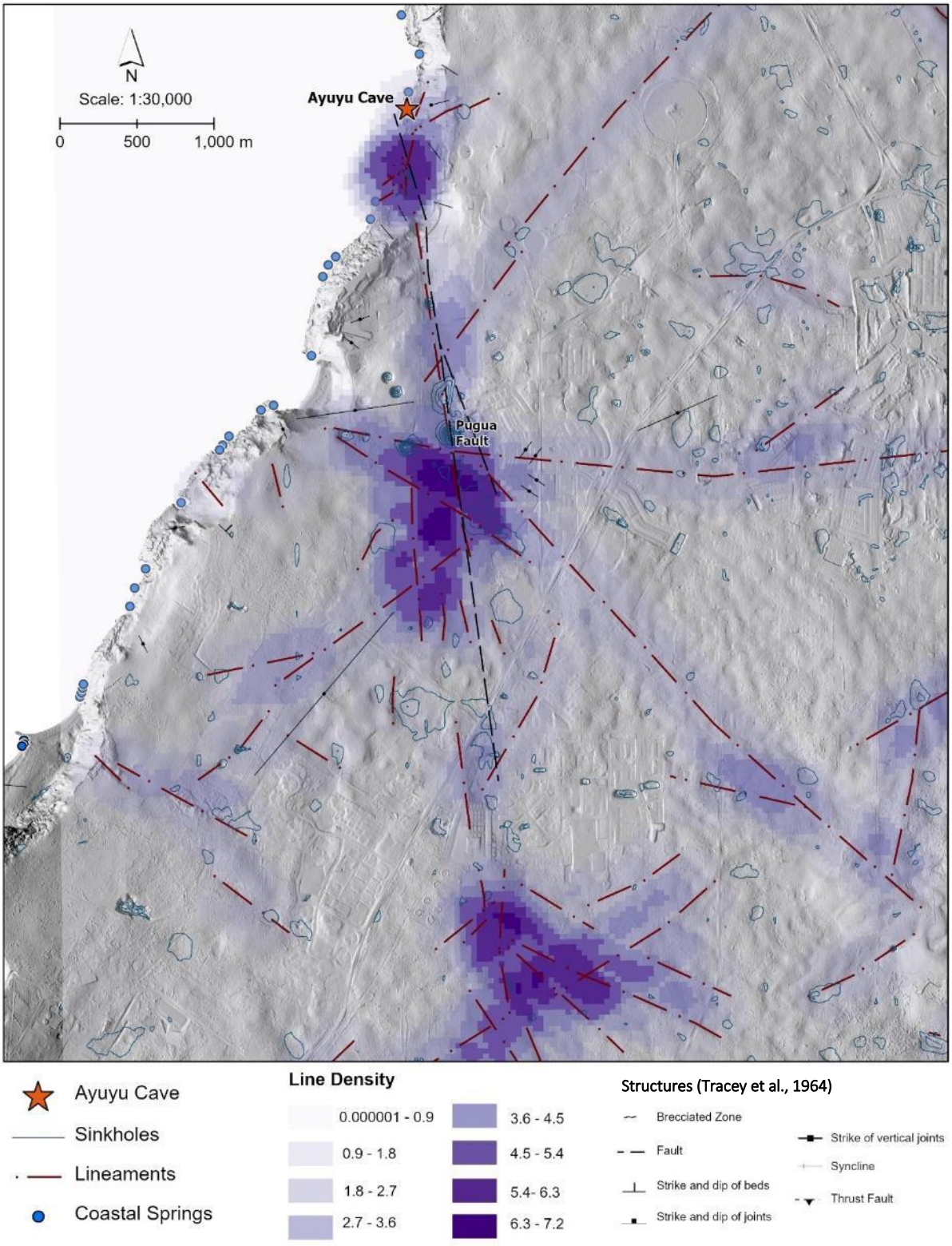

Figure 4.3. Lineament density map of retraced structures in study area.

4.1.2 Closed topographic depressions along Pugua Fault

This study builds directly on Shalilian (2017), including the application of advanced methods and new tools for comprehensive, detailed, and high-resolution mapping and geospatial analysis of Ayuyu Cave and related features in the study area. Closed topographic depressions were derived from DEM using simple hydrology geoprocessing functions – Fill and Sink, built into the ARCGIS Pro software. A preliminary sinkhole map (Figure 4.4) was created, still as part of characterizing the karst surface.

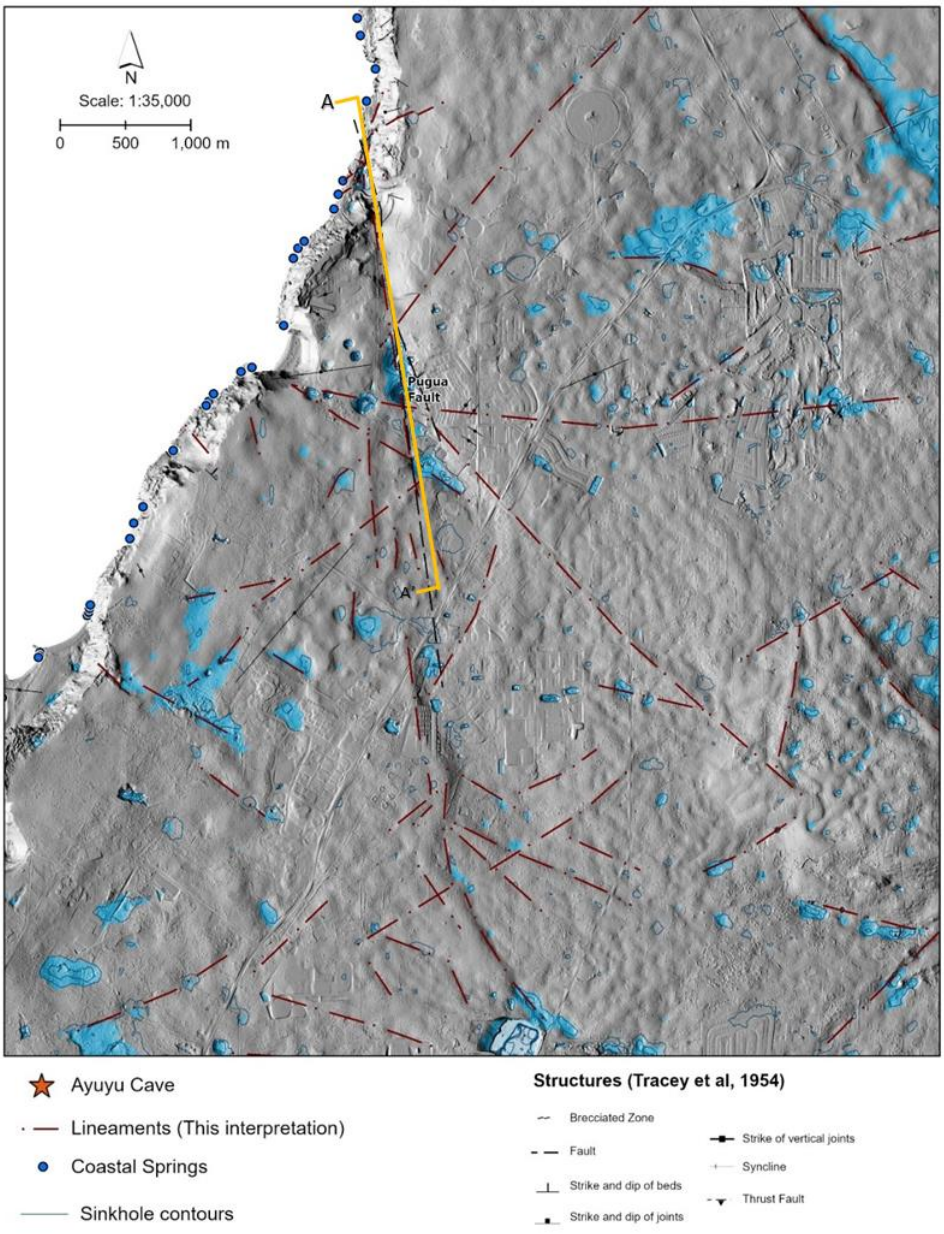

Figure 4.4. Preliminary sinkhole map and interpreted lineaments

The distribution of the sinkholes at first glance, illustrates a somewhat random and haphazard distributions. But when correlated to the interpreted linear features (Figure 4.3), patterns emerged, and our interpretations are described here. Several sinkholes were visibly strewn within the fracture network of Pugua Fault especially where lineaments intersect. Recent work on the sinkhole features and properties of the study area, Shalilian (2017) noted that fractures and fault traces in Finegayan Basin are associated with sets of aligned circular closed depressions. The section profile along Pugua Fault illustrates this (Figure 4.5). Several sinkholes were identified in LiDAR imagery along the 4369-m extent of the NNW-trending Pugua Fault. The most notable is a large, elongated sinkhole along the coastal end of the fault that Shalilian (2017) named the *Pugua Sink* (Figure 4.6). At its deepest point, *Pugua* Sink contains a cenote where the thin water lens is exposed to the surface and responds to the rise and fall of tide.

Also, at extensional segments associated with the overstepping of Pugua Fault and where lineaments intersect, are nestling complex and elongated sinkholes. In contrast, at compressional bends, there are few to no sinkholes.

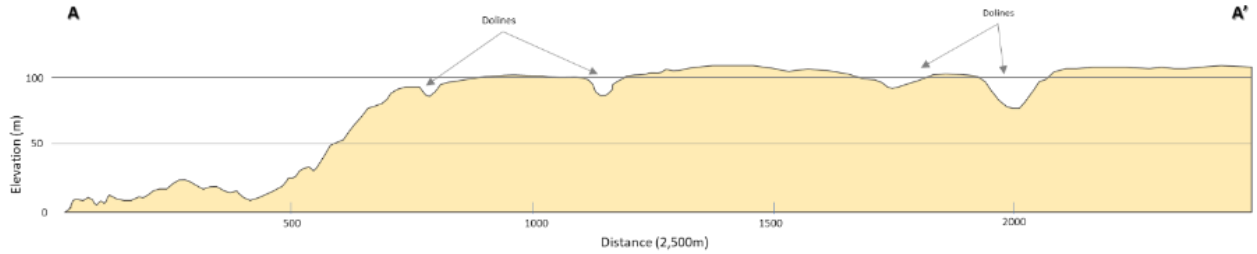

Figure 4.5. Elevation profile (A-A') showing sinkholes aligned along the strike of Pugua Fault.

4.1.3 Field Observations of Surface Karst features and Pugua Fault

Karren and sinkhole features documented by Shalilian (2017) in her study of the hydrogeology of Finegayan basin provided the groundwork of this research since we are unable to conduct fieldwork in the areas above the cave. Perhaps the most significant surface features identified in Shalilian's (2017) work is the *Pugua Sink*, an elongate sinkhole along the strike of Pugua Fault which has a small cenote in its deepest point (Figure 4.6a). The water table is intersected in the cenote, observed to rise and fall with tide. Figure 4.6b is the view looking north to Ayuyu Cave photographed in one of Shalilian's (2017) field surveys of areas above the cave.

Figure 4.6. Relevant karst and fault features observed in the field by previous worker, a) Cenote in the deep end of Pugua sink (Photo by John Jenson); *b) View* overlooking the NW coast (Photo by John Jenson).

4.2 Cave Exploration and Survey Mapping

As noted in the previous section, the cave network in the subsurface is linked with surface features to form a single integrated hydrogeologic system. Cave development is thus linked to surface geomorphic evolution. Morphological features in caves, however, include depositional features (e.g., speleothems) which are more likely to be preserved than landform features at the surface where dissolution and weathering are dominant. The study of caves thus can provide well preserved clues of historical events and processes operating at local scale (e.g., paleoclimatic changes), and their correlation with events and processes operating at a regional scale (e.g., eustatic sea level changes, tectonic uplift, and subsidence).

Our recent explorations in Ayuyu Cave reveal new information and important hydrogeological, speleogenetic and structural features in the cave. We discovered previously unmapped tiered passages, upper-level rooms, and speleothems that reflect past hydrogeologic and sea level conditions. Cave features were inventoried based on what hydrogeologic conditions they likely reflected. The Water Table Pool at the end of the cave was one highlight of our discoveries. Several breakdown rooms, fracture chimneys and fissure passages were mapped as well, reinforcing the hypothesis that

Ayuyu Cave patterns are guided by structures. As we found more structural features in the cave, the complexity of Ayuyu Cave became more apparent.

A total of 43 stations were surveyed in Ayuyu Cave. The linear extent of the cave itself is limited, only about 65 m from station 0 at the entrance to the last survey point at Station 16 at the water-table pool. There are several side and upper-level passages which adds up to the total survey length of 184.4 m. Survey data are compiled and summarized in Appendix 3. Cave passage altitudes range from -0.9 m at its deepest portion to 7.3 m at its highest, or a total depth of 8.2 m. The conservative volume estimate of Ayuyu Cave based on rendered 3D maps is 3486 m^3. Ayuyu Cave profile showing surface above is attached as Appendix 4. The map (Figure 4.7) and profile (Figure 4.8) of Ayuyu Cave was made using cave mapping softwares – *Topodroid* and *Therion*.

4.3 Cave Rooms and Passages

At first glance of the cave map and profile (Figures 4.7 and 4.8), three striking observations comes to mind – first is the basic linearity of the 65-m-long cave system; second, the WSW orientation of the 65-m axis of the system—exactly perpendicular to the WNW orientation of the Pugua Fault; and third, the disproportionately wide and relatively equidimensional size of the initial room that opens onto the coast (Figure 4.9). As alluded to earlier and to be discussed in detail later, these properties reflect affinities with flank margin cave model at the room behind the mouth of the cave (proximal end of the cave), but with the linear passage type of cave for the remaining portion extending to the distal end of the cave. The perpendicular orientation of the cave relative to the orientation of Pugua Fault indicates a more complex pattern of flow than simple linear flow along the general axis of the fault as mapped by Tracey *et al.* (1964).

Passage length, or cave development, as applied in standard speleological mapping, is a defining parameter of caves, and is conventionally interpreted as the length of flow that formed the passage (Klimchouk, 2000). The complexity of this cave, however, precludes simple, straightforward application of such parameters. Although there is at the latest estimate 2.3 MGD of discharge at the mouth of the cave, the distal passageway arches above the water table, and there is no flowing water in the distal passageway. In the distal end of the cave, the passageway intercepts the water table in a pool, which this study is the first to document (Figure 4.7).

Ayuyu Cave Map

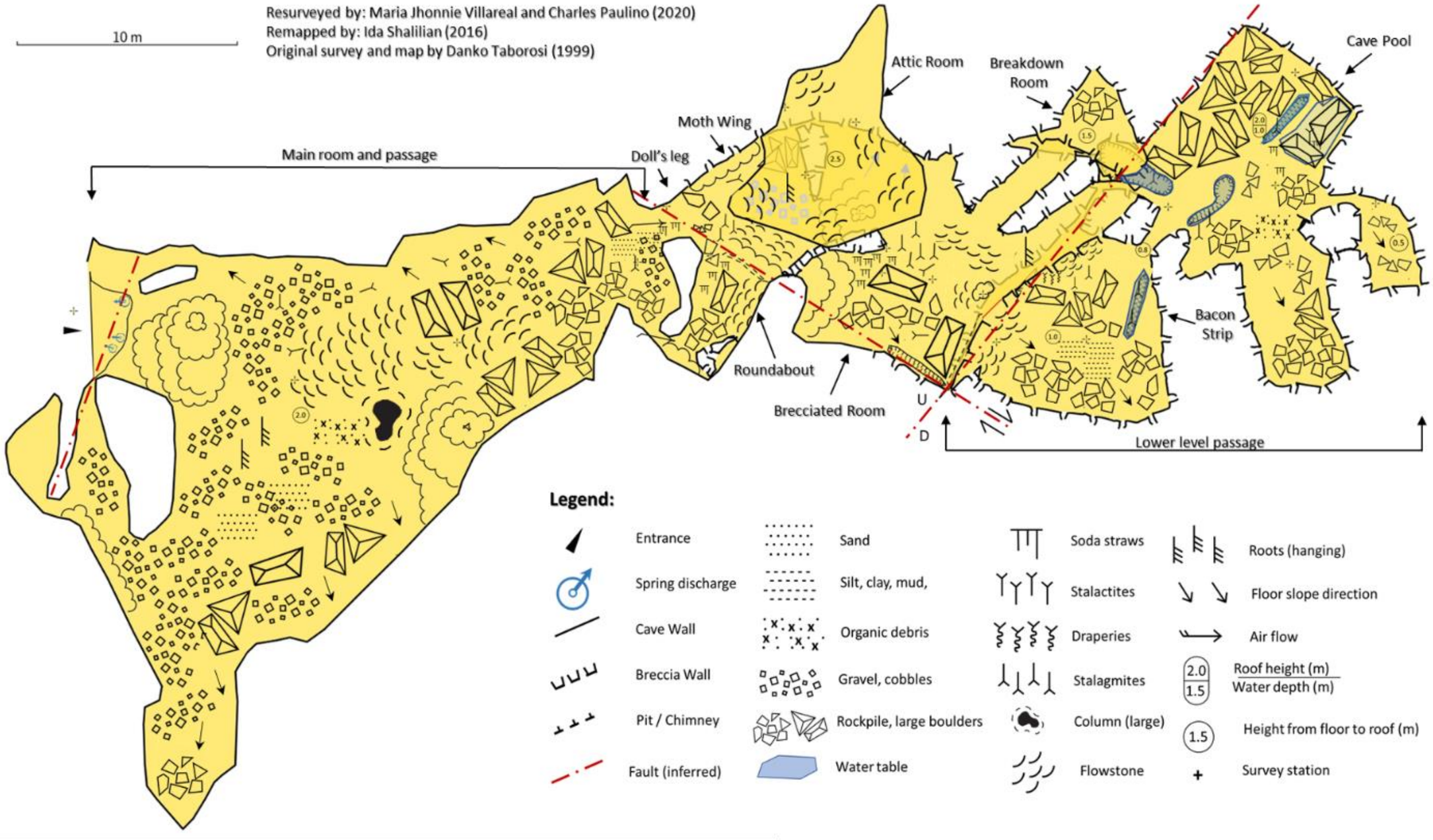

Figure 4.7. Map of Ayuyu Cave

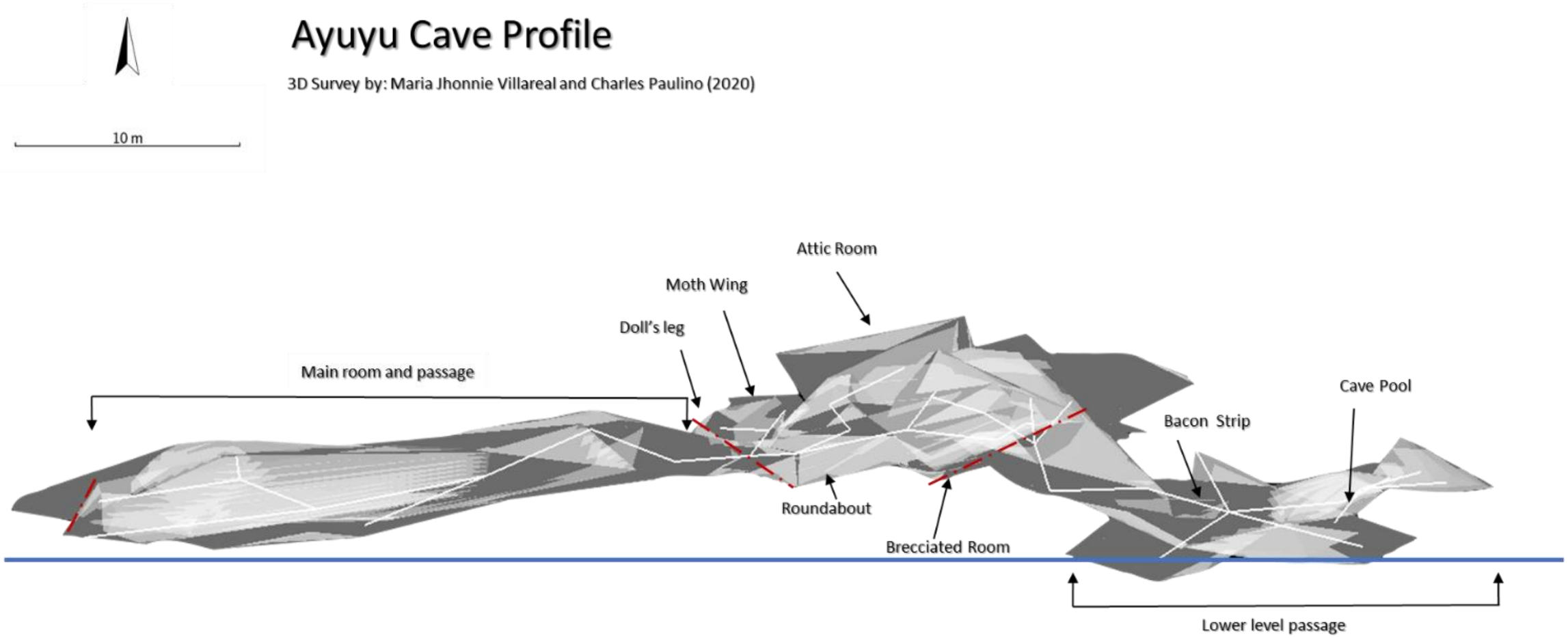

Figure 4.8. Ayuyu Cave Profile

Caves formed by linear passageways are generally categorized by passage cross-sectional morphology as either *vadose*, *phreatic* or *breakdown* (Ford and Williams, 2007). Given the coastal location of Ayuyu Cave, it is expected that tide and surf also contribute to the hydrogeological properties of the cave. To add further complexity, tide and surf conditions have varied over geologic time, with eustatic and tectonic changes in relative sea levels.

Vadose passages are only partially filled with water, such that flow in them is essentially open-channel flow. They tend to have steep gradients and canyon-shaped cross-sections, reflecting their having formed above the water table. Unless they are occasionally flooded, various kinds of speleothem (e.g., draperies, soda straw) typically develop in vadose conditions.

Where water fills the passageway entirely, the condition is said to be *phreatic*. Phreatic cave passages are formed only below base level, which for coastal systems means below sea level. Phreatic passages typically have gentle gradients, are tubular in shape, with near-circular cross-sections. *Breakdown* passages or chambers generally contain sharp or blocky clasts and are primarily structural in origin but can also be caused by collapse from withdrawal of water. Single provenance caves are relatively easy to identify, however, mature karst systems usually develop a combination of these cave morphology types (Klimchouk *et al.,* 2000).

Ayuyu Cave is a complex, multi-stage karst system, in which various portions of the cave exhibit affinities with each of the models described above and the entire cave has undergone episodes of prolonged emergent vadose conditions alternated with occasional episodes of submergent phreatic conditions. Areas of the caves are sectioned and classified (Figure 4.7, Figure 4.8, and Table 4.1) based on their morphological features and associated speleogenetic conditions. Summarized in Table 4.1 are the room and passages in Ayuyu Cave and their hydrogeologic and morphologic controls**.** In the sections that follow, the relevant observations are described for each of the distinct portions of passage, beginning with the entrance and progressing to the distal (inland) end of the cave.

Table 4.1. Rooms and passage in Ayuyu Cave and their hydro-morphologic control

Cave Area	Extent	Morphologic Control		Summary of features
		Present	Past	
Entrance		TS	P, SL	Scarped dripline, ~1.5m ledge; huge volume spring discharge; vaulted or half domed conduit entrance suspected formed under phreatic conditions. Trash and plant debris brought in by surf
Main room and passage	Entrance to Doll's Leg	TS, V	V, SL, B, P	Cave floor covered in rounded cobble-sized rock fragments and coral heads with occasional breakdown boulders. Overall morphology indicates a past flank margin affinity even phreatic, but at present more influenced by tide, surf, and vadose recharge. Degraded and broken speleothems
Moth Wing Room	After Doll's Leg and before Ayuyu passage	B, V	SL, P, V	Separated from the main room and passage through the Doll's Leg squeeze. Air draft at the Doll's Leg. Floor is covered with angular rock fragments and broken stalactites
Roundabout	Looping passage loop to the Doll's Leg.	V, B	V, B	Intermediary room between Doll's Leg and Upper-level room. Connected to the Attic room through a fracture chimney.
Ayuyu Corridor	Passage between Moth Wing Room and Brecciated Room	V	SL	Gently sloped flowstone dipping to the NW between the Moth Wing Room and Brecciated Room; Abundant soda straws that become active after heavy rain.
Attic Room	Upper-level room above Moth Wing Room and Ayuyu passage	V	B	Abundant dripstones and flowstones, main access at Moth Wing Room, connected to the lower-level room roundabout through a fracture chimney and to the top of Ayuyu corridor through a small squeeze.
Brecciated Room	Big room after Ayuyu Corridor	V	B	Massive complex stalagmites, some of which are buried by huge ceiling boulder breakdowns. Abundant soda straws that become active after heavy rain.
Lower-level passage	After Brecciated Room	B, V, SL	SL, P, V	Blocky, low ceiling passage predominantly breakdown materials, very active dripping after heavy rain, degraded draperies, half submerged stalagmites,
Cave Pool Breakdown Room	Above left of cave pool passage	B, V	B	Small room bounded by boulder breakdowns, intermittent drips
Water table pool		P, B, TS, V, SL	SL, P, V	Rises and falls with tide. Submerged speleothems and breakdown materials, Aggressive dissolution at the water-air interface

Key: V = Vadose, P = Phreatic, B = Breakdown, S = Structural SL = Sea level changes, TS = Tide and surf

4.3.1 Entrance

Ayuyu Cave has a single entrance, opening at sea level above a reef flat (Figure 4.9a-c). The height of the entrance is at the same level as the base of the tidal notch formed during the mid-Holocene when sea level was at least 2-4 m above present. At the entrance, the cave floor rises at least 1 m to 1.5 m from the reef flat, which requires stepping up a rock ledge to enter the cave. At the base of the rock ledge are cavities and conduits where laminar to turbulent groundwater discharges along the bottom horizontal interface (Figure 4.9d). This unique discharge mode is best observed during negative low tides.

The dripline overhang at the entrance is noticeably scarped, striking N15^{o}E, dipping near vertical to the NNW (Figure 4.9b). Although we looked for indicators of movement and shearing along the face of the scarp, the presence or absence of slickensides on the scarped surface cannot be confidently determined due to the extensive dissolution and weathering of the rock face. Crosscutting and conjugate fracture sets are present to the right of the entrance (Figure 4.9c), deeply indented on the limestone. In front of the cave is a large boulder that serves as location marker of the entrance (Figure 4.9e). It is suspected that the boulder is breached material that might have been part of the platform in front of the cave. On satellite image, the boulder looks like a puzzle piece that fits right into the breached cave entrance. The top of the boulder exhibits a dissolution texture typical of microkarren. The sides of the boulder also exhibit a tidal notch noticeably tilted which suggests even more that the boulder was displaced to its present location.

4.3.2 Main room and passage

The main room and passage are the longest section (25m) in the cave, beginning at the big room by the entrance with slight meanders heading northeast to the Doll's Leg (Figure 4.10a). The main room and passage display the hydrogeological influence of the presently predominant vadose and tide-surf environment while maintaining features diagnostic of a past phreatic environment as well as tectonic or water-withdrawal induced breakdowns. This section of the cave is well exposed to and strongly affected by tide, surf, and storm-induced waves, as attested by the abundance of plant materials and lightweight trash (e.g., water bottles, slippers, buoys) that have accumulated in the main room (Figure 4.10b). Plant materials and lightweight trash (which float in water) are brought in when the surf is high enough to go above and past the ~1.5m ledge at the entrance. The floor of the main room and passage is covered in rounded cobble-sized rock fragments and coral heads (Figure 4.10a). These are most probably eroded materials from the cave walls and ceiling itself. Their abundance and the uniform degree of roundness suggests these cobble-sized rocks have accumulated over time and are repeatedly rounded in place by high-energy water such as wrought by storms.

There are occasional stalagmites—indicative of extended quiescent periods of vadose conditions without exposure to the intrusion of surf—in the main room and passage, albeit broken or toppled, and already reworked with the other sediments and trash in this section (Figure 4.10c). The main passage exhibits features consistent with vadose evolution overprinted by occasional phreatic conditions, including freshwater phreatic, i.e., flank margin, conditions. There are several clues that point to this. The presence of massive stalagmites is evidence that vadose activity has been more isolated from coastal processes than at present. Flowstones draping the walls to the floor also support this interpretation.

The flank margin affinities of this section of the cave are also apparent. Stalagmites and flowstones in this section are smoothed and show modification which might be expected if they have been partially submerged in freshwater after their formation. For example, the tallest stalagmite in the main room was found to be hollowed at the base (Figure 4.11). Freshwater-saltwater mixing would be capable of such rapid and localized dissolution. Another feature of the cave that indicate its flank margin affinity can be demonstrated in profile of this section of the cave. The profile of the main room and passage is lenticular gently dipping to the north. This thinned out lateral horizon beneath all the rubble and sediments is inferred as a dissolution horizon attributed to the Mid-Holocene Sea level. Another indicator of phreatic conditions is the semi-arched entrance (Figure 4.9b), which reflects the sphericity diagnostic of flank margin caves.

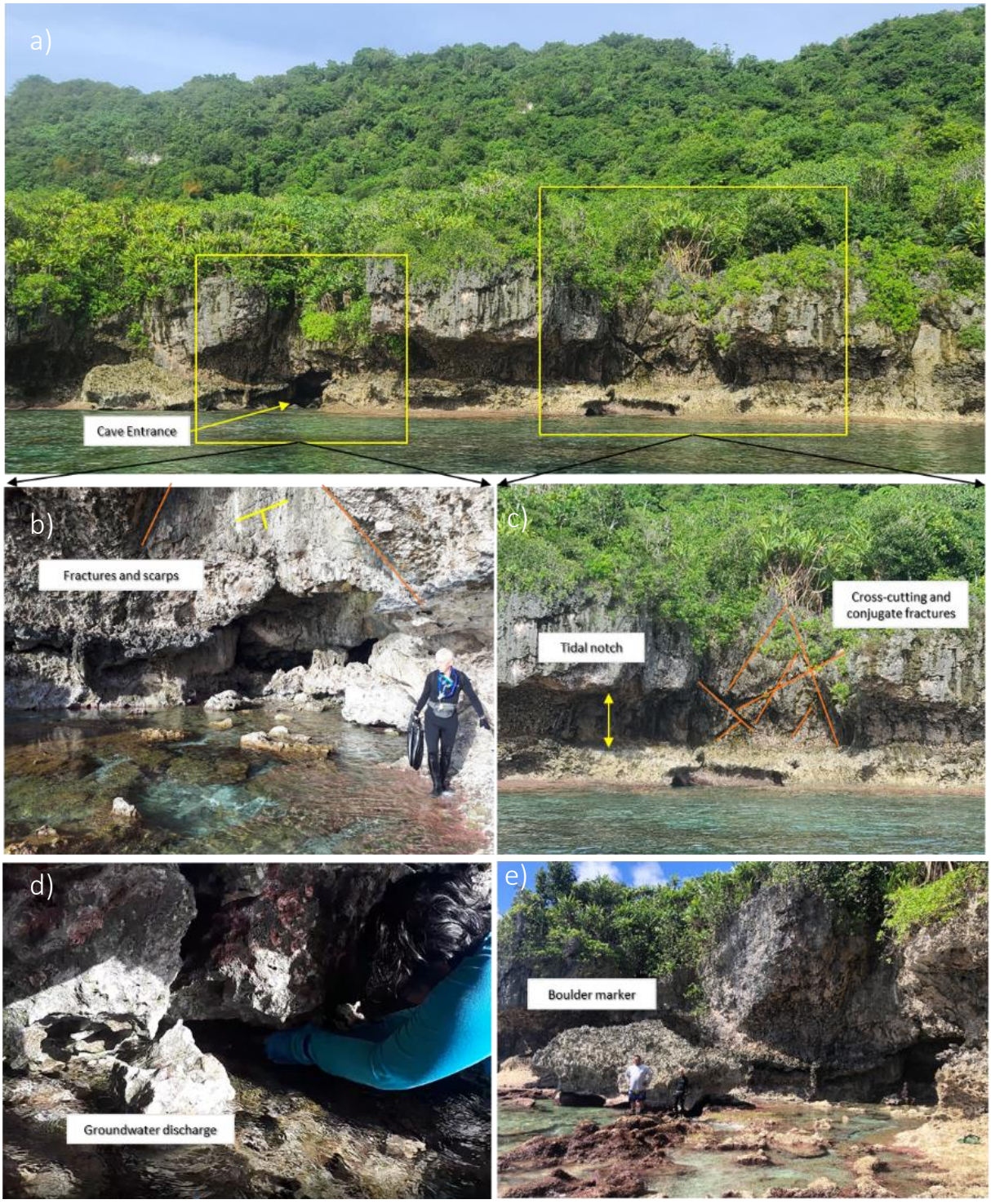

Figure 4.9. Geological features at study site a) Ayuyu Cave entrance showing tidal notches. b) Scarped overhang and ledge at entrance, c) Cross-cutting and conjugate fractures on rock face; d) Groundwater discharge at base of ledge; e) Boulder location marker in front of cave possibly breached platform material.

Figure 4.10. The main room and passage are predominantly exposed to the effects of tide, surf, and storm surge a) Rounded cobbles and shell fragments near the cave entrance b) All sort of debris brought in by the sea; c) High-energy storm surges can rework the sediments in the cave and quite possibly topple stalagmites.

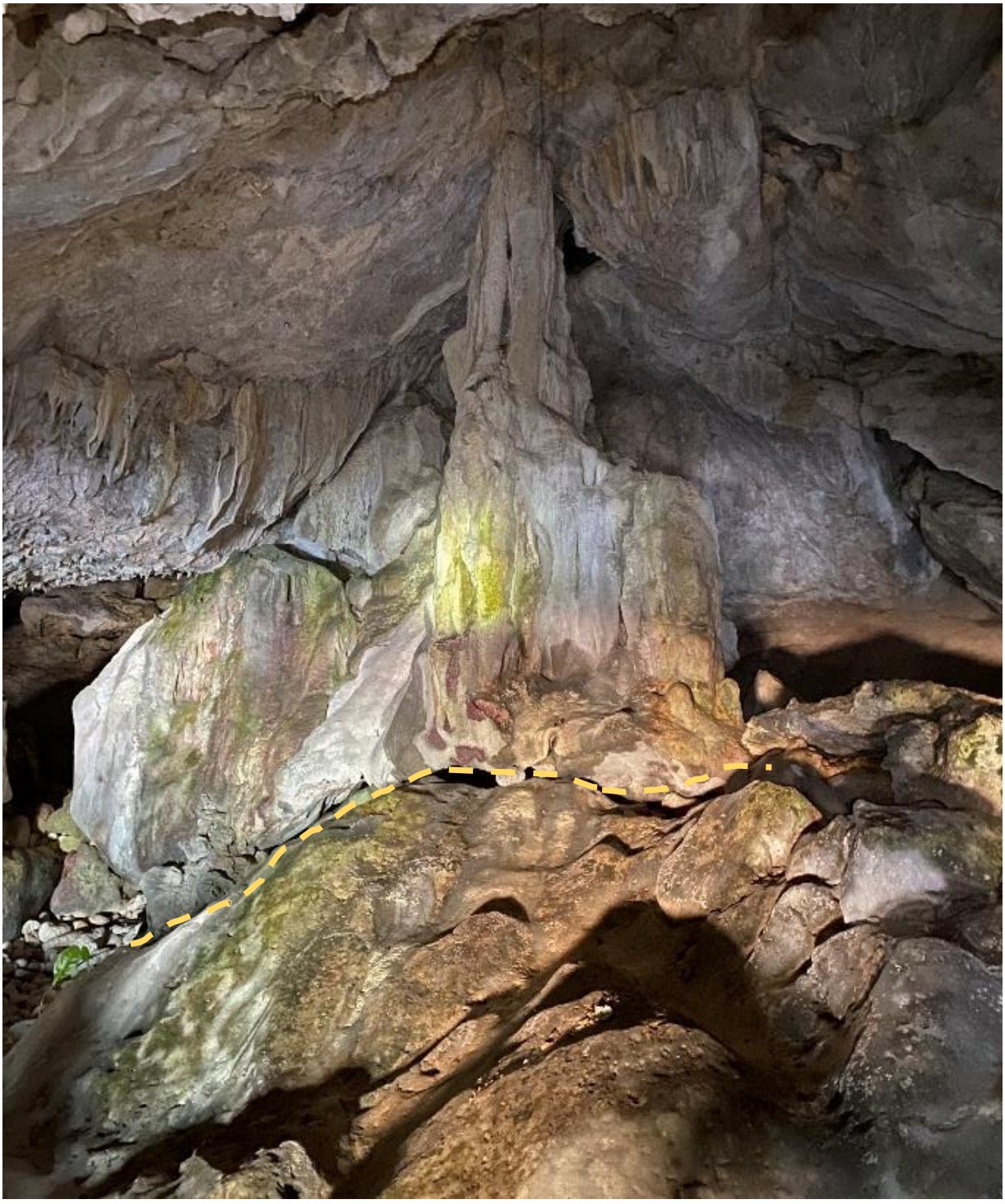

Figure 4.11. Complex stalagmite-flowstone that have been hollowed and detached at base.

4.3.3 Moth Wing Room

The Moth Wing Room is the central station of Ayuyu Cave because most cave sections can be accessed from here. The main access to the upper-level, Attic Room is by the north side through a pile of boulders. The passage to the Brecciated Room that leads to the rest of the cave is by the northeast side through Ayuyu Corridor.

The Moth Wing Room is separated from the main room and passage by the Doll's Leg (Figure 4.12a). The Doll's Leg is a tight crawl space through a fractured flowstone formation (Figure 4.12b). After the tight squeeze, the room opens to the Moth Wing Room. The cave is ventilated here. When crawling out from the Moth Wing Room on the way out, a strong and steady draft of air frequently gushes through the Doll's Leg. The floor cover in the Moth Wing Room is predominantly angular rock fragments and broken stalactites. This sharp contrast of angular floor sediments versus the rounded cobbles in the main room is one criterion for identifying the Moth Wing Room as a separate section.

Stalagmite morphologies in the Moth Wing Room are varied, consisting of the clustered, stumpy stalagmites by the Doll's Leg; flat-topped ones towards the Ayuyu Corridor; and the lone, massive, toppled stalagmite by the NNE wall. The toppled stalagmite is a significant clue that the ceiling has dropped at various sections of the cave, which could only be tectonic in nature (Figure 4.12e). If the stalagmite were to be raised back up, there would not be enough ceiling clearance to do so. The stalactite that fed dripwater to this massive stalagmite is nowhere to be found; pieces of it are possibly part of the floor sediments by now. Another feature that supports structural control in the Moth Wing Room section is the discovery of the *Roundabout Room*, intermediary between the Doll's Leg and the Attic Room (Figure 4.12d). The Roundabout Room we found is connected to the Attic Room through a narrow fracture chimney (Figure 4.12f).

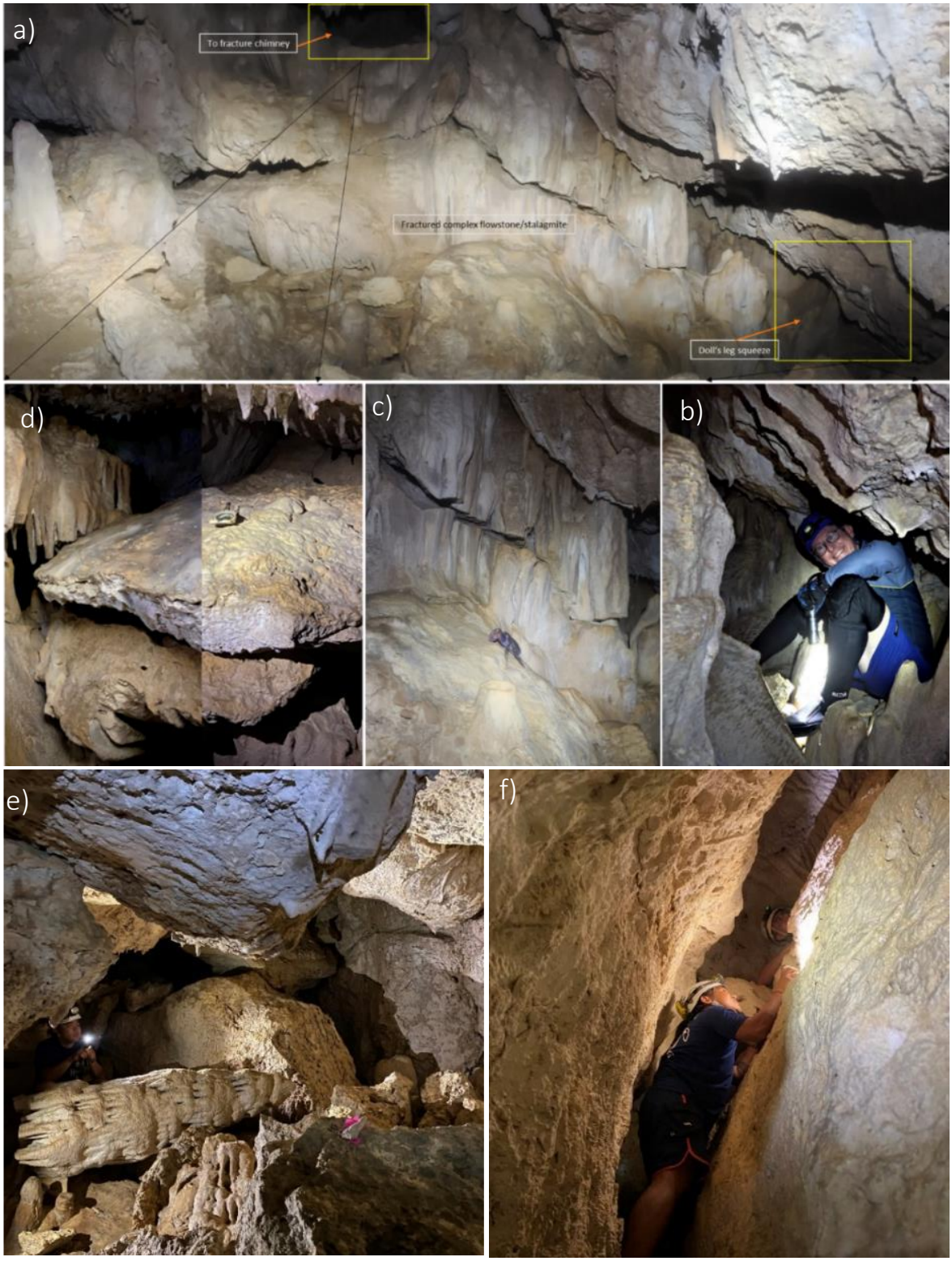

Figure 4.12. Structural features in Moth wing. a) Southwest wall of the Moth wing. b) Boulder piles and active speleothems in the Roundabout room. c) Doll's leg tight crawl-space d) Fracture damage on the southeast wall formation. e) Toppled stalagmite. f) Fracture chimney connecting the Roundabout and Attic rooms

Figure 4.13. Attic Room vadose depositional features a) Profuse soda straw and stalagmite b) Roots from plants above the cave can reach the cave 5 m below through fractures. c) Persistent growth of stalagmite even when its base support is gone.

4.3.4 Brecciated Room

The Brecciated Room (Figure 4.14a) is the most distal passage mapped in previous surveys (specifically, Shalilian, 2017) of Ayuyu Cave. It is slightly lower in elevation than the Attic Room, which makes it the second highest room. The cave roof-to-surface thickness above it is at least 6 m. Their co-positioning implies that the Brecciated Room and Attic Room have similar histories and properties, and this is evident. The Brecciated Room contains massive, and complex stalagmites, some of the biggest in the cave (Figure 4.14b). Soda straws and small stalactites on the ceiling are profuse and actively drip after a heavy rain.

Despite their similarities, the Brecciated Room is unique from the Attic Room in terms of its palpable breakdown features, which are not found in the Attic Room. One striking type of breakdown feature seen here is the boulder-sized pieces from the ceiling that are now part of the floor on which we stood in the cave. These massive roof slabs buried equally massive stalagmites that lay broken beneath them (Figure 4.14c).

Another cave feature of structural origin in the Brecciated Room is the linear dissolution pit (Figure 4.14d) trending NW-SE at the southeast corner of the room. At the same southeast corner of the Brecciated Room but perpendicular to the linear dissolution pit is a NE-SW trending fracture chimney. This fracture chimney is not wide enough to fit a person like the fracture chimney at the Roundabout Room. The northeast flowstone wall in the Brecciated Room also exhibits a multitude of joints and fractures (Figure 4.14e).

We found no features in the Brecciated Room that might be attributed to phreatic conditions. The next cave section from the Brecciated Room is the Lower-Level Passage that leads to the Water Table Pool.

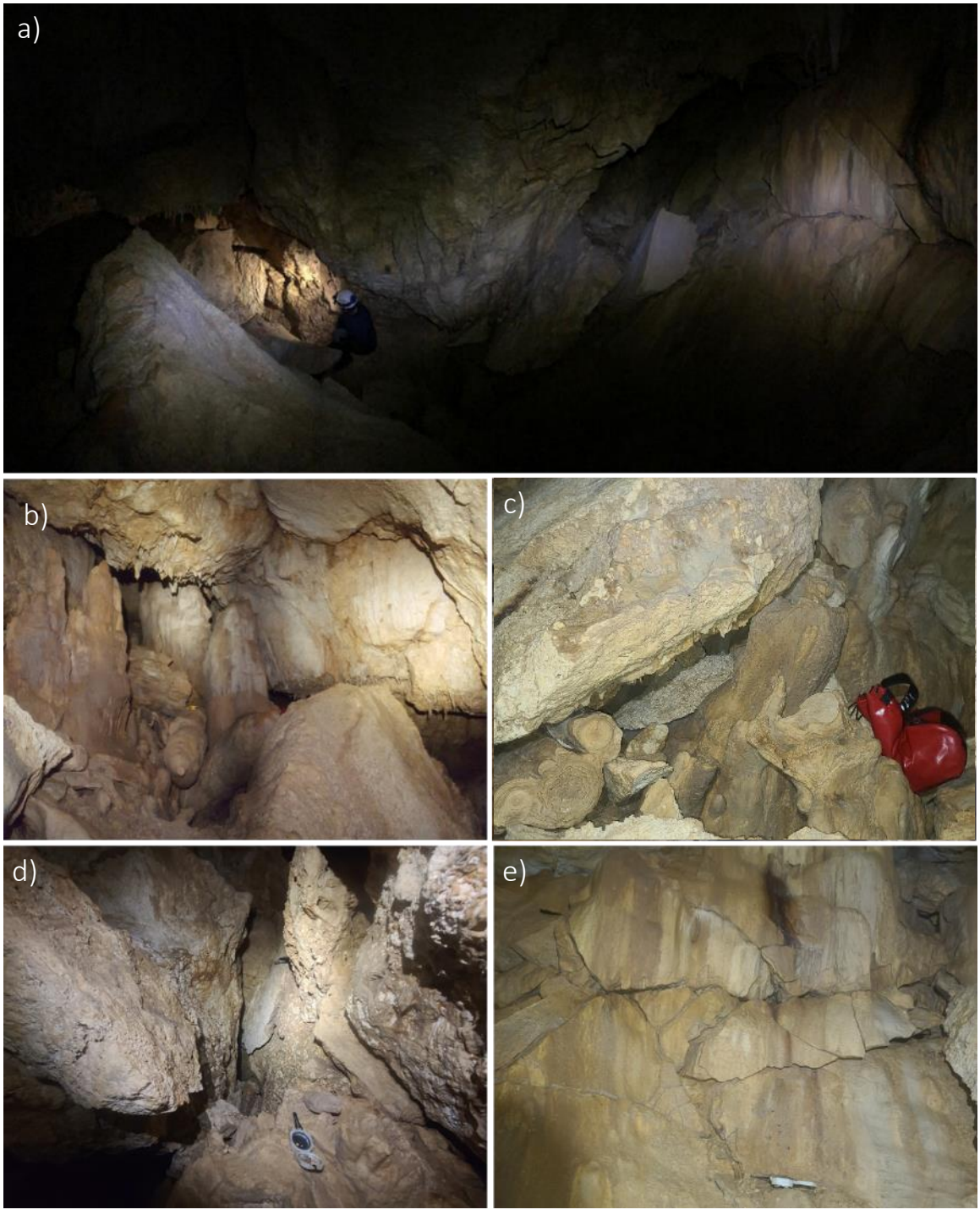

Figure 4.14. Tectonic-induced breakdown features in the Brecciated room a) Massive slabs of ceiling breakdowns. b) Huge and complex stalagmites that can only develop in vadose conditions. c) Stalagmites buried under ceiling boulder breakdowns d) Linear dissolution pit e) Fractured flowstone wall in the northeast side of the room.

4.3.5 Lower-Level Passage

The cave passage continues from the Brecciated Room to the Lower-Level Passages that extend all the way to the distal end of the cave. This part of the cave is a new section discovered and mapped during the course of this research. The Lower-Level Passage is between 5-6 m lower in elevation than the Brecciated Room. The cave roof-to-surface thickness is 11 m, the thickest across the entire cave. The Lower-Level Passage can be described as structurally controlled based on the blocky separation of rooms and passage at this level. At the approach of the passage, the morphology is distinctly breakdown type (Figure 4.15a) and the shape of the passage becomes lenticular like that of the main room.

At the Bacon Strip, just 5 m from the breakdown area by the passage approach, vadose morphology is notably more prevalent. Bacon Strip is named after the draperies (Figure 4.15b) in this room and the narrow strip of passage floor bounded by a linear dissolutional pit (right side going in) and hollows beneath the rubbles on both sides (left side going in). The speleothems in the Bacon strip are profuse. Flowstone make up the entire northwest wall (Figure 4.15c), stalagmites on the pit. with stalactites, stalagmites, and draperies. Based on the degradation of the draperies, it seems it has stopped growing for a while. We found a stalagmite which was detached at its base, leaning against the flowstone wall, to which was recemented. Stalagmites inside the dissolution pits are partly submerged by the rise and fall of the water table level, but also fed by dripwaters when vadose flow becomes active from rain. Another stalagmite appears to have been broken at base from the weight of the breakdown that fell on it. The growth of speleothems is at times interrupted by sudden breakdowns but so long as the vadose conditions still operate, the growth of new speleothems continues.

From the Bacon Strip, the only way to get to the Water Table Pool is through a triangular hole (Figure 4.15e) through a massive, boulder breakdown. This crawl passage is beneath a hanging wall that exhibits slickensides (Figure 4.15f). Beyond the crawl passage, the passage morphology becomes indicative of breakdowns again, and at the end of the passage is the Water Table Pool.

Figure 4.15. Lower-level room and passage morphology a) Breakdown at the lower-level passage approach b) Draperies at the bacon strip suggests vadose. c) *Northeast flowstone wall at the Bacon Strip. d) Partly submerged speleothems inside dissolutional pit. e)* Tight passage through breakdown boulders. d) Slickensided wall hanging over tight breakdown passage below

4.3.6 Water Table Pool

The water table pool was observed to rise and fall with tide. The cave pool is only ~65m from the entrance. The pool water is relatively fresh and generally calm with no obvious flow. This contrast with the turbulent, high-discharge flow of the spring at the entrance. Boulder breakdowns make up the floor of water table pool area. The water table pool is accessible in pockets and cavities in between these boulders (Figure 4.16b). Above the water table pool are low hanging ceiling rocks that exhibit a unique sponge-like texture (Figure 4.16b) indicative of aggressive dissolution at the water-air interface. A thin deposit of reddish soil with organic debris on rock piles were noted in the deepest part of the cave. This is evidence of the vadose flow transporting sediments through fractures in the formation.

Beneath the breakdown boulders are cavities into which we sent a submersible rover (Fifish) to explore the phreatic environment and characterize submerged cave features. The development and growth of speleothems is necessarily subaerial; their occurrence submerged in caves unequivocally indicates a vadose history, hence a lower sea level in the past. The submerged speleothems are as diverse as their subaerial counterparts in the cave. Complex clusters of stalactite and draperies underwater remain intact but in places show distinct dissolution degradation (Figure 4.17a). The same vuggy texture was seen on the formation underwater as in the limestone above water, bearing crosscutting fractures and joints as well (Figure 4.17b). Partly submerged stalagmites (Figure 416d) continue to grow above the high-water line, fed by intermittent drip waters that percolate immediately after each heavy rain. Like the submerged stalactites, the stalagmites could have only formed when the water table was lower than its present level.

A thin layer of reddish clayey-silt sized sediments mixed with coarse sand to pebble-sized angular rock fragments has settled on top of the submerged pile of breakdown boulders (Figure 17c). The unconsolidated sediments were quick to stir, the coarse pieces settling quickly, but the clayey silt taking about a few minutes. If there were finer or more clays in the sediment, it would have taken more time to settle. We suspect that the fine-grained sediments do not stay long on top of the boulder pile based on how thin the deposit was and would readily be removed by the onset of lateral flow.

Although the age of the speleothems cannot be accurately placed, their submergence is very strong evidence of the rapid changes in sea level conditions that occurred in the last thousand years.

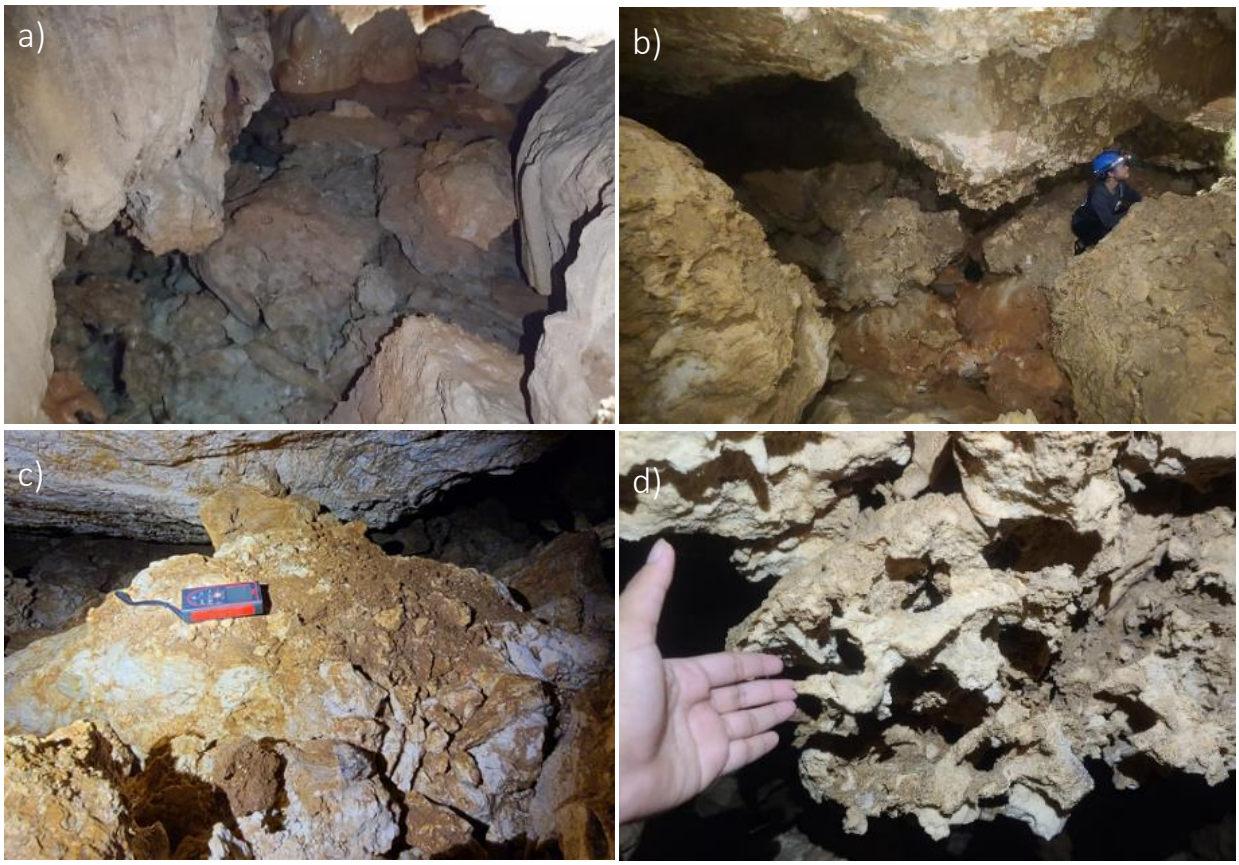

Figure 4.16. Water table pool features a) Pool water that rise and fall with tide. b) Massive, boulder breakdowns, c) Sponge-like texture of low hanging ceiling rocks suggests aggressive dissolution at the water-air interface, d) Soil and organic debris found at the deepest level of the cave.

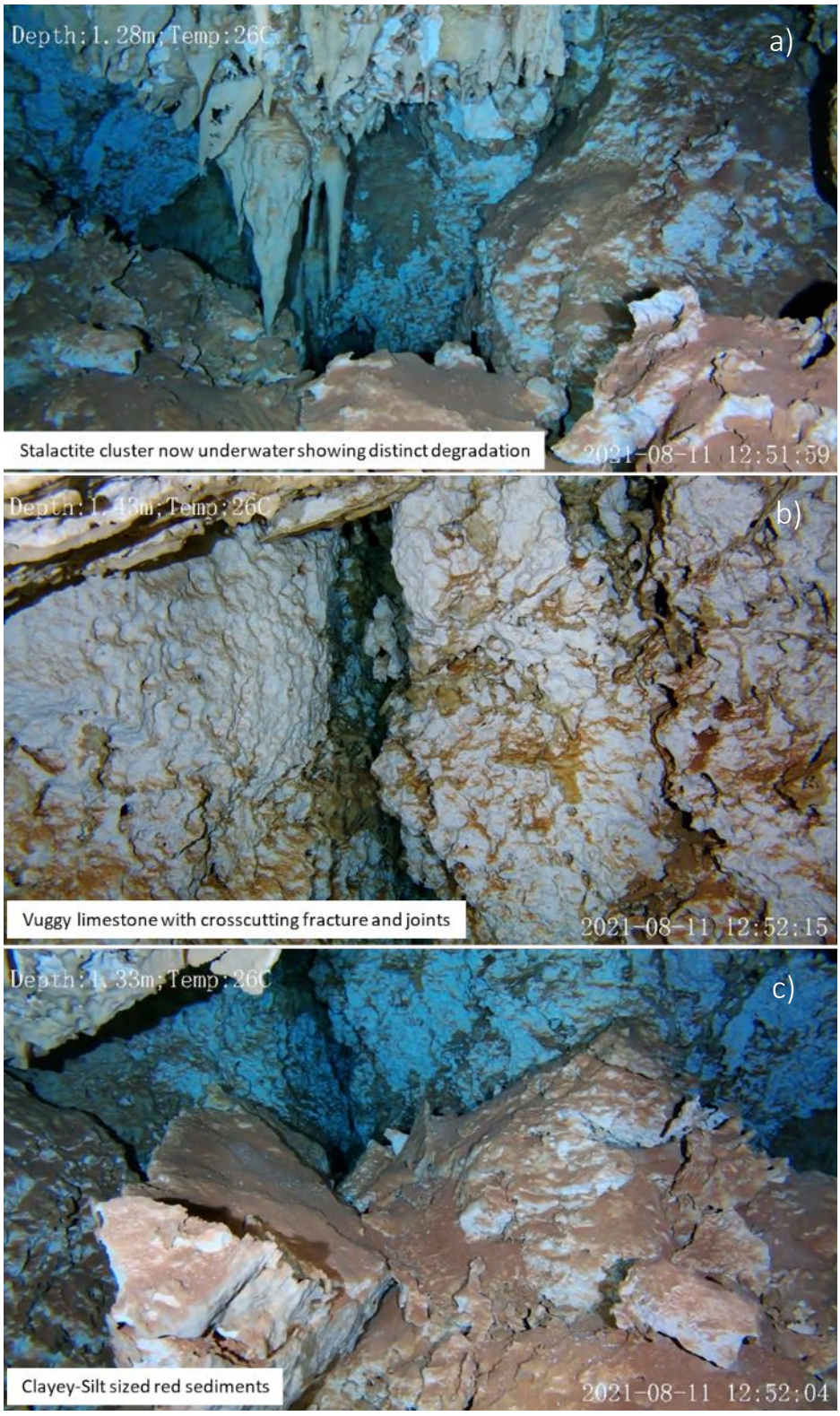

Figure 4.17. Cave pool underwater features includes a) submerged stalactites and draperies showing degradation b) vuggy texture with crosscutting fracture and joints; c) clayey-silt sized reddish sediments accumulated on rubbles. (Images courtesy of Carl Henderson)

4.4 Cave Pool Water and Spring Discharge Data

Water samples were collected from the cave pool at the distal end and from the spring discharge at the entrance of Ayuyu Cave, to determine conductivity which is an index of brackishness. Samples were taken during several trips to the cave at times when the tide was negative. Cave pool water and spring discharge samples were collected simultaneously.

Table 4.2. Summary of results of water samples collected from Ayuyu Cave pool water and spring discharge from 2019 to 2021.

		Cave Pool	***Cave Pool***	***Entrance***	***Cave Pool***	***Entrance***	***Cave Pool***	***Entrance***
	Unit	28-Sep-19	11-Jun-20	24-Jun-20	12-Mar-21		11-Aug-21	
Classification		Slightly Brackish	Slightly Brackish	Brackish	Slightly Brackish	Brackish	Slightly Brackish	Brackish
Conductivity	µS/cm	1719	1862	5000	2097	8520	1480	6186
TDS					1346	6788		
pH					7.6	7.5	7.5	7.5
Hardness					280	349		
Ca	mg/L	86.1			89.8	132	91	130
Mg	mg/L	27.7			13.6	4.46	46	203
Fe		< 0.1			< 0.1	< 0.10		

In-situ measurements were also taken using a YSI Multimeter on February 24, 2021, at high tide. The results are tabulated below:

Table 4.3. In-situ measurements of Ayuyu Cave pool water and Spring discharge at cave.

February 24, 2021		***Cave Pool***			***Entrance***
Parameter *Units*		**11:07:27 AM**	**11:08:27 AM**	**11:08:41 AM**	**11:54:03 AM**
Classification					*Brackish*
Conductivity	µS/cm	2423	3291	3287	8871
Dissolved Oxygen	%	58.8	60.5	55.7	68.5
pH	(units)	7.36	7.34	7.34	7.49
Salinity	ppt	1.22	1.69	1.68	4.84
Temperature	°C	25.8	25.9	25.9	26

Conductivity values for the cave pool water taken with the YSI probe are higher than those from the laboratory analyzed samples. This is probably due to the water samples for the laboratory having been collected from the top of the pool while the YSI multimeter probe was lowered to the bottom (about 1m) of the pool to measure conductivity.

CHAPTER 5. DISCUSSION

Presented in Chapter 4 are surface and subsurface karst geological characteristics identified and analyzed for Pugua Fault and Ayuyu Cave, respectively. We have correlated surface and subsurface karst features to answer three research questions:

(1) What are the structural, speleogenetic, and hydrogeological controls on the occurrence and distribution of coastal discharge from Ayuyu Cave?

(2) What generalizations can be drawn from them for applications elsewhere?

(3) What are the relationships of the cave and the associated discharge to Pugua Fault and other structural features associated with the cave?

In this chapter, we discuss our findings with respect to the relevant conceptual models to characterize and explain this unique high-discharge coastal freshwater spring system in NW Guam.

5.1 Ayuyu Cave in the context of Submarine Groundwater Discharge.

Exploration for and investigation of SGD along the NW coast were the main interests at the initial stages of this research project. Coastal discharge and seeps on the NW coast were substantially explored up close and from above using UAV (Walker, 2020) and will be reported separately. Upon visiting and documenting the spectacular discharge from Ayuyu Cave, it became apparent that this unique feature merited an investigation of its own. Moreover, to explain the high-discharge freshwater spring system in Ayuyu Cave required not only a detailed understanding of the cave itself, but also of the karst processes at the surface and towards the subsurface. There is no immediately obvious answer as to how Ayuyu Cave discharges 2.3 MGD of freshwater. The investigation therefore led to examining the possible role of Pugua Fault, a region-scale structure, in channeling flow into Ayuyu Cave.

5.2 New insights to the Pugua Fault Zone and implications to surface hydrology

There is only a handful of references and descriptions of Pugua Fault. It was identified by Tracey *et al.,* (1964) and incorporated by (Siegrist and Randall, 2008) in their revision of the Geologic map of Guam. To our knowledge, there has yet to be a focused structural or geophysical study of the fault. Very little is known about Pugua Fault, except for it being interpreted and mapped so far as a NNW-trending normal fault that cuts across the

Mariana Limestone in the NW side of the *Machanao* Block (see Tracey *et al.,* 1964). In these reports, the interpreted tectonic sense of movement of Pugua Fault was extensional, with steep vertical dip, downthrown to the SW. The original estimated 4369 m trace of Pugua Fault transects Naval Base Guam North Finegayan Telecommunications Site (NCTS) and strikes towards the NW coast veering slightly away from Ayuyu Cave. It splays to the right at about a third of its strike length, with the same sense of movement as the main Pugua Fault strand. Pugua Fault is referred and treated as a single strand of structure. We propose to refer to Pugua Fault in a broader structural sense, not just as a strand of fault line, but as a ***fault zone***[6] of significantly complex nature; that it occurs on a young, diagenetically immature limestone formation adds to the geologic complexities of Pugua Fault.

Based on the LiDAR study, new insights regarding the extent and nature of Pugua Fault are presented. In this work, the interpretation of Pugua Fault is that of a segmented, left-stepping sinistral fault with extensional components where they overstep[7]. Pugua Fault oversteps to the left where a releasing bend developed in between the parallel fault segments (Figure 5.1). A shutter ridge was also distinguished by the south end of the first stepover segment. The group of short lineaments delineated north end of Pugua Fault towards Ayuyu Cave are apparent transtensional[8] positive flower structures, features typically found in strike-slip duplexes. Transtensional, positive flower structures have normal dip slip sense of displacement to them.

These new insights to the structural characteristics of Pugua Fault have significant implications to the surface hydrology in the study area. Extensional bends and transtensional sections are areas where high permeability can be expected. In contrast, compressional bends would typically have low permeability. In karst, extensional bends would be areas where sinkholes will likely develop while transtensional sections would be areas where surface flow may be channeled and become water's fast flow route into the subsurface. Ideally, strike slip faults are compressional feature having low permeability that may function as a barrier to flow. But their complex oversteps, and minor extensional component creates pockets of high permeability zones within a typical compressive

6 Fault zones have three primary components namely, a *fault core*, a *damage zone* and a *protolith* (Caine *et al*., 1996). The fault core is the central structure where most displacement occurs. The damage zone is the network of subsidiary structures that bounds the fault core. The protolith surrounds the damage zone and displays properties of the unfaulted host rock.

7 An *overstep* is where the strain at the tip of the fault is transferred to a parallel fault of the same sense of displacement, creating a restraining or releasing bend at the overstep. Restraining bends are compressional features which can be recognized at the surface by pressure or shutter ridges. Releasing bends are extensional features that are best exemplified by sag ponds or pull-apart basins. (Aydin *et al*., 2010)

8 *Transtension* is a combination of strike-slip (dominant) and extension; also called oblique slip. If the strike-slip component is compressional, it is regarded as *transpression*. (Aydin *et al.,* 2010)

setting. Many more lineaments cross-cutting Pugua Fault were delineated in the study area. In the framework of strike slip fault zones, these could be synthetic and antithetic faults related to displacements along the master fault. We did not characterize them, as such complexities are beyond the scope of this study.

There were three areas shown in the line density map (Figure 4.3) where fault convergence is highest. These areas are likely to undergo focused channeling of large volumes of water and therefore undergo rapid, extensive, and severe dissolution. The north segment of Pugua Fault is a high-line-density area with subparallel, NE-striking short linear features, which are apparent splays forming positive flower structures.

Shalilian (2017) calculated the hydraulic conductivity of the north segment of Pugua Fault using a range of storativity values (0.01 to 0.4) from previous NGLA models (Rotzoll *et al.,* 2013 and Gingerich, 2013). The estimated hydraulic conductivity of Pugua Fault (north segment) ranges between 5,000 to 200,000 m/d. Based on the calculated discharge of 2.3 MGD from Ayuyu Cave, and high hydraulic conductivity potential along Pugua Fault, Shalilian (2017) proposed that the boundaries of Finegayan basin be revised to include Ayuyu Cave and the mapped extent of Pugua Fault.

The inferred faults and lineaments in the LiDAR study warrant a more focused structural study. Field verification of the delineated structures of the Pugua Fault zone is vital moving forward, else they remain hypothetical. In complex carbonate island karst systems, structural features can guide conduit inception and cave pattern development in the subsurface. The unique high-discharge freshwater spring system in Ayuyu Cave can be attributed to the structural geological complexities of the Pugua Fault zone presented in this thesis.

5.3 Pugua Fault in the context of the Carbonate Island Karst Model

The Carbonate Island Karst Model was conceptualized in 1990 by Mylroie and Carew to explain the development of karst features on young carbonate islands in the Caribbean and western Atlantic. Jenson *et al.* (2004) investigated the more geologically complex Mariana Islands in terms of the model and demonstrated that island karst is more complex than previously observed and reported. The model was revised to improve the composite island type based on features observed in Guam and to include the complex island type based on Saipan.

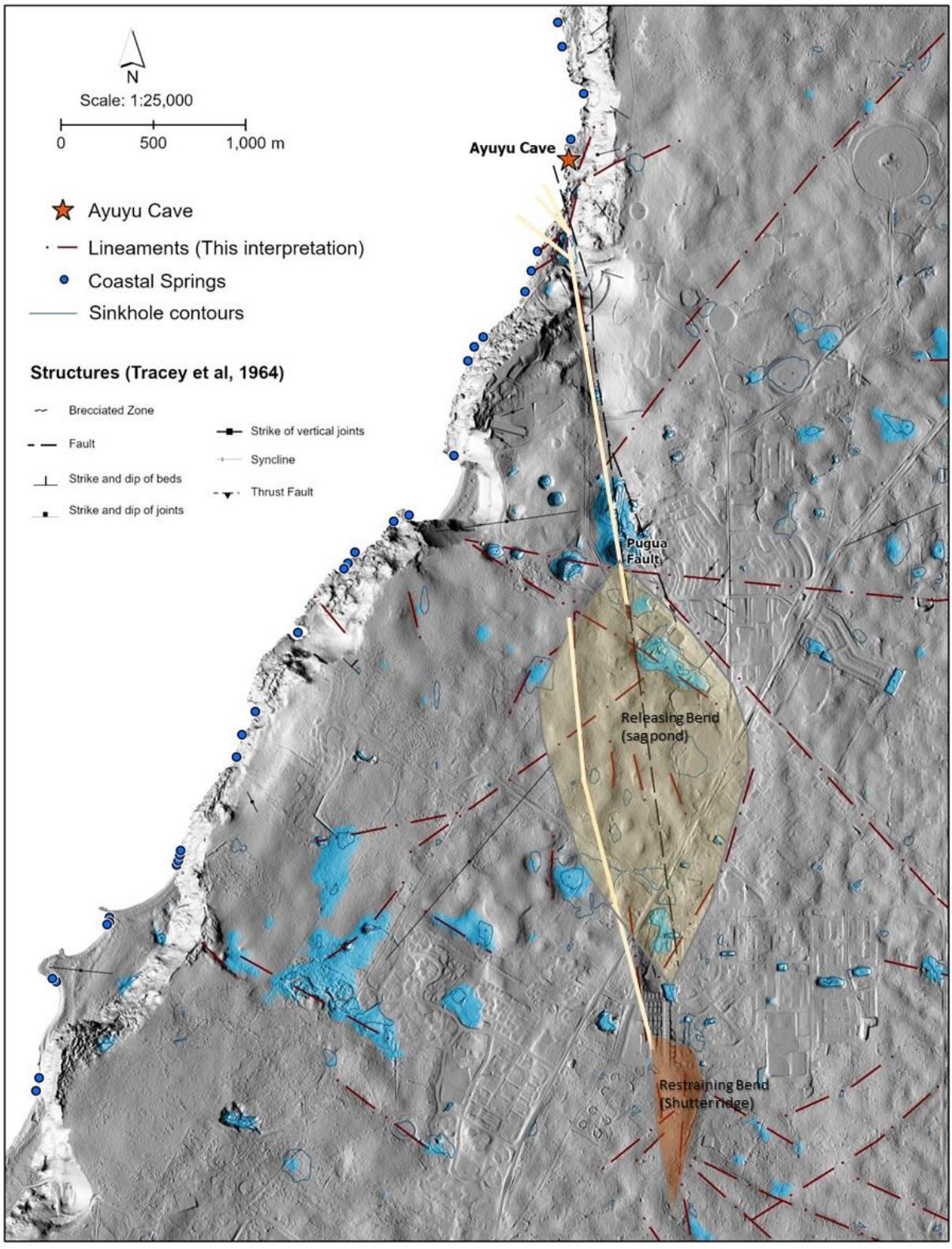

Figure 5.1. Interpreted structural features of Pugua Fault Zone in the context of a strike slip fault.

New insights into the structural characteristics of the regional-scale, NNW-trending Pugua Fault, suggest that this portion of northern Guam is best described as Complex Carbonate Island Karst in terms of the CIKM, and that structural control of or influence in conduit geometry be considered in configuring and interpreting the results of numerical models. Such features are important departures from classic Darcian flow and require careful consideration in the application of standard numerical models, which assume Darcian flow.

In Tracey *et al.,* (1964), Pugua Fault was described as a normal fault. However, from the LiDAR study, Pugua Fault was reinterpreted as a left-stepping left- lateral fault with extensional bends along their oversteps. Tracey *et al.,* (1964) aptly described Pugua Fault cutting across the top-lying Mariana Limestone in the NW coast. Therefore, based on classic application of stratigraphic and cross-cutting relationships, the estimated age of Pugua Fault is <2Ma-old, or younger than the Upper Pleistocene Reef Facies of the Mariana Limestone that it cuts across. Based also on the relatively good geomorphic impressions of Pugua Fault observed on the LiDAR study, which remain discernable despite the high solubility of the carbonate bedrock, it is highly likely that Pugua Fault may still be active.

Given these proven complex geological relationships of the NGLA, (i.e., Pugua Fault zone, high-discharge freshwater spring system), we propose that this portion of the northern Guam Plateau be classified as a ***Complex Island*** type. We also suggest that structural features be considered in modeling karst aquifer boundaries, in particular in delineating aquifer basins of the NGLA. Shalilian (2017) proposed the boundaries of Finegayan basin to be revised to include Ayuyu Cave and Pugua Fault. We agree to this in principle but advise that more study of structures in the NGLA be undertaken to characterize structural control in sufficient detail. Fault systems, depending on their manner of deformation (i.e., extensional, compressional, and lateral) may act as either conduits or a barrier to groundwater flow.

5.4 Ayuyu Cave in the context of the Flank Margin Cave Model

A subset of the Carbonate Island Karst Model is the Flank Margin Cave Model, which is also based on Mylroie and Carew's study of the Caribbean and the Bahamas. Flank margin caves have a characteristic morphology that makes them useful and important markers of past and present sea levels (Figure 1.3). There are two schools of thought that attempt to explain to the dissolution that generates water-table and flank margin caves. Mylroie and Carew (1990) invoked a mixing-corrosion mechanism to explain the diagnostic morphology of flank margin caves. Gulley *et al*. (2015) have suggested that biologically-generated CO_2 may be more important for dissolution and karstification than mixing water dissolution.

As we have demonstrated, Ayuyu Cave is a surprisingly complex cave, with a complex morphology reflecting a complex history. For example, northern Guam has been emergent for the last 2 Ma (Pleistocene), within which there have been many cycles of eustatic sea level fluctuation, contemporaneous with episodes of tectonic uplift and subsidence of unknown timing and magnitude. Flank margin caves in Guam are ubiquitous in cliff faces, 2 m above modern sea level for the Mid-Holocene Highstand, 7 m above modern sea level for the MIS 5e Highstand. Caves at intermediate level are most likely products of local tectonic uplift and subsidence (Miklavič, 2012).

Cave morphology characterized in Ayuyu Cave which reflect affinities with the flank margin model is disproportionately wide and relatively equidimensional size of the initial room that opens onto the coast. In the cave profile (Figure 4.8), this is the area from the Main Room and passage up to the Doll's Leg where a fault was inferred. Past the main passage of the cave, flank margin cave affinity dissipates as vadose and breakdown morphologies become more prevalent. Vadose conditions and their associated depositional morphologies are the most consistent and enduring process in the cave, halted only when sea level rises high enough to completely submerge the cave and phreatic conditions prevail. There may have been plenty of time in the past for vadose conditions to dissolve and develop vadose galleries such as the Attic Room and the Brecciated Room (pre-collapse breakdown). It is possible for vadose galleries above and flank margin caves below to develop at the same time, especially with structural guidance (e.g., fractures and faults).

To explain the development of Ayuyu Cave, Taborôsi *et al.,* (2003) departed from the original flank margin model of the tectonically quiescent Bahamas (Mylroie *et al.,* 1995) because of the unusual high-discharge freshwater spring discharge which he described as the termini of conduit systems. He hypothesized that there must be some unique geologic and hydrologic conditions that would allow such unique discharge phenomenon. We agree to this observation and propose the Pugua Fault zone as the structural control to surface hydrology capable of creating the high-discharge freshwater spring system in Ayuyu Cave.

Today, at the lower-level passage, and certainly below the water table, is where flank margin cave processes continue to operate. Beneath the breakdown piles and along the submerged speleothems, the mixing water and/or CO_2 dissolution and karstification processes continue, unobserved and certainly difficult to characterize. If sea level lowers some more, as it did from the Mid-Holocene to the present, these new flank margin caves will be ready to be explored by future generations of UOG environmental science students.

CHAPTER 6. CONCLUSIONS AND RECOMMENDATIONS

The surface and subsurface karst features discussed in this report illustrate the heterogenous structure and complex hydrogeology that may be found in carbonate island karst systems. The use of LiDAR study was valuable in characterizing karst surface features in the study area and instrumental to the reinterpretation of Pugua Fault as a strike-slip fault. In the context of the CIKM (Figure 1.2), northern Guam is classified as a *Composite Island*, but our interpretation of Pugua Fault suggests that at least this and perhaps other areas where regional-scale faults are present may be better described as fitting the Complex Island model.

Morphological observations in the cave were crucial to understanding the hydrogeological and structural processes that drove the evolution of Ayuyu Cave. These morphological features in the subsurface are undoubtedly related to surface processes. Morphological features inventoried in Ayuyu Cave were categorized as either vadose, phreatic, or breakdown, and distinguished further if they are features developed in the past or still active at present. Characterization of the passage levels, patterns, and profile reveals a very complex history of speleogenesis and hydrogeological evolution of Ayuyu Cave.

The unique high-discharge freshwater spring system in Ayuyu Cave can be explained by the geological complexities presented in this thesis. The region-scale Pugua Fault zone is a structural feature capable of exerting major influence on surface hydrology to create the high-discharge freshwater spring system in Ayuyu Cave. Characterizing the dynamics of flow in the Ayuyu Cave - Pugua Fault zone was beyond the scope of this study and, if desired, will require dye tracing methods.

6.1 Suggested Future Research

The surface and subsurface karst features documented in this thesis presents several opportunities for future research in Northern Guam. Updating the regional geology of Guam using remote sensing data (e.g., Landsat, LiDAR) combined with UAV technology is recommended for future study. The fault and structures map of Guam was created as part of Tracey et al.'s study of the Geology of Guam in 1964, that has only been revisited and updated briefly by Siegrist and Reagan (2008). The combined use of high-resolution, remotely sensed satellite imagery, LiDAR and UAVs are the latest technological advancement available today in geological, structural and karst geomorphological mapping, where datasets at successive scales, can be applied to complement one another can be employed in this study.

To better understand groundwater flow dynamics in island karst and to ascertain the role of faults (e.g., Pugua fault) in channeling flow, specifically to determine the Ayuyu Cave – Pugua Fault Zone connection, dye tracing method is suggested. Radioactive isotope (Radon and Tritium) and groundwater flow models to estimate the residence time and catchment area for Ayuyu Spring water is a similar method that may be considered in the future. Both are relatively expensive methods but can provide definitive information of groundwater flow paths in the subsurface.

The drilling of seven new wells in northern Guam, which are currently underway, is another opportunity for gathering subsurface information for the NGLA. Detailed lithology can be reconstructed from the drill cuttings recovered from drilling. And where voids and cavities are encountered, an assessment of their preferential horizons for development can be conducted as well.

REFERENCES

Aydin A., and Berryman J.G. (2010). Analysis of the growth of strike-slip faults using effective medium theory. Journal of Structural Geology*, 32(11), 1629-1642. d*oi:10.1016/j.jsg.2009.11.007

Burnett WC, Bokuniewicz H, Huettel M, Moore WS, and Taniguchi M. (2003). Groundwater and pore water inputs to the coastal zone. Biogeochemistry 66(1–2):3–33. doi:10.1023/b:biog.000000606 6.21240.53

Burnett, W. C., Aggarwal, P. K., Aureli, A., Bokuniewicz, H., Cable, J. E., Charette, M. A., Turner, J. V. (2006). Quantifying submarine groundwater discharge in the coastal zone via multiple methods. Science of The Total Environment, 367(2-3), 498–543. doi:10.1016/j.scitotenv.2006.05.009

Charette, M. A. (2007). Hydrologic forcing of submarine groundwater discharge: Insight from a seasonal study of radium isotopes in a groundwater-dominated salt marsh estuary. Limnology and Oceanography, 52(1), 230–239. doi:10.4319/lo.2007.52.1.0230

Contractor, D.N. (1983). Numerical modeling of saltwater intrusion in the Northern Guam Lens. Water Resources Bulletin, 19, 745–751

Contractor, D.N. and Jenson J.W. (2000). Simulated effect of vadose infiltration on water levels in the Northern Guam Lens Aquifer. Journal of Hydrology, v.229, p232-254

Contractor, D.N. and Srivastva, R., (1990). Simulation of saltwater intrusion in the Northern Guam Lens using microcomputer: Journal of Hydrology, v.118, p.87-106

Csoma, A.E., Goldstein, R.H. and Pomar L. (2006) Pleistocene speleothems of Mallorca: Implications for paleoclimate and carbonate diagenesis in mixing zones. *Sedimentology, 53(1), 213–236.* doi:10.1111/j.1365-3091.2005.00759.x

Emery, K.O. (1962). Marine Geology of Guam. U.S. Geological Survey Professional Paper 403-B. Washington, DC: U.S. Geological Survey

Fleury, P., Bakalowicz, M., & de Marsily, G. (2007). Submarine springs and coastal karst aquifers: A review. Journal of Hydrology, 339(1-2), 79–92. doi:10.1016/j.jhydrol.2007.03.009

Ford D. and Williams P. (2007). Karst Hydrogeology and Geomorphology, West Sussex, England, John Wiley &sones, Ltd., 129-142 p.

Gardner, J.V. (2010). The West Mariana Ridge, western Pacific Ocean: Geomorphology and processes from new multibeam data. Geological Society of America Bulletin, Sept./Oct 2010, 1378-1388

Ginés, A. (2009). Karrenfield landscapes and karren landforms. In: Ginés, A., Knez, M., Slabe, T., Dreybrodt, W. (eds.) (2009) Karst Rock Features: Karren Sculpturing. Ljubljana: ZRC Publishing. 13-24

Gingerich, S. B. (2013). The effects of withdrawals and drought on groundwater availability in the Northern Guam Lens Aquifer, Guam. Retrieved from https://pubs.usgs.gov/sir/2013/5216/pdf/sir2013-5216.pdf

Hickey-Vargas,R. and Reagan, M.K. (1987). Temporal variation of isotope and rare earth element abundances in volcanic rocks from Guam: implications for the evolution of the Mariana arc. Contributions to Mineralogy and Petrology, 497-508.

Lander M.A., Guard CP (2003). Creation of a 50-Year Rainfall Database, Annual Rainfall climatology, and annual Rainfall distribution Map for Guam. WERI Technical Report No. 102, pp 31.

Jenson, J.W. (2016). Recommended Sites for the New Deep Observations Wells for the Northern Guam Lens Aquifer. Internal Report, Water and Environmental Research Institute of the Western Pacific – University of Guam.

Jenson, J.W.; Jocson, J.M.U., and Siegrist, H.G. (1997). Groundwater discharge styles from an uplifted Pleistocene Island karst aquifer, Guam, Mariana Islands. In: Beck, B.F. and Stephenson, J.B. (eds.), The Engineering Geology and Hydrology of Karst Terranes.

Jenson, J. W., Keel, T. M., Mylroie, J. R., Mylroie, J. E., Stafford, K. W., Taboroši, D., & Wexel, C. (2006). Karst of the Mariana Islands: The interaction of tectonics, glacio-eustasy, and freshwater/seawater mixing in island carbonates. Special Paper 404: Perspectives on Karst Geomorphology, Hydrology, and Geochemistry - A Tribute Volume to Derek C. Ford and William B. White, 129–138. doi:10.1130/2006.2404(11)

Jocson, J.M.U.; Jenson, J.W., and Contractor, D.N., (1999). Numerical Modeling and Field Investigation of Infiltration, Recharge, and Discharge in the Northern Guam Lens Aquifer. WERI Technical Report 88. Mangilao, Guam: Water and Energy Research Institute of the Western Pacific, University of Guam.

Jocson, J.M.U.; Jenson, J.W., and Contractor, D.N., (2002). Recharge and aquifer response: northern Guam lens aquifer, Guam, Mariana Islands. Journal of Hydrology, 260, 231–254.

Johnson, A.G. (2012). A water-budget model and estimates of groundwater recharge for Guam: U.S. Geological survey Scientific Investigations Report 2012-5028.

Karig, D. E., (1971). Structural history of the Mariana Island arc system. Geological Society of America Bulletin, Volume 83 s.2 p.p. 323- 344, doi:10.1130/0016-7606(1971)82[323]2.0.CO;2

Kato T., Beavan J., Matsushima T., Kotake Y.J., Camacho T., Nakao S. (2003). Geodetic evidence of back-arc spreading in the Mariana Trough. Geophys Res Lett 30(12):1625. doi:10.1029/2002GL016757

Kaufmann, G. (2003). Numerical models for mixing corrosion in natural and artificial karst environments. Water Resources Research, 39(6). doi:10.1029/2002wr001707.

Kayanne, H., Yonekura, N., Ishii, T., and Matsumoto, E. (1988). Geomorphic and geologic development of Holocene emerged reefs in Rota and Guam, Mariana Islands. In 'Sea-level changes and Tectonics in the Middle Pacifics' (HIPAC Team), pp.35-57. Report of the HIPAC Project in 1986 and 1987 IThird Research), University of Tokyo, Tokyo

Kayanne, H., Yonekura, N., Ishii, T., Matsumoto, E., and Yonekura, N. (1993). Late Holocene Sea-Level Change on Rota and Guam, Mariana Islands and its Constraint on Geophysical Predictions (1993).Quaternary Research v40 pp.189-200.

Labourdette, R., Lascu, I., Mylroie, J., & Roth, M. (2007). Process-Like Modeling of Flank-Margin Caves: From Genesis to Burial Evolution. Journal of Sedimentary Research, 77(11), 965–979. doi:10.2110/jsr.2007.086

Lallemand S. (2016). Philippine Sea Plate Inception, evolution, and consumption with special emphasis on the early stages of Izu-Bonin-Mariana subduction. Progress in Earth and Planetary Science 3:15

Lemeille, F., Cushing, M., Carbon, D., Grellet, B., Bitterli, T., Flehoc, C., & Innocent, C. (1999). Co-seismic ruptures and deformations recorded by speleothems in the epicentral zone of the Basel earthquake. Geodinamica Acta, 12(3-4), 179–191. doi:10.1080/09853111.1999.11105341

Matson, E.A., (1993). Nutrient flux through soils and aquifers to the coastal zone of Guam (Mariana Islands): Linmology and Oceanography, v.38, No.2, p.361-171.

Miklavič B. (2011). Formation of geomorphic features as a response to sea-level change at Ritidian Point, Guam Mariana. Master's Thesis, Mississippi State University.

Mink, J.F., Vacher, H.L., (1997). Hydrogeology of northern Guam. In Vacher, H.L., Quin, T. (Eds): Geology and Hydrogeology of Carbonate Islands. Developments in Sedimentololgy, 54. Elsevier Science B.V., p. 743-761

Mylroie, J. E., & Carew, J. L. (1990). The flank margin model for dissolution cave development in carbonate platforms. Earth Surface Processes and Landforms, 15(5), 413–424. doi:10.1002/esp.3290150505

Mylorie, J. E., Carew, J. L. (1995). Karst development on carbonate islands. In: Unconformities and porosity in carbonate strata, Budd, D. A., Saller, A. H., Harris, P.M. (eds). American Association of Petroleum Geologists Memoir 63, p. 55-76.

Mylroie, J. E., Carew, J. L. (1999). Speleogenesis in young limestones in coastal and oceanic settings, in Klimchouk, A.B., Ford, D.C., Palmer, A.N., and Dreybrodt, W., eds., Speleogenesis: Evolution of Karst Aquifers: Huntsville, AL, National Speleological Society, p. 496.

Mylroie, J.E.; Jenson, J.W., Taborôi D.; Jocson, J.M.U., Vann, D.T., and Wexel, C., (2001). Karst features in Guam in terms of a general model of carbonate island karst. Journal of Cave and Karst Studies, 63, 9-22.

Mylroie, J.R., Mylroie, J.E., (2007). Development of the carbonate island karst model. Journal Of Cave and Karst Studies, v. 69, n. 1, p. 59-75.

Mylroie, J.E., Mylroie, J.R., (2009) Flank margin caves as syndepositional caves: examples from the Bahamas. In White, W.B., (ed): Proceedings, 15th International Congress of Speleology, Kerville, Texas, 1(1), p. 533-539.

Mylroie, J. E., & Mylroie, J. R. (2011). Void development on carbonate coasts: creation of anchialine habitats. Hydrobiologia, 677(1), 15–32. doi:10.1007/s10750-010-0542-y

Randall, R.H. (1979). Geologic Features within the Guam Seashore Study Area. U.S. National Park Service, University of Guam Marine Laboratory Technical Report No. 55.

Randall, R.H., Siegrist, H.G., (1996). The Legacy of Tarague Embayment and Its Inhabitants, Anderson AFB, Guam, Volume III: Geology, Beaches, and Coral Reefs. Prepared for Andersen Air Force Base. International Archaeology, Inc., Honolulu, 462 pp.

Rotzoll, K.; Gingerich, S.B.; Jenson, J.W., and El-Kadi, A.I., (2012). Estimating hydraulic properties from tidal attenuation in the Northern Guam Lens Aquifer System, Territory of Guam, USA. Hydrogeology Journal, in press

Schlanger, S.O., (1964). Petrology of the Limestones of Guam. U.S. Geological Survey Professional Paper 403-D. Washington, DC: U.S. Geological Survey

Schuler, P., Duran, L., McCormack, T., & Gill, L. (2018). Submarine and intertidal groundwater discharge through a complex multi-level karst conduit aquifer. Hydrogeology Journal, 26(8), 2629–2647. Doi:10.1007/s10040-018-1821-3

Shalilian, I. (2017). Hydrogeology of Finegayan Basin, Northern Guam Lens Aquifer. Master's Thesis., University of Guam

Siegrist, H. G., Jr., and R.H. Randall (1992). Carbonate geology of Guam: summary and field trip guide. 7th International Coral Reef Symposium, Guam, USA, June 18–20, 1992. Water and Energy Research Institute of the Western Pacific, University of Guam, Mangilao, Guam, USA.

Siegrist, H.G., Reagan, M.K., R. H. Randall, and J. W. Jenson. (2008). Geologic Map and Sections of Guam, Mariana Islands (1:50,000), Water and Environmental Research Institute, University of Guam, Mangilao, Guam, USA.

Sasowsky I. D. (Eds.) Hydrogeology and Biology of Post-Paleozoic Carbonate Aquifers, Proceedings of the symposium Karst Frontiers: Florida and Related Environments, Gainesville, Florida, Karst Waters Institute, 79-83.

Stafford, K. W., J. W. Jenson, and J. E. Mylroie. (2009). Eogenetic karst of the carbonate islands of the northern Marianas. Proceedings of the International Congress of Speleology 15(1):542–547.

Stearns, H.T. (1937). Geology and Water Resources of the Island of Guam, Mariana Islands. U.S. Navy Manuscript Report

Stern, R. J., Fouch, M. J., & Klemperer, S. L. (2003). An overview of the Izu-Bonin-Mariana subduction factory. Geophysical Monograph Series, 175–222. doi:10.1029/138gm10

Taborosi, D. (2006). Karst inventory of Guam, Mariana Islands. WERI Technical Report 112. Mangilao, Guam: Water and Energy Research Institute of the Western Pacific, University of Guam.

Taborosi, D.; Jenson, J.W.; Jocson, J.M.U., and Mylroie, J.E. (2009). Coastal discharge features from an uplifted carbonate island aquifer: Northern Guam, Mariana Islands. In: Proceedings of the 15th International Congress of Speleology (Kerrville, Texas), Volume 2, pp. 548–553.

Taborosi, D.; Jenson, J.W., and Mylroie, J.E. (2003). Zones of enhanced dissolution and associated cave morphology in an uplifted carbonate island karst aquifer, northern Guam, Mariana Islands. Speleogenesis and Evolution of Karst Aquifers, 1(4), 16p.

Taborosi, D., Jenson, J. W., & Mylroie, J. E. (2012). Field Observations of Coastal Discharge from an Uplifted Carbonate Island Aquifer, Northern Guam, Mariana Islands: A Descriptive Geomorphic and Hydrogeologic Perspective. Journal of Coastal Research, 289, 926–943. doi:10.2112/jcoastres-d-12-00054.1

Taborosi , D. (2006). Karst inventory of Guam, Mariana Islands. WERI Technical Report 112. Mangilao, Guam: Water and Energy Research Institute of the Western Pacific, University of Guam.

Tracey, J.I. Jr.; Schlanger, S.O.; Stark, J.T.; Doan, D.B., and May, H.G. (1964). General Geology of Guam. U.S. Geological Survey Professional Paper 403-A. Washington, DC: U.S. Geological Survey.

United States Geological Survey Pacific Islands Water Science Center (2016). Groundwater Resources for the Northern Guam Lens Aquifer (2016-2025). Internal report. Water and Environmental Research Institute of the Western Pacific, University of Guam.

Veress, M. (2020). Karst Types and Their Karstification. Journal of Earth Science, 31(3), 621–634. doi:10.1007/s12583-020-1306-x

Walker E. (2021). Mapping Coastal freshwater discharge of the Northern Guam Lens Aquifer – Impacts of tide. Lightning talk presentation at the International Tropical Islands Water Conference, April 12-15, 2021.

Ward, P.E.; Hoffard, S.H., and Davis, D.A. (1965). Hydrology of Guam. U.S. Geological Survey Professional Paper 403-H. Washington, DC: U.S. Geological Survey

White, S., & Webb, J. A. (2015). The influence of tectonics on flank margin cave formation on a passive continental margin: Naracoorte, Southeastern Australia. Geomorphology, 229, 58–72. doi:10.1016/j.geomorph.2014.09.003.

APPENDICES

Appendix 1. Earlier Maps of Ayuyu Cave by (a) Taborôsi and Plunkett (1999) and (b) Shalilian (2017)

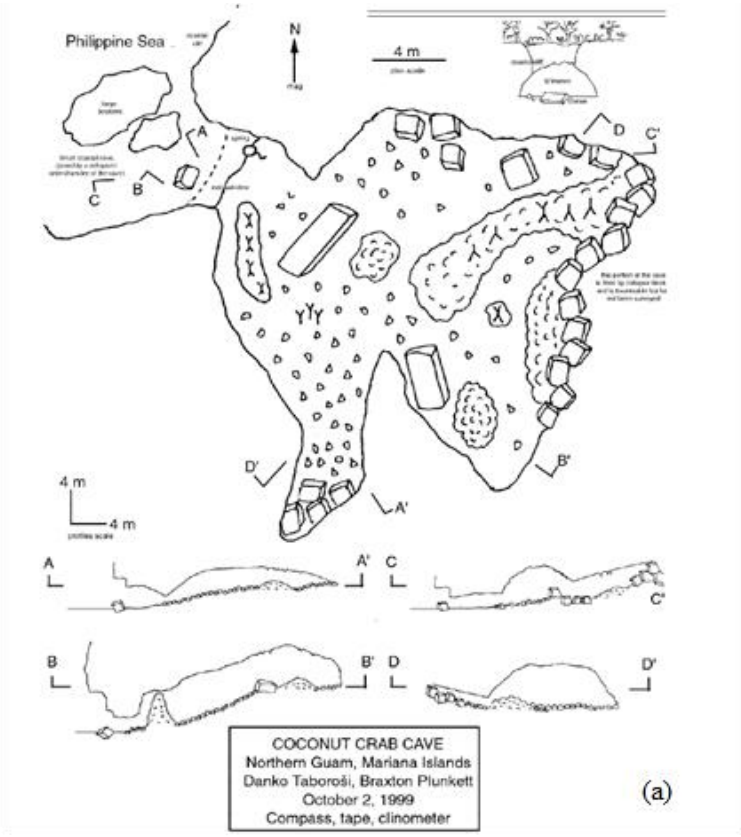

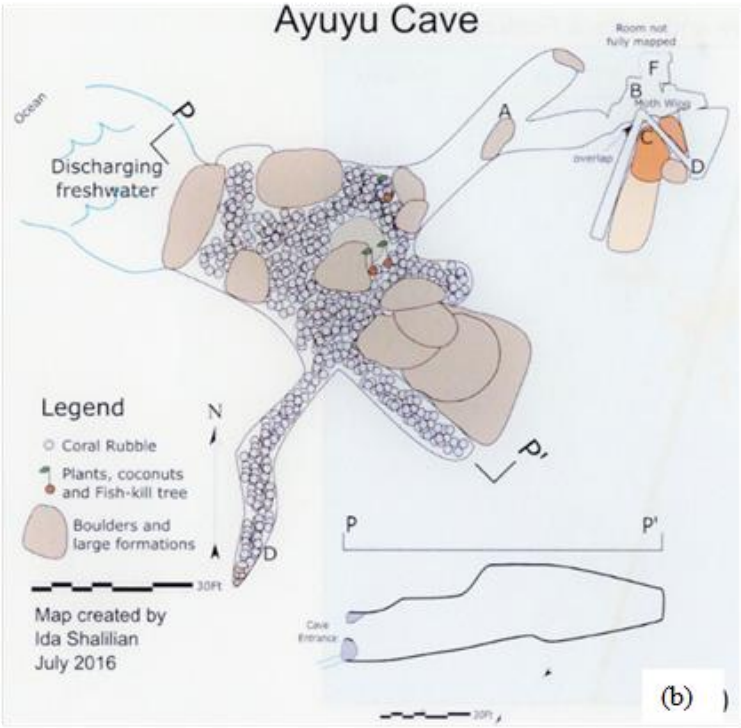

Appendix 2. Structural Map of Guam (Modified from Tracey et al.,1964)

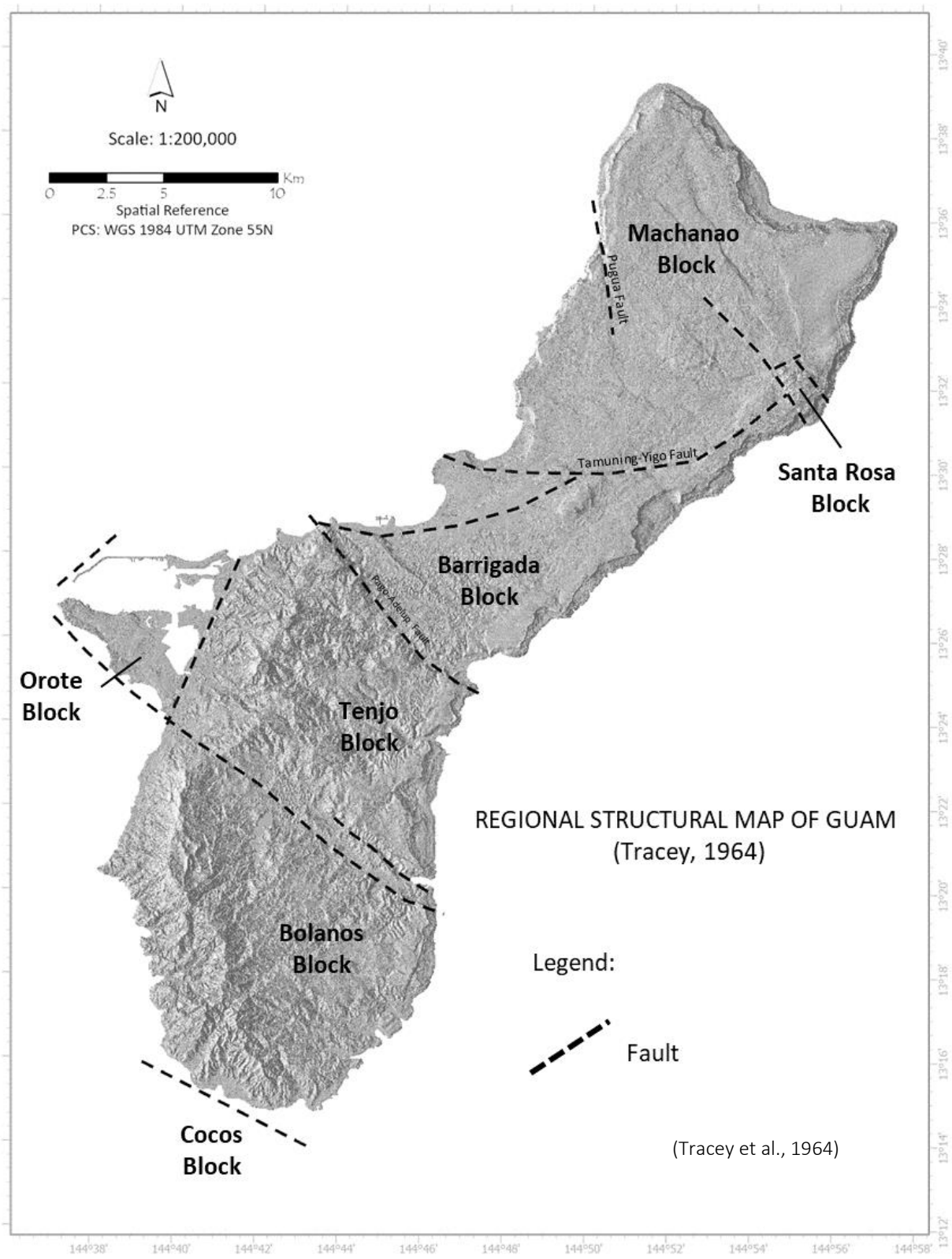

Appendix 3. Ayuyu Cave Survey Data

From	To	Distance	Azimuth	Inclination	Left	Right	Up	Down
AS0	AS1	10.52	106.90	6.70	3.34	3.78	∞	1.00
AS1	AS2	7.53	77.20	10.80	2.10	4.83	1.15	0.48
AS1	AS1R	11.75	196.30	6.20	-	-	-	-
AS1R	AS1R1	6.32	181.30	9.40	0.88	3.32	0.28	0.45
AS1R1	AS1R2	8.01	310.20	-6.70	2.64	0.61	0.86	1.00
AS2	AS3	4.97	92.20	23.90	4.58	2.15	0.70	1.10
AS2	AS2L	6.13	296.60	-20.00	4.94	1.67	0.86	0.48
AS3	AS4	5.42	43.10	-14.80	6.97	2.15	0.70	1.10
AS4	AS5	2.84	27.30	2.00	1.23	2.60	0.46	0.74
AS5	AS6	3.03	140.20	2.70	2.81	2.65	0.43	0.59
AS6	AS7	2.63	46.90	2.10	0.90	0.90	0.63	0.37
AS6	AS6R	1.78	144.90	37.90	0.79	1.78	1.41	0.72
AS6R	AS6R1	3.69	214.90	1.40	1.84	1.32	0.77	0.47
AS6R	AS6R2	2.26	160.50	22.90	0.49	2.36	0.66	0.65
AS7	AS8	4.88	87.90	12.00	2.07	3.51	0.83	1.42
AS7	AS7L0	3.17	52.10	18.7	-	-	-	-
AS7L0	AS7L1	3.39	343.60	18.7	3.39	0.00	1.13	1.53
AS7L1	AS7L2	3.64	102.20	25.6	1.47	0.91	0.55	0.70
AS8	AS9	2.61	141.40	39.50	3.25	1.33	0.90	0.67
AS8	AS8L	3.45	66.40	-6.00	-	-	-	-
AS8L	AS8L1	1.91	22.3	-1.90	3.08	0.17	0.70	0.66
AS8L1	AS8L2	1.48	100.80	28.70	4.11	0.31	0.56	0.19
AS8L2	AS8L3	0.36	125.70	-4.10	3.52	1.82	1.40	0.28
AS9	AS10	1.13	191.00	-12.20	0.91	1.04	0.64	0.65
AS10	AS11	2.39	97.80	-16.60	2.07	1.26	1.29	0.97
AS11	AS12	2.61	105.80	-30.10	1.60	2.77	0.76	1.20
AS12	AS13	3.07	163.20	-41.80	0.91	1.03	1.32	0.57
AS12	AS12R	2.66	56.40	43.60	-	-	-	-
AS12	AS12S	3.33	355.60	36.40	-	-	-	-
AS13	AS14	4.09	87.80	1.90	1.42	1.64	0.75	0.85
AS14	AS15	6.93	31.50	-8.60	1.92	2.73	0.72	1.22
AS15	AS16	8.40	43.70	-10.10	3.40	2.03	-	-
AS15	AS15R	4.99	78.5	4.90	-	-	-	-
AS15R	AS15R2	4.92	170.00	7.00	-	-	-	-
AS15R2	AS15R3	5.44	41.90	2.50	-	-	-	-
AS15R2	AS15R4	4.78	195.5	-18.1	-	-	-	-
AS15R2	AS15R5	4.31	143.5	9.30	-	-	-	-
AS15	AS15L	3.48	321.30	49.30	1.19	1.60	1.91	0.96

Appendix 4. Ayuyu Cave showing surface profile and roof thickness

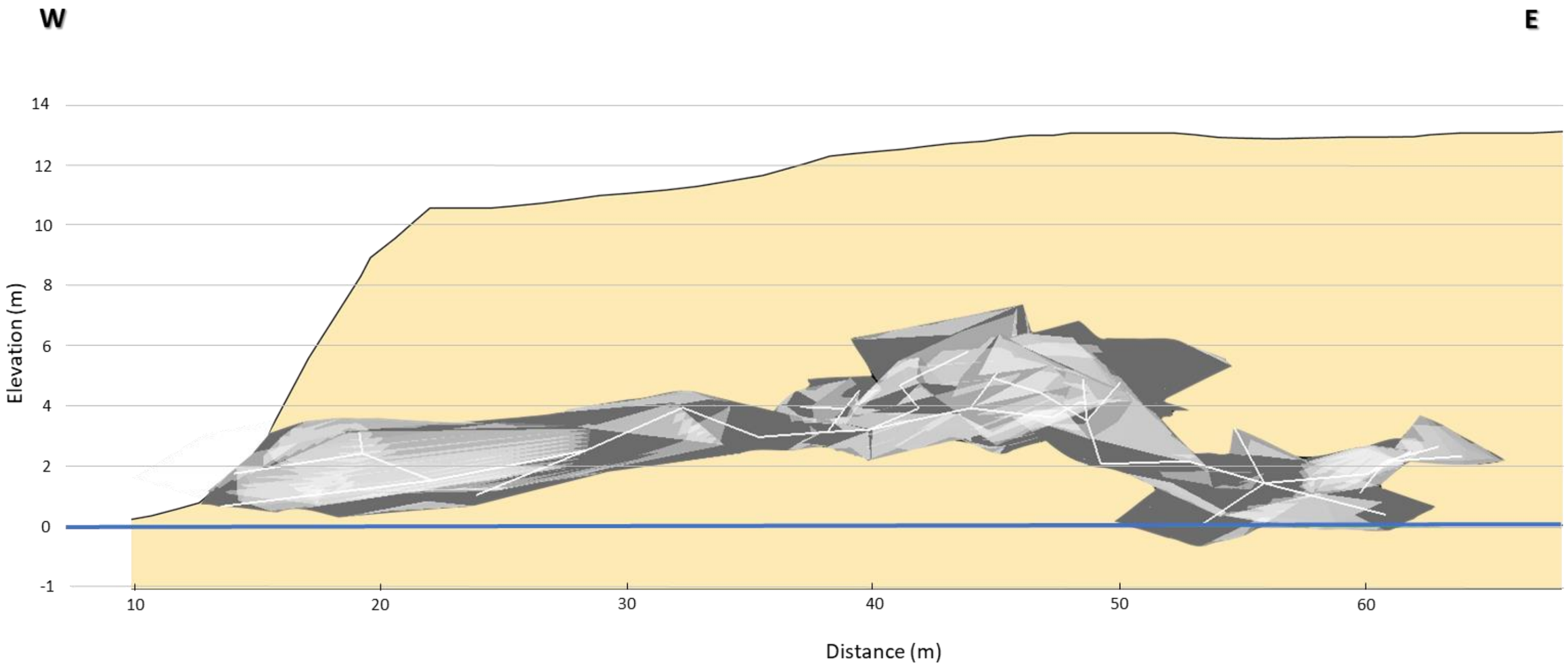

Appendix 5. Ayuyu Cave Plan and Profile showing points of interest

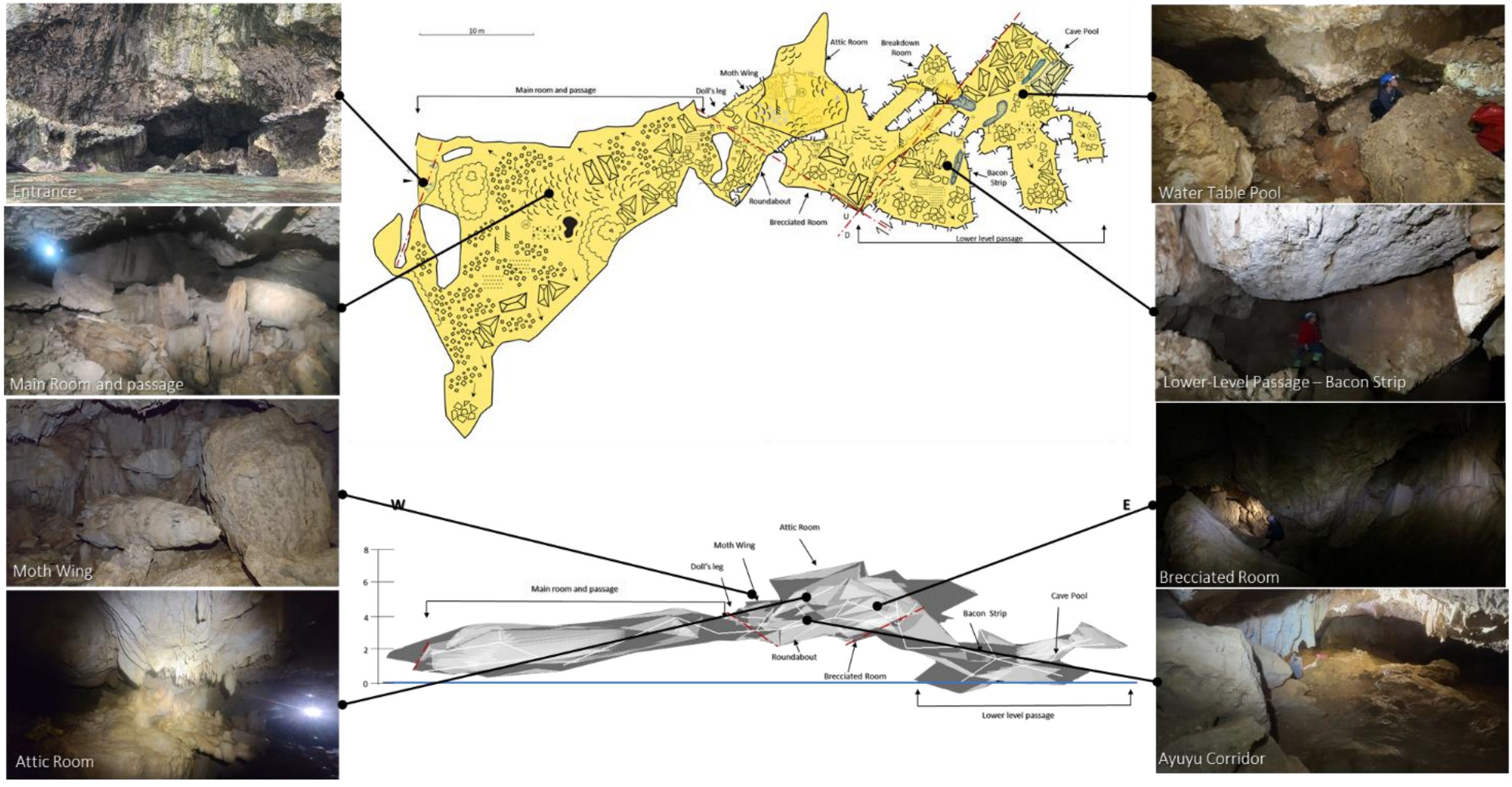

Appendix 6. Ayuyu Cave 3D Profile-DEM made in Therion Software